

# SHAPE OPTIMIZATION USING INTRINSIC GEOMETRY AND BOUNDARY ELEMENT METHOD

by  
**JAKKA VENKATESH**

ME

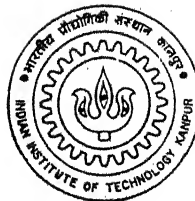
1994

D

VEN

SHA

GA



**DEPARTMENT OF MECHANICAL ENGINEERING  
INDIAN INSTITUTE OF TECHNOLOGY KANPUR**

**November, 1994**

**SHAPE OPTIMIZATION USING  
INTRINSIC GEOMETRY  
AND  
BOUNDARY ELEMENT METHOD**

**A Thesis Submitted  
In Partial Fulfilment of the Requirements  
for the Degree of  
DOCTOR OF PHILOSOPHY**

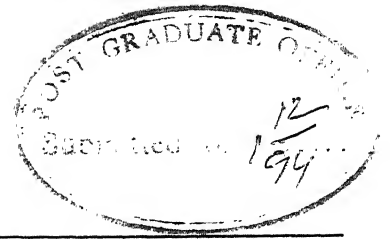
**by  
JAKKA VENKATESH**

**to the  
Department of Mechanical Engineering  
INDIAN INSTITUTE OF TECHNOLOGY KANPUR  
November, 1994**

---

**Dedicated to  
my ever loving brother  
Jakka Ramohan Scientist-D DRDL Hyderabad**

---



---

## CERTIFICATE

---

*This is to certify that the present research work entitled SHAPE OPTIMIZATION USING INTRINSIC GEOMETRY AND BOUNDARY ELEMENT METHOD was carried out by JAKKA VENKATESH under my supervision and it has not been submitted elsewhere for a degree.*

A handwritten signature in black ink, which appears to read "Dhande", followed by a horizontal line.

Dr. Sanjay G. Dhande  
Professor, ME & CSE  
Head, Mechanical Engineering  
IIT Kanpur

November 29, 1994

---

# SYNOPSIS

---

## SHAPE OPTIMIZATION USING INTRINSIC GEOMETRY AND BOUNDARY ELEMENT METHOD

A Thesis Submitted  
In Partial Fulfilment of the Requirements  
for the Degree of  
Doctor of Philosophy  
by  
Jakka Venkatesh

to the  
Department of Mechanical Engineering  
Indian Institute of Technology, Kanpur  
INDIA  
November, 1994

The design stages of synthesis, analysis and optimization constitute the core of any engineering design methodology. The concept of optimization is intrinsically tied to humanity's desire to excel. Though we may not consciously recognize it and though the optimization process takes different forms in different fields of endeavour, this drive to do better than before consumes much of our energy. Optimization is the process of maximizing a desired quantity or minimizing an undesired one. The process of mechanical design, or synthesis, may often be viewed as an optimization task. In optimization, the goal is to minimize an objective, such as weight or peak stress, subject to constraints on strength and performance. Optimization problems may be classified into the following categories:

- (i) Standard or Size optimization.
- (ii) Combinatorial optimization.
- (iii) Shape optimization.
- (iv) Topology optimization.

Size optimization relates to determining values of design parameters such as thickness and cross-sectional areas and inertias. Whereas in combinatorial optimization, the problems considered are called discrete optimization problems. In such problems some or all the decision variables are restricted to assume values within specified discrete sets. In combinatorial problems the optimum combination out of a possible set of combinations has to be determined. Some applications of this class of optimization include: airline crew scheduling, metal trimming and nesting problems. In trim problems, sheets of various sizes have to be cut from a big master sheet of given dimensions to minimize total wastage. In nesting problems, a set of component pieces in the form of specific shapes and sizes are to be nested on a given sheet so as to minimize the wastage of the resource material. Shape optimization problems deal with determining the outline or shape of a component and its associated dimensions such as, for example, the shape and size of a fillet or the shape and size of a cutout. Shape optimization is an important class of structural optimization problems. The exterior and interior boundary shapes of structures should be controlled and determined in the shape optimization process. Therefore, the parameters describing the changing boundary shapes of structures will be taken as design variables (referred to as Shape Design Variables). Topology optimization addresses the basic question of designing an optimum topological structure of a continuum so as to satisfy a set of functional requirements and achieve the minimum or maximum of an objective function. Shape optimization problems deal with the design of the boundary while topological optimization problems deal with the nature of the interior continuum in terms of the distribution of its solid/void nature.

Design optimization methods have been used successfully for optimization problems which involve selecting a set of optimal values for scalar design variables. The methods developed have been widely used for structural design as well as mechanical component design activities. Shape optimization is also a major consideration in many engineering design problems. The problem of shape optimization for a component can be described as deciding the geometry of a curve or a surface which will maximize or minimize an objective function as well as satisfy a set of constraints. The success of any shape optimization method depends on how the shape synthesis module has been defined. The most frequently published approach is that of representing the shape in terms of either an array of control points or a spline like representation. This representation does not evaluate shape explicitly and does not indicate clearly how shape should be modified for improving a design. Generally shape is synthesized using a mathematical model. In the present work, the shape synthesis is proposed to be done in the intrinsic geometry domain. The term shape is considered to describe the intrinsic properties of geometry that define a curve or surface. This representation of shape is then mapped into a cartesian domain, in which different analyses are performed based upon the particular application. The results are evaluated and updated till the optimum shape is found. In the last two decades, analysis using FEM/BEM (Finite Element Method/Boundary Element Method) have been used for engineering applications, in general, and for the

analysis part of any shape optimization procedure, in particular. Numerical methods are needed to optimize engineering components that generally have complex loading and geometry. Moreover, material reduction optimization needs simultaneous consideration of design and manufacturing. Shape optimization has been successfully applied to a variety of engineering problems in the automotive, aircraft and other industries. A few examples are fillets, turbine disks and blades, pre-forms in forging, channels or ducts, minimum-stress forms for elastic solids, and air-foil shapes.

A review of the current state-of-the-art shows that the geometrical description of a component is specified by using a set of auxiliary points or a set of points lying on the geometry of the curve or surface. Auxiliary points may not lie on the curve or surface. For example, the control polygon points of a Bezier or B-spline curve or surface are the auxiliary points of a particular curve or surface being designed. They, however, do define the shape of the curve or the surface. The review of the current literature shows that introducing the concept of intrinsic shape definition will definitely provide a better foundation for solving shape optimization problems.

Among all the numerical techniques available for engineering analysis, Boundary Element Method is more suitable for shape optimization since one needs solutions only on the boundary. The shape optimization problems described above can also be formulated and solved using the shape optimization methodology based on intrinsic geometry proposed in this research work. The method of shape optimization, proposed here, consists of selecting a shape model, defining a set of intrinsic shape design variables and then evaluating cartesian co-ordinates of the curve. A shape model is conceived as a set of continuous piecewise LINEar Curvature Elements (LINCEs), each element defined as a function of the arc length. The SDVs (Shape Design Variables) are the values of curvature and/or arc lengths at some of the linear curvature elements. Then, the mapping from the intrinsic space to the cartesian space will be carried out. Thus, shape synthesis will be accomplished. The shape synthesis module can be integrated through BEM analysis and an exhaustive search NLP (Non-Linear Programming) in one approach, and via first-order method of NLP in the other approach, to show how intrinsic geometry based shape definition can be used for engineering analysis and shape optimization. The proposed research also involves the method of calculating sensitivities of the objective functions like the frontal areas and the peak stress with respect to the intrinsic shape design variables. The optimal shapes of the following components have been obtained using the proposed shape optimization methodology: a thick cylinder subjected to constant internal pressure, an elastic ring under diametral compression, a torque arm subjected to axial and transverse loading, a fillet subjected to an axial load, and a ladle hook subjected to a tensile loading. The complete proposed methodology has successfully been implemented as a computer aided design tool by developing a multi-window concept for cartesian and intrinsic space using SUN-view graphics on SUN-workstation with Unix environment and also using HP-9000/800 series-workstation

with STARBASE graphics on Unix platform. As a conclusion, it can be said that the proposed approach requires fewer shape design variables as compared to the methods where shape is represented using spline-like functions.

The overall objective of this work is to develop an approach for shape optimization using intrinsic geometry and Boundary Element Method and to show how this methodology can be applied to various structural and mechanical design problems. The specific objectives of this research work can be stated as follows:

(1). For the proposed methodology of shape optimization, it is required to develop and test a robust numerical scheme in order to solve Serret-Frenet equations. The Serret-Frenet equations play an important role in the curve synthesis. Since these are non-linear equations in intrinsic variables, to be solved simultaneously in order to satisfy geometric constraints during the first stage of shape synthesis, proper caution must be taken in deciding free and dependent design variables. Suitable attention also must be given to select a stable numerical scheme and its implementation. The robust numerical scheme eliminates the designer intervention during the design process. This involves selection and development of a numerical integration module from amongst various numerical integration schemes such as Trapezoidal rule, Simpson's rule and Gaussian quadrature etc. in order to develop a suitable scheme of shape synthesis & optimization. These numerical integration schemes will provide the necessary mapping from intrinsic domain to cartesian domain by solving the Serret-Frenet equations.

(2). It is also required to develop a generalized BEM analysis computer code based on existing sub-modules for 2D-elastostatic plane-stress, plane-strain, and axi-symmetric problems which take into account the geometrical definition of the boundary in the form of an intrinsic curve. Boundary Element Method for 2D-elastostatic problems will be applied as an analysis tool in the proposed shape optimization methodology and the problems considered are characterized by a state of either plane-stress or plane-strain.

(3). The key idea is to employ geometric modeling concepts of curve synthesis typical of the CAD technology in order to produce sensitivity analysis results. These sensitivities with respect to intrinsic shape design variables can then be used by an optimizer to generate an improved design. Presently, analysis of engineering problems requires either FEM/BEM approach or either algebraic or numerical analysis methods. All these techniques are carried out in cartesian domain. The intrinsic geometry should provide the information about the cartesian geometry and any change in the shape made through the intrinsic design variables should update the cartesian geometry. In short, it is necessary to develop a method in which intrinsic geometry along with the cartesian geometry will be used for engineering analysis. To study and develop the numerical aspects of sensitivity of the curve or boundary of the component and hence the frontal area of the cross-section and the magnitude of the peak stress (Maximum Von Mises stress) with

respect to the intrinsic shape design variables. Determination of the sensitivity of the design to variations of the parameters is important in design and design optimization. This seems particularly important since the intrinsic definition of the curve has been used to define the boundary of the component being designed in the present work. It is expected that changes in some of the intrinsic shape design variables will have a large impact on the resulting cartesian coordinates.

(4). The next objective is to develop an interactive redesign system that integrates optimization methods in order to have a flexible and efficient computational tool that can be used easily by design engineers. The interactive module is intended to create the missing link between BEM and CAD technologies and therefore it should constitute one of the key elements to computerize the shape optimization cycle. It has been found that the intrinsic definition of shape seems to suffer from a handicap that one doesn't get the feel of the geometry of a curve. This problem can be eliminated by creating a multi-window facility with provisions for cartesian space, intrinsic space and various option buttons and information. The shape optimization cycle is composed of non-linear equation solver, numerical integration solver for mapping from intrinsic domain to cartesian domain, BEM module and a non-linear programming optimizer.

(5). Illustrative examples are to be considered and solved in order to show the capabilities of the proposed shape optimization methodology. However, emphasis will be focused on structural and mechanical applications.

The organization of the dissertation can be outlined as follows:

Chapter 1 introduces the relevant background information pertaining to the present research work. This includes a state-of-the-art review of optimization methods, an introduction of shape optimization, review of the relevant literature of intrinsic geometry and shape optimization problems, the objectives and scope of work, and the organization of the presentation of the dissertation.

Chapter 2 deals with the shape synthesis using intrinsic geometry. The basic concepts of differential geometry are presented in this chapter. The intrinsic geometrical aspects of the LINear Curvature Element model of a curve are introduced. Some fundamental definitions such as curvature, torsion, arc length are discussed. The Serret-Frenet equations which are the basis for curve synthesis are examined. For the case of planar curves, the differential equations relating to cartesian co-ordinates as a function of arc length are derived for the Serret-Frenet equations. The solution approach for synthesizing 2D curves are introduced. Intrinsic definition of the 3D surface is presented. Mapping procedure from intrinsic to cartesian domain is discussed. Some illustrative examples are discussed to show the capabilities of intrinsic geometry based curve synthesis. Finally, some observation on 2D curve synthesis have been discussed.

Chapter 3 addresses the concepts of BEM analysis using intrinsic geometry. Geometry, load, and restraints specifications have been discussed. BEM analysis formulation for 2D-elastostatic problems characterized by plane-stress, plane-strain, and axi-symmetric cases have been discussed. Sensitivity analysis aspects with respect to the SDVs are introduced. Finally, numerical example has been considered to show the numerical procedure of stress-sensitivity with respect to the shape design variables and the graphical plot of the same has been shown.

General approach of shape optimization methodology using intrinsic geometry and BEM has been addressed in Chapter 4. The integrating procedure between geometry, analysis and an exhaustive search NLP technique has been discussed. Similarly the procedure of linking between geometry, analysis, and first-order optimization method has also been discussed. Issues of sensitivities of objective function with respect to the shape design variables are addressed. The concepts of multi-window graphics environment to eliminate the handicap of intrinsic geometry has been discussed. Illustrative examples of some graphics environment have been presented. Finally, comparison and efficiency of the proposed shape optimization methodology is made with respect to the existing methods.

Case studies via Zero-order method are illustrated in Chapter 5. The illustrative examples using 2-LINCEs model include: a thick cylinder subjected to constant internal pressure and an elastic ring under diametral compression are presented. The illustrative examples using 3-LINCEs model include: a torque arm subjected to axial and transverse loading, a fillet under an axial load, and a ladle hook subjected to a tensile load. All these examples show how the intrinsic geometry based shape optimization can be used. An appreciable amount of reduction in the frontal area has been achieved depending upon the initial geometry of the component. Stress plots corresponding to the above examples are also presented.

Case studies via first-order method have been presented in Chapter 6. As an illustrative example the optimal shape of an elastic ring under diametral compression using 3-LINCEs model is obtained. The problem formulation and results have been discussed. The problem formulation include establishing the constrained optimization problem by imposing suitable geometric and stress constraints and transforming to an unconstrained optimization problem using interior penalty function method. The DFP (Davidon-Fletcher-Powell) method has been used as an unconstrained optimization solver.

Chapter 7 deals with the conclusions of the present work, which include a technical summary and the description concerning the scope for future work. The use of intrinsic geometry as a geometric modeling tool in shape optimization has been evaluated.

---

# ACKNOWLEDGEMENTS

---

I am sincerely thankful with my heart and soul to my ever loving guide Dr. Sanjay G. Dhande for rendering his valuable knowledge, excellent guidance, unmeasurable help. I had never experienced so far a professional and personality like Professor S. G. Dhande who has got excellent qualities of guiding postgraduate students, especially doctoral students in particular.

My experiences with professor Dhande tempts me to pursue my remaining career with him. I experienced from Professor Dhande that the degree of precision and perfection in delivering good ideas for carrying out this valuable doctoral dissertation and I am deeply thankful to him regarding the same. Such valuable hints and ideas of Dr. S. G. Dhande helped me to accomplish this doctoral dissertation successfully without any hinderence. I am highly grateful to him and his family. I am paying my great regards to him for sparing me his valuable time in completing this dissertation work successfully.

I immensely grateful to my beloved mother, brother Ramohan, and sister Lalitha who had obliged me from time to time in providing moral and financial support. I could not find the words that can express the greatness of the above three people of my family in encouraging one way or the other in order to accomplish this doctoral dissertation perfectly. I express my sincere regards to my ever loving brother Ramohan for his non-returnable help throughout my academic and non-academic life.

I am very thankful to my good friends Mr. P. V. M. Rao, N. Srinivas, Dr. B. K. Misra, Mrs. Biswas, I. Sridher, N. V. Reddy, P. S. Venkatesh, K. V. N. D. Ramesh and others for fruitful discussions I had with them. My thanks are also due to my best friend Mr. P. M. V. Subbarao and his family. I am grateful to Dr. S. C. Pradhan, Dr. Kalyanmoy Deb, Mr. Nathani, Mr. C. P. Singh, and K. S. Singh for their help and company.

I also would like to thank the group of CAD-Project, Mr. S. C. Gupta and Mr. Babulal who helped me in several ways during my stay at I.I.T Kanpur.

- Jakka Venkatesh

---

# TABLE OF CONTENTS

---

Certificate	iii
Synopsis	iv
Acknowledgements	x
Table of Contents	xi
List of Figures	xiii
Nomenclature	xix
<b>1. Introduction</b>	<b>1</b>
1.1 An Overview of Optimization Methods	1
1.2 Shape Optimization - An Introduction	4
1.3 Literature Review	10
1.4 Objectives and Scope of Work	18
1.5 Organization	19
<b>2. Shape Synthesis Using Intrinsic Geometry</b>	<b>22</b>
2.1 Basic Concepts of Differential Geometry	22
2.2 Intrinsic LINear Curvature Element (LINCE) Model of a Curve	30
2.3 Intrinsic Definition of a Surface	35
2.4 Intrinsic-Cartesian Mapping	39
2.5 Illustrative Examples	47

<b>Table of Contents</b>	<b>xii</b>
2.6 Some Observations	51
<b>3. BEM Analysis Using Intrinsic Geometry</b>	<b>52</b>
3.1 Geometry, Load, and Restraint Specifications	52
3.2 BEM Analysis	56
3.3 Sensitivity Analysis	67
3.4 Numerical Examples	68
<b>4. Shape Optimization Methodolgy</b>	<b>74</b>
4.1 General Approach	74
4.2 Zero-order Method (Exhaustive Search Method)	78
4.3 First-order Method	80
4.4 Issues of Sensitivity Analysis	84
4.5 Comparison and Efficiency of Proposed Method	87
<b>5. Case Studies via Zero-order Method</b>	<b>89</b>
5.1 Computer Software Developement	89
5.2 Illustrative Examples	89
5.2.1 A Thick Cylinder Problem	90
5.2.2 An Elastic Ring Problem	91
5.2.3 A Torque Arm Problem	100
5.2.4 A Fillet Problem	109
5.2.5 A Ladle Hook Problem	116
5.2.6 Sensitivity Analysis of An Elastic Ring Problem	130
<b>6. Case Studies via First-order Method</b>	<b>135</b>
6.1 Software Development	135
6.2 Numerical Example	135
6.2.1 An Elastic Ring Problem	135
<b>7. Conclusions</b>	<b>141</b>
7.1 General Observations	76
7.2 Future Work	145
<b>References</b>	<b>147</b>

---

# LIST OF FIGURES

---

Figure 1.1	Stages of Engineering Design Process	5
Figure 1.2	Shape Design by Co-operation Between Man and computer	6
Figure 1.3	Schematic Block Diagram of the Shape Optimization Methodology	8
Figure 1.4	Shape in Engineering Design Cycle	9
Figure 2.1	The Space Curve t-n-b frame $f(s)$	23
Figure 2.2	The Local Planes of Moving Trihedron	26
Figure 2.3	Intrinsic Geometry of 3-D Curve	27
Figure 2.4	Plane Curve Definition Using Cartesian Co-ordinates and Tangent Angles	32
Figure 2.5	Generalized n-LINCEs Model	33
Figure 2.6	Shape Models : (a) 1-LINCE Model (R Model $n=1, l=1$ ) (b) 2-LINCE Model (R-R Model $n=2, l=0$ ) (c) 3-LINCE Model (R-R-R Model $n=3, l=0$ ) (d) 3-LINCE Model (R-R-R Model $n=3, l=1$ )	34

<b>List of Figures</b>		xiv
Figure 2.7	Tangent Plane and Normal of a Biparametric Surface	37
Figure 2.8	Normal Curvature of a Biparametric Surface	38
Figure 2.9	Newton-Raphson Iterative Scheme	42
Figure 2.10	Graphical Output of $\kappa$ - $s$ $x$ - $y$ Curves of Example 2.1	48
Figure 2.11	Graphical Output of Example 2.2	49
Figure 2.12	Graphical Output of Example 2.3	50
Figure 3.1	A 2-Dimensional Physical Domain	53
Figure 3.2	An Isoparametric Quadratic Element	57
Figure 3.3	Local and Cartesian Components of the Traction Vector	66
Figure 3.4	(a) Definition of An Elastic Ring Problem (b) BEM Mesh for the Elastic ring problem	70
Figure 3.5	(a) Cartesian Profile for an Initial Shape of An Elastic Ring (b) Intrinsic Profile for an Initial Shape of An Elastic Ring	71
Figure 3.6	(a) Cartesian Profile for an Intermediate Shape of An Elastic Ring (b) Intrinsic Profile for an Intermediate Shape of An Elastic Ring	72
Figure 3.7	Graph Shows Stress Sensitivity Vs Change in Curvature Plot	73
Figure 4.1	Multi-Window Graphics Environment Designed on SUN-Workstations via SUN-View Graphics	75
Figure 4.2	General Definition of the Shape Optimization Problem Using Intrinsic Geometry and BEM	77
Figure 4.3	(a) Cartesian Geometry (b) Intrinsic Geometry	85

---

Figure 5.1	Thick Cylinder Subjected to an Internal Pressure	92
Figure 5.2	(a) Definition of Thick Cylinder Problem with Displacement and Stress Boundary Conditions (b) Boundary Element Mesh for Thick Cylinder	93
Figure 5.3	(a) Cartesian Profile for the Initial Shape of a Thick Cylinder (b) Intrinsic Profile for the Initial Shape of a Thick Cylinder	94
Figure 5.4	(a) Cartesian Profile for the Optimal Shape of a Thick Cylinder (b) Intrinsic Profile for the Optimal Shape of a Thick Cylinder	95
Figure 5.5	(a) Cartesian Profiles for the Initial and Optimal Shapes of a Thick Cylinder (b) Intrinsic Profiles for the Initial and Optimal Shapes of a Thick Cylinder	96
Figure 5.6	Cartesian and Intrinsic Profiles of Initial and Optimal Shapes of a Thick Cylinder on a Multi-Window SUN-view Graphics Environment	97
Figure 5.7	Equivalent Stress Vs Node Number along the Boundary of a Thick Cylinder	98
Figure 5.8	(a) Colour Stress Plot for an Initial Shape of a Thick Cylinder (b) Colour Stress Plot for an Optimal Shape of a Thick Cylinder	99
Figure 5.9	(a) Definition of An Elastic Ring Problem with Displacement and Stress Boundary Conditions (b) Boundary Element Mesh for an Elastic Ring	101
Figure 5.10	(a) Cartesian Profile for the Initial Shape of An Elastic Ring (b) Intrinsic Profile for the Initial Shape of An Elastic Ring	102
Figure 5.11	(a) Cartesian Profile for the Optimal Shape of An Elastic Ring (b) Intrinsic Profile for the Optimal Shape of An Elastic Ring	103
Figure 5.12	(a) Cartesian Profiles for the Initial and Optimal Shapes of An Elastic Ring (b) Intrinsic Profiles for the Initial and Optimal Shapes of An Elastic Ring	104
Figure 5.13	Design History of An Elastic Ring on a Multi-Window SUN-View Graphics Environment	105

<b>List of Figures</b>		<b>xvi</b>
Figure 5.14	Cartesian and Intrinsic Profiles of An Elastic Ring on a Multi-Window SUN-View Graphics Environment	106
Figure 5.15	Graph Shows Stress Vs Node Number Along the Boundary of An Elastic Ring	107
Figure 5.16	(a) Colour Stress Plot for an Initial Shape of An Elastic Ring (b) Colour Stress Plot for an Optimal Shape of An Elastic Ring	108
Figure 5.17	(a) Definition of a Torque Arm Design Problem with Displacement and Stress Boundary Conditions (b) Boundary Element Mesh for a Torque Arm	110
Figure 5.18	(a) Cartesian Profile for the Initial Shape of a Torque Arm (b) Intrinsic Profile for the Initial Shape of a Torque Arm	111
Figure 5.19	(a) Cartesian Profile for the Optimal Shape of a Torque Arm (b) Intrinsic Profile for the Optimal Shape of a Torque Arm	112
Figure 5.20	(a) Cartesian Profiles for the Initial and Optimal Shapes of a Torque Arm (b) Intrinsic Profiles for the Initial and Optimal Shapes of a Torque Arm	113
Figure 5.21	Cartesian and Intrinsic Profiles of Initial and Optimal Shapes of a Torque Arm on a Multi-Window SUN-view Graphics Environment	114
Figure 5.22	(a) Colour Stress Plot for an Initial Shape of a Torque Arm (b) Colour Stress Plot for an Optimal Shape of a Torque Arm	115
Figure 5.23	(a) Definition of a Fillet Problem with Displacement and Stress Boundary Conditions (b) Boundary Element Mesh for a Fillet	117
Figure 5.24	(a) Cartesian Profile for the Initial Shape of a Fillet (b) Intrinsic Profile for the Initial Shape of a Fillet	118
Figure 5.25	(a) Cartesian Profile for the Optimal Shape of a Fillet (b) Intrinsic Profile for the Optimal Shape of a Fillet	119
Figure 5.26	(a) Cartesian Profiles for the Initial and Optimal Shapes of a Fillet (b) Intrinsic Profiles for the Initial and Optimal Shapes of a Fillet	120

Figure 5.27	Cartesian and Intrinsic Profiles of a Fillet on a Multi-Window SUN-view Graphics Environment	121
Figure 5.28	(a) Colour Stress Plot for an Initial Shape of a Fillet (b) Colour Stress Plot for an Optimal Shape of a Fillet	122
Figure 5.29	(a) Definition of a Ladle Hook Problem with Displacement and Stress Boundary Conditions (b) Boundary Element Mesh for a Ladle Hook Problem	124
Figure 5.30	(a) Cartesian Profile for the Initial Shape of a Ladle Hook (b) Intrinsic Profile for the Initial Shape of a Ladle Hook	125
Figure 5.31	(a) Cartesian Profile for the Optimal Shape of a Ladle Hook (b) Intrinsic Profile for the Optimal Shape of a Ladle Hook	126
Figure 5.32	(a) Cartesian Profiles for the Initial and Optimal Shapes of a Ladle Hook (b) Intrinsic Profiles for the Initial and Optimal Shapes of a Ladle Hook	127
Figure 5.33	Cartesian and Intrinsic Profiles for the Initial and Optimal Shapes of a Ladle Hook on a Multi-Window SUN-view Graphics Environment	128
Figure 5.34	(a) Colour Plot for an Initial Shape of a Ladle Hook on SUN-View Graphics Environment (b) Colour Plot for an Optimal Shape of a Ladle Hook	129
Figure 5.35	Graph Shows Frontal-area Vs Change in Curvature ( $\Delta\kappa_1$ )	131
Figure 5.36	Graph Shows Area Sensitivity Vs Change in Curvature ( $\Delta\kappa_1$ )	132
Figure 5.37	Graph Shows Frontal-area Vs Change in Arc Length ( $\Delta s_1$ )	133
Figure 5.38	Graph Shows Area Sensitivity Vs Change in Arc Length ( $\Delta s_1$ )	134
Figure 6.1	(a) Definition of an Elastic Ring Under Diametrical Compression with Displacement and Stress Boundary Conditions (b) Boundary Element Mesh for An Elastic Ring Problem	136

List of Figures		xviii
Figure 6.2	(a) Cartesian Profiles for the Initial and Optimal Shapes of An Elastic Ring (Via First-order Method) (b) Intrinsic Profiles for the Initial and Optimal Shapes of An Elastic Ring (Via First-order Method)	139
Figure 6.3	Cartesian and Intrinsic Profiles for the Initial and Optimal Shapes of An Elastic Ring (Via First-order Method) on Multi-Window SUN-view Graphics Environment	140
Figure 7.1	Multi-Window Concept on HP-9000/800 series Work Station	142

---

# NOMENCLATURE

---

$t$	-	Tangent Vector at a generic point P
$b$	-	Binormal Vector at a generic point P
$n$	-	Normal Vector at a generic point P
$r$	-	Position Vector a Point
$s$	-	Arc length from a reference point to a generic point measured along the curve
SDV	-	Shape Design Variable
$x, y, z$	-	Cartesian Co-ordinates of a generic point P
$W$	-	Objective function
$\kappa$	-	Curvature of a generic point p
$\tau$	-	Torsion of a generic point P
$\psi$	-	Tangent angle
$u_n$	-	Normal Component of displacement
$T_{ij}(p, Q)$	-	Traction kernel
$t_i$	-	traction vector

$U_{ij}(p, Q)$	-	Displacement kernel
$N_c(\nabla)$	-	Quadratic shape functions in two-dimensional problems
$E$	-	Young's Modulus
$J(\nabla)$	-	Jacobian of transformation in two-dimensional problems
$\mathbf{m}$	-	Tangential Vector in two-dimensional problems
$L_{\max}$	-	Maximum distance between any two points on the boundary
$S$	-	Scaling factor
$w_g$	-	Weight function in ordinary Gaussian quadrature
$w_{gl}$	-	Weight function in logarithmic Gaussian quadrature
$\sigma_{ij}$	-	Cartesian stress components
$\epsilon_{ij}$	-	Cartesian strain components
$\nu$	-	Poisson's ratio
$\mu$	-	Shear modulus
$\alpha$	-	angle
$\Gamma$	-	Surface or boundary in two-dimensional problems
$\tau_{\max}$	-	Maximum Von-Mises stress
$\tau_{all}$	-	Allowable stress

# INTRODUCTION

---

## 1.1 An Overview of Optimization Methods

The concept of optimization is intrinsically tied to humanity's desire to excel. Though we may not consciously recognize it and though the optimization process takes different forms in different fields of endeavour, this drive to do better than before consumes much of our energy. Optimization is the process of maximizing a desired quantity or minimizing an undesired one. The process of mechanical design, or synthesis, may often be viewed as an optimization task. In optimization, the goal is to minimize an objective, such as weight or peak stress, subject to constraints on strength and performance. Optimization problems may be classified in to the following categories ([3], [41], [54]):

- (i) Standard or Size optimization.
- (ii) Combinatorial optimization.
- (iii) Shape optimization.
- (iv) Topology optimization.

**Standard or Size optimization :** Size optimization relates to determining values of design parameters such as thickness and cross-sectional areas and inertias. The mathematical optimization of a design assumes that a single measure of merit, objective function, or merit function exists and can be expressed formally in terms of the design parameters. The scalar merit function can be denoted by  $W(\mathbf{X})$ . Thus, the optimization problem can be stated as follows.

$$\text{Minimize } W(\mathbf{X}) \tag{1.1}$$

subject to

$$g_i(\mathbf{X}) \leq 0, \quad i = 1, 2, \dots, m$$

$$\text{and } h_j(\mathbf{X}) = 0, \quad j = 1, 2, \dots, p$$

where

$$\mathbf{X} = \begin{Bmatrix} x_1 \\ x_2 \\ \vdots \\ x_n \end{Bmatrix}.$$

It should be noted that  $\mathbf{X}$  is an  $n$ -dimensional vector called the design vector,  $W(\mathbf{X})$  is called the objective function and  $g_i(\mathbf{X})$  and  $h_j(\mathbf{X})$  are respectively, the inequality and the equality constraints. The number of variables  $n$  and the number of constraints  $m$  and/or  $p$  need not be related in any way. The problem stated in Eqn. (1.1) is called a constrained optimization problem.

If an optimization problem is simply stated as below:

$$\text{find } \mathbf{X} = (x_1, x_2, \dots, x_n)^T \text{ which minimizes } W(\mathbf{X}) \quad (1.2)$$

then such problems are called unconstrained optimization problems.

It is likely that there may exist one or more values of  $\mathbf{X}$  at which the function  $W$  will have a local minimum. Furthermore, it can be stated that the optimization problem is essentially to find an extremum value of the objective function. It can either be in the form of a minimum value of a function  $W(\mathbf{X})$  or it can also be in the form of a maximum value of  $-W(\mathbf{X})$ .

There are many approaches to find the solution of an optimization. Basically, there are search methods that use the function values,  $W$ , alone; gradient methods that use the function values and its first partial derivatives,  $\frac{\partial W}{\partial x_i}$ ; and finally, methods that also require the second partial derivatives,  $\frac{\partial^2 W}{\partial x_i \partial x_j}$ . The most common solution methods include ([3], [41], [54]) :

- (1) Search Methods.
- (2) Gradient Methods.
- (3) Second Derivative Methods.
- (4) Linear Programming.
- (5) Non-linear Programming.

Search methods include : exhaustive search, bisection search, grid search, random search, simplex search and golden search. Popular gradient methods are Steepest descent, Conjugate gradients, Newton's method. The most popular methods include the method of Steepest descent, Conjugate directions, Powell's direct search, method of least squares, and the Simplex search method. The search methods are easier to understand and are computationally inexpensive, since they do not require computing derivatives. Obviously, there are problems where utilizing derivative information will speed up the convergence to a local minimum.

**Combinatorial Optimization :** In the standard optimization problems the decision variables are all continuous variables, that is they can assume all possible values within their range of variation. In combinatorial optimization, the problems considered are called discrete optimization problems in which some or all the decision variables are restricted to assume values within specified discrete sets. In combinatorial problems the optimum combination out of a possible set of feasible combinations has to be determined.

If some or all the decision variables of a linear programming problem can assume only integer values then such a problem can be classified as a combinatorial optimization problem. Such problems are also called as integer linear programming or simply integer programming problems. The versatility of the integer programming model in several applications stems from the fact that in many practical problems, activities and resources, like machines, ships, and operators are indivisible. Also, most optimization problems of a combinatorial nature can be formulated as integer programs.

**Shape Optimization :** Shape optimization relates to determining the outline of a component and its dimensions such as, for example, the shape and size of a fillet or a hole. Shape optimization is a major consideration in many structural and mechanical engineering design problems. The problem of shape optimization for a component can be described as deciding the geometry of a curve or a surface which will maximize or minimize an objective function as well as satisfy a set of constraints. The exterior and interior boundary shapes of structures should be controlled and determined in the shape optimization process. Therefore, the parameters describing the changing boundary shapes of structures will be taken as design variables (referred to as Shape Design Variables).

Shape optimization is more complex than sizing optimization ([3], [41], [54]). Since the shapes of structures or mechanical components are continuously changing in the design process, a number of points need careful consideration: describing changing boundary shape, how to maintain adequate finite element/boundary element mesh, how to enhance the accuracy of the sensitivity analysis, how to impose proper constraints, and how to utilize existing optimization methods to solve the shape optimization problems.

**Topology Optimization :** Topology optimization addresses the basic question of where material should and should not be. In various practical structural design problems, decision of a layout of a structure or stiffeners in a given design space satisfying some design requirements is the most difficult task for design engineers since they must consider many possible conditions for safety, performance and so on. It is also very difficult to solve the topology (layout) problem by any conventional structural optimization technique because mathematical modeling of topology is too complex. To solve such problems, topology/layout optimization techniques are used based on various methods ([19]). The topology optimization is applicable to actual design problems in automobile design such as frame and stiffener layout problems of a car body.

## 1.2 Shape Optimization - An Introduction

Engineering design is a methodology involving several stages starting with the statement of a need and ending with the final presentation of a design. Figure 1.1 shows the stages involved in the engineering design process. It can be observed that the design stages of synthesis, analysis and optimization constitute the core of any engineering design methodology. The synthesis stage involves type synthesis, dimensional synthesis, material synthesis, synthesis of component tolerances as well as assembly clearances, and synthesis for manufacturability. The overall objective of dimensional synthesis is to design the geometry of physical objects. The geometrical aspects of the dimensional synthesis involve shape as well as size determination. The geometrical parameters could be described as scalar variables or as continuous functions. The diameter of a shaft is an example of a sizing design variable, the profile of a cam and a fillet of a structural member's cross-section are examples of shape design functions. The shape design process can be carried out by co-operation between man and computer and can be visualized as shown in Figure 1.2. The shape design process can start by using a physical model and then convert it to a mathematical model. If necessary, the mathematical model can be modified, edited or updated. Moreover, one can create a physical model from this revised version of the mathematical model.

The success of any shape optimization method depends on how the shape synthesis module (Figure 1.3) has been defined. The most frequently published approach is that of representing the shape in terms of either an array of control points or a spline like representation. This representation does not evaluate shape explicitly and does not indicate clearly how shape should be modified for improving a design. Although it is difficult to define, shape is still a basic property for design and manufacture. For example, the design of a cam or a fillet is the design of its geometry. The crucial decision is about the shape. Lord and Wilson (1984) defined shape as "Those aspects of geometrical form which have to do with the external aspect that an object presents to

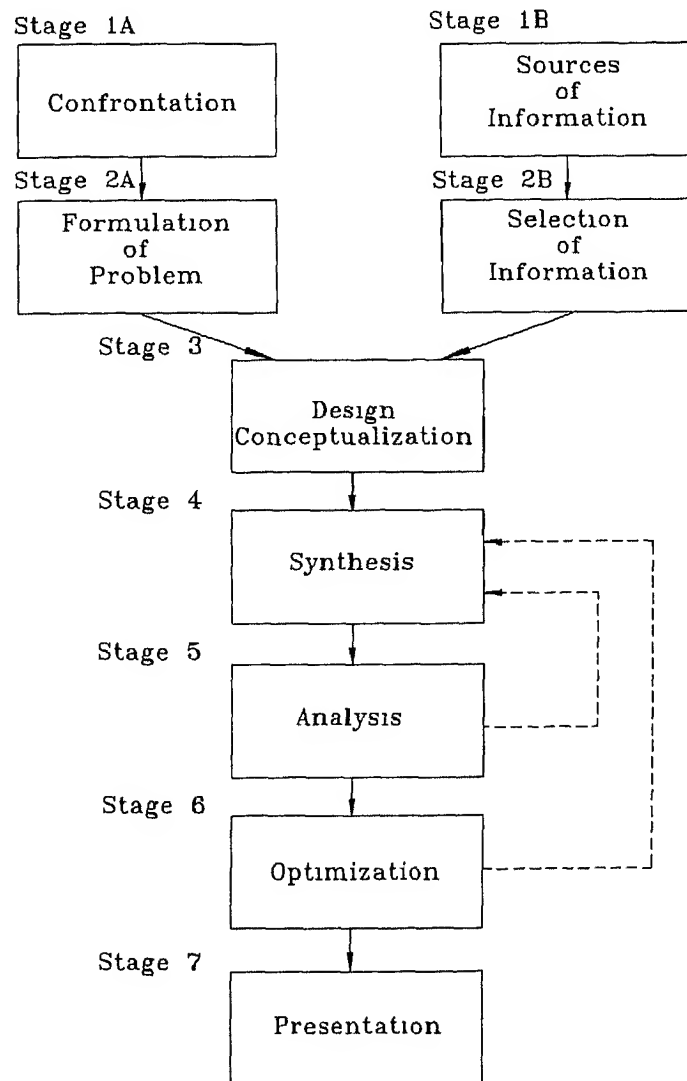


Figure 1.1 Stages of Engineering Design Process.

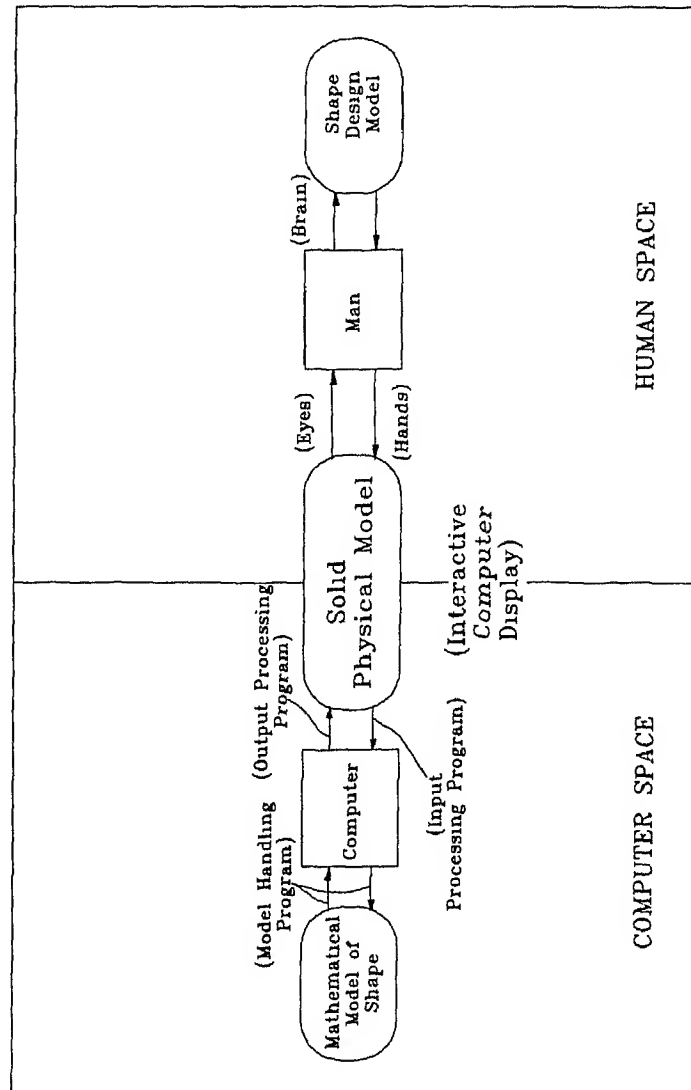


Figure 1.2 Shape Design by Cooperation Between Man and Computer.

the world". Mathematical representation of a shape is difficult. Shape is like an overall attribute or characteristic. Unlike microscopic properties of a geometry like co-ordinates and slopes, shape is a macroscopic attribute. One can also find aspects of geometrical form that deal with extrinsic and intrinsic geometrical properties. The co-ordinates that represent the geometry are extrinsic shape properties and are analogous to mass and temperature and other thermodynamic and rigid body dynamic properties. Shape, on the other hand is independent of scale, position and orientation and can be viewed as an intrinsic property of geometry much like entropy is an intensive thermodynamic property. Examples of shape intrinsic properties are the curvature and torsion of a three-dimensional space curve. Figure 1.4 shows the role of shape in the engineering cycle. Shape is synthesized using a mathematical model. This is done in the intrinsic geometry domain. This representation of shape is then mapped into a cartesian domain, in which different analyses are performed based upon the particular application. The results are evaluated and updated till the optimum shape is found. Shape optimization is a field of research which is in rapid development and is of increasing importance in engineering. For example, notches or holes of inappropriate shape, size, or orientation are known contributors to premature failure of mechanical components. Shape optimization can be used to determine the positions and sizes of notches or holes to minimize stress concentrations.

Research into the optimization of structures dates back to the 17th century classical treatise of Galileo, who investigated the optimum shapes of beams. In the 18th century, mathematicians posed certain classical shape optimization problems. For example, the "isoperimetric problem" required finding the shape of a closed curve of fixed length that encloses the greatest area (answer: a circle). From 1960 through 1980, considerable research was done using classical mathematical approaches to determine the optimal shapes of columns, plates, arches, and shafts. The objective in these efforts was to maximize the buckling load (or lowest natural frequency) or to minimize the displacement in the structure for a given amount of material.

In the last two decades, advances in FEM/BEM analysis using high-speed computers have shifted the focus to using numerical methods for shape optimization. Numerical methods are needed to optimize engineering components that generally have complex loading and geometry. Moreover, material reduction optimization needs simultaneous consideration of design and manufacturing. Shape optimization has been successfully applied to a variety of engineering problems in the automotive, aircraft and other industries. A few examples are fillets, turbine disks and blades, pre-forms in forging, channels or ducts, stress minimum forms for elastic solids, and air-foil shapes.

The method of shape optimization, proposed in this research work, consists of selecting a shape model in an intrinsic space, defining a set of shape design variables (SDVs) and then mapping into cartesian space. A shape model is represented as a set of LINear

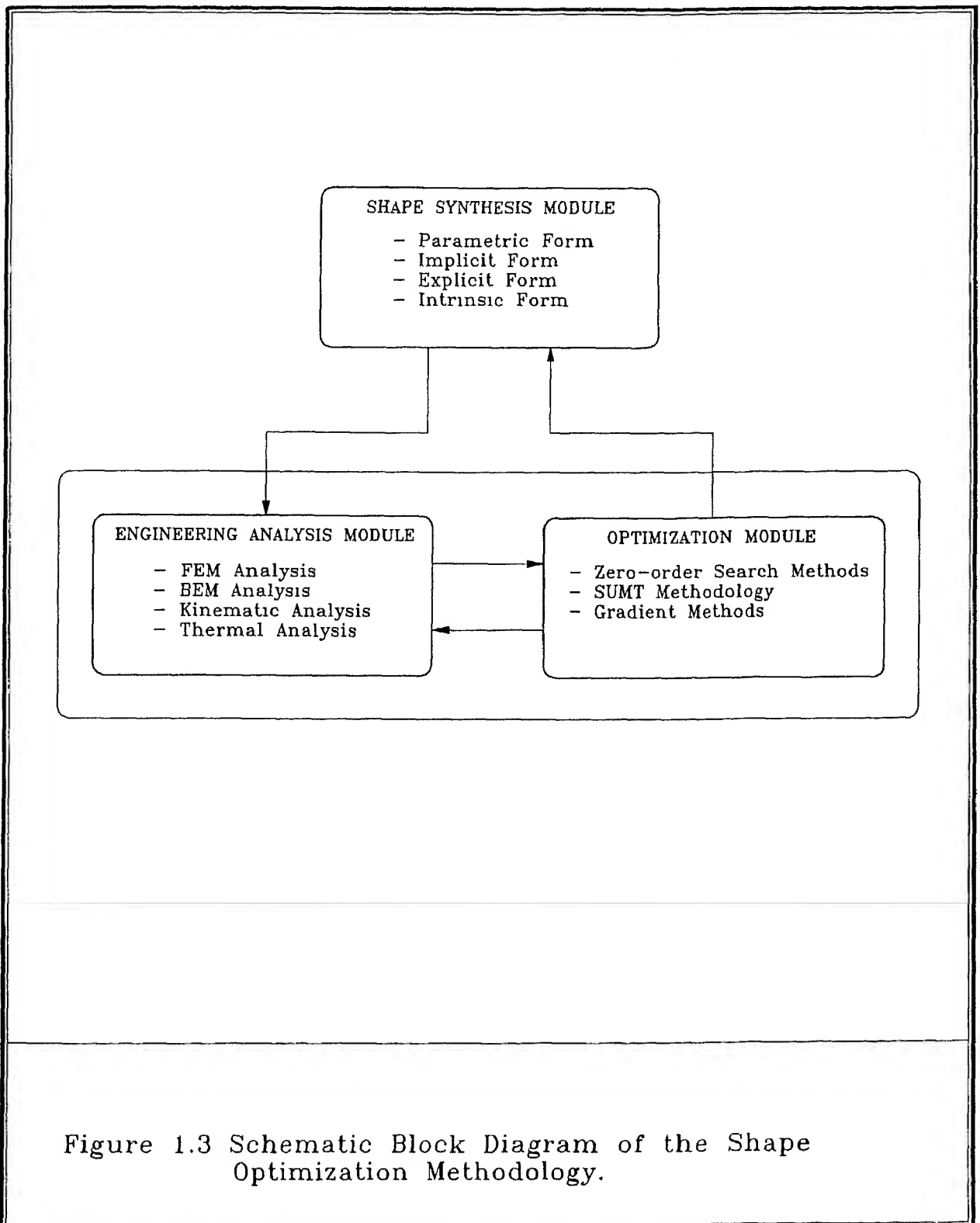


Figure 1.3 Schematic Block Diagram of the Shape Optimization Methodology.

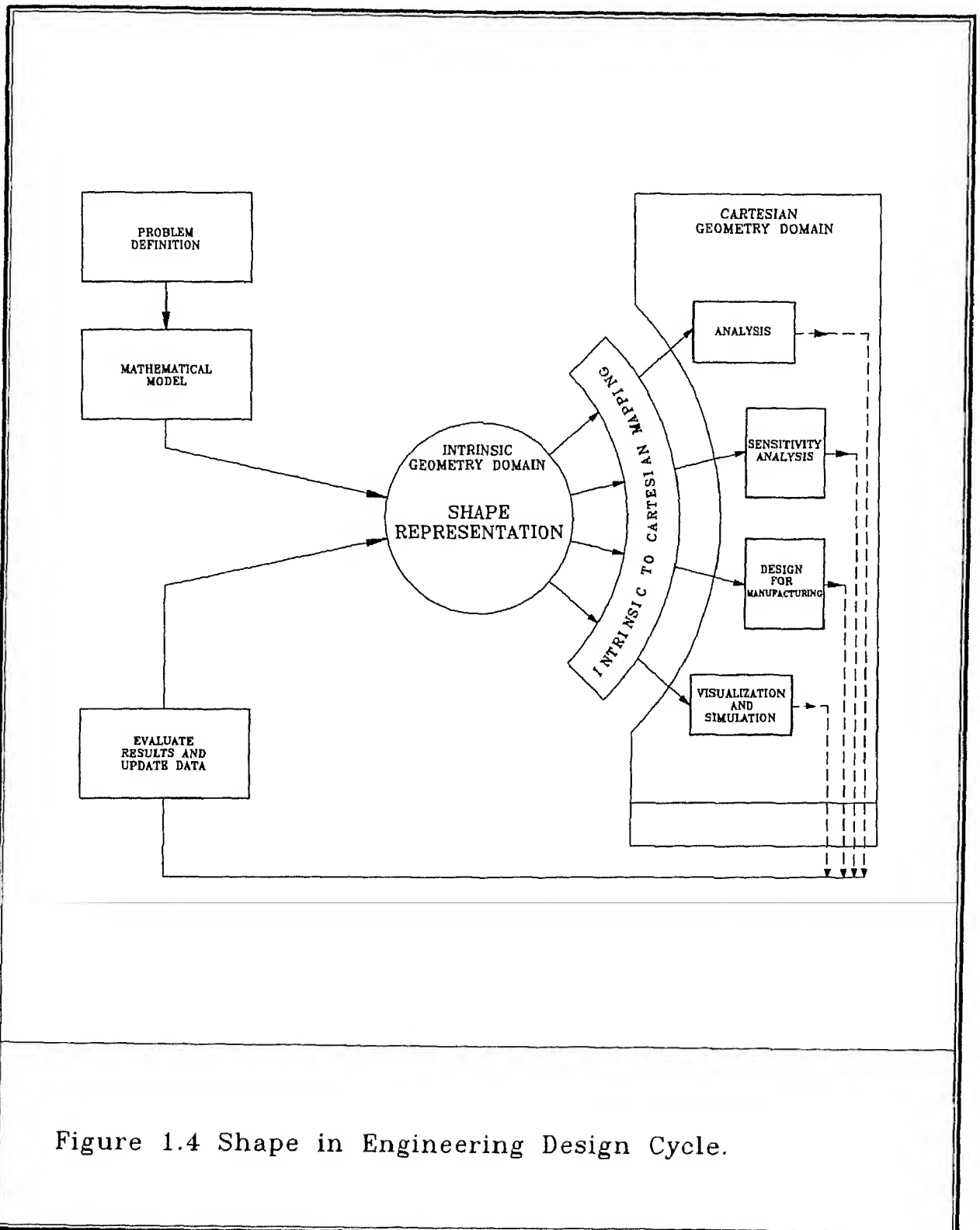


Figure 1.4 Shape in Engineering Design Cycle.

Curvature Elements (LINCEs). The shape design variables are the values of curvature and/or arc length at some of the LINCEs.

### 1.3 Literature Review

The study of geometry is one of the most fascinating fields in the world of mathematics. Among the different branches of mathematics, geometry is probably the most appealing to our intuition. Historical reviews indicate that geometry was one of the fundamental branches of science developed by the Babylonians and the Egyptians. Euclid, one of the Greek Philosophers, established the foundation of what is known as the Euclidian Geometry. In the Euclidian Geometry, one studies the actual shape of objects. More accurately, one studies those properties of objects that are unchanged by rotation, translation and reflections of objects.

Different branches of geometry have evolved in the past few centuries, projective geometry and differential geometry are two examples. Both these fields are extensions of Euclidian Geometry. In projective geometry, one studies the way objects are seen in contrast to Euclidian Geometry in which one studies metric properties of real objects. Projective geometry has been of more interest to engineers than it has to mathematicians. It has become a tool for design engineers for conveying their ideas effectively. Differential geometry on the other hand deals with the geometry of curves and surfaces studied by means of differential calculus. Concepts of intrinsic geometry have been described in well known texts of differential geometry ([49], [13], [34]). In the literature on differential geometry, the Cornu spiral, known in American literature as a clothoid, but also called a transition spiral, or railway curve, since it is often used in rail track layout to increase or decrease curvature linearly is probably the widely illustrated example of a curve for intrinsic geometry. Intrinsic definition of a Cornu spiral is a linear curve in the curvature-arc length,  $\kappa$ - $s$ , plane.

The developments in the area of computational geometry during the 70's and 80's gave an impetus for developing computational algorithms for many geometrical problems. In particular, curve and surface design became an active topic of research. One can now see a series of excellent texts which describe, in detail, how curves and surfaces can be designed using a variety of spline models ([17], [31], [34], [57])). The major drawback of using a spline approach for shape synthesis is that the information about curvature and torsion is not explicitly available. This makes it difficult to provide a feedback from the analysis-optimization sequence to the shape synthesis algorithm.

The works of Adams, Pal, Nutbourne, Remash Chandran, and Tavakkoli ([1],[37], [36], [42], [51], and [52]) form an interesting section of the literature reviewed here. The concepts of curve synthesis using linear curvature elements, termed as LINCEs, had been

developed by Nutbourne. This concept has been implemented in the form a detailed procedure by Adams (1975) and Nutbourne and Pal (1977) ([1], [37]). There are two difficulties in reviewing the works of Nutbourne, Adams and Pal. The first one being that they do not solve the boundary condition constraints of Serret-Frenet equations explicitly. This makes the computational procedure lengthy. The second aspect is that they have not shown how the method can be used for analysis-optimization process and hence sensitivity analysis. Remash Chandran (1982) ([42]) had used a spline curve to model the intrinsic shape definition. He had shown how a planar cam profile can be designed using their approach. It should be noted, however, that the method has not been extended for any shape optimization work. Tavakkoli and Dhande ([52]) worked on shape synthesis and optimization methodology using intrinsic geometry had shown only optimal configuration of Variable Geometry Truss design problems. It has not been extended for generalized shape optimization methodology involving FEM/BEM stress analysis and first-order optimization methods and hence sensitivity analysis. Although, the SDVs are the values of curvatures and/or arc lengths at some of the LINCes during shape synthesis, the freedom and restrictions involved in choosing the number of arc length SDVs (i.e.  $s_i$ 's) as dependent design variables while solving the Serret-Frenet non-linear simultaneous equations and the robustness of numerical scheme have not been discussed. It is important to note that, out of three dependent shape design variables, the number of arc length (i.e.  $s_i$ 's) variables can not be more than one. For example, in 2-LINCes model, the design variables will be  $\kappa_0$ ,  $s_0$ ,  $\kappa_1$ ,  $s_1$ ,  $\kappa_2$ , and  $s_2$ . Out of these six SDVs by keeping  $s_0 = 0$ ,  $\kappa_0$  and  $s_1$  are chosen as free shape design variables, and hence  $\kappa_1$ ,  $s_1$ , and  $\kappa_2$  will become dependent design variables which usually obtained by solving three non-linear Serret-Frenet geometric constraint equations, which is a successful case. Whereas  $\kappa_0$  and  $\kappa_1$  are chosen as free SDVs,  $s_1$ ,  $\kappa_2$ , and  $s_2$  will become dependent design variables. Since the arc length variables are highly non-linear as compared to curvature variables, this choice will provide a difficult situation of not being able to converge to a solution. Such a behaviour of the Serret-Frenet equations has been verified using various non-linear equation solving schemes. The solution to the Serret-Frenet equations involve computation of Fresnel integrals. Unfortunately, the expressions of the Fresnel integrals are not available in closed-form. Hence, it is necessary to select a proper set of variables and also select an efficient as well as a robust numerical scheme for the solution of the Serret-Frenet equations.

The finite element method has been extensively used for the analysis of mechanical components and in structural optimization during the last two decades, including successful application to shape optimal design of shafts, automobile components, aircraft and elastic structural components. In contrast, the boundary element method has only recently been applied to shape optimization of structural and mechanical components.

The FEM application for shape optimization problems of structural and mechanical components has been successfully demonstrated, but at the same time it has some

drawbacks. It is often necessary to redefine new finite-element meshes as the geometry of the structure changes. Inaccurate evaluations of stresses at the boundary can be responsible for the evaluation of very inaccurate design sensitivity analysis, thus leading to a large number of optimization iterations or even unrealistic designs. These difficulties with the FEM can be partially overcome by using the BEM to discretize the structure. Results of the boundary element analysis of elasticity problems are more accurate than the corresponding solutions of the FEM models, and they are expected to yield improved design sensitivity information. Consequently, a smaller number of iterations is needed to find the optimum shape. In the last two decades large number of papers have been published in the evolution of the BEM for shape optimization of engineering design problems ([4], [9], [32], [33], [45], and [56]).

The BEM is less versatile for structural analysis than the FEM. Its applicability to shape optimization of structures is presently limited to elasticity problems subjected to static constraints.

The merits of BEM against FEM can be summarized as follows:

1. Less data preparation time.
2. High resolution of stress.
3. Less computer time and storage.
4. Less unwanted information (since internal points in BE solutions are optional).
5. Easily applicable to incompressible materials. The displacement based plane-strain FE formulation fails when Poisson's ratio equals 0.5 exactly (i.e. the material is incompressible). The boundary element formulation, however handles these materials without any difficulty. Therefore, in problems involving rubber like materials the BEM is much more suitable than FEM.

Perhaps a more severe weakness is the difficulty in modeling thin-shell structures using BEM. While BEM is capable of handling thickness ratios of 10:1 - and in some cases upto 25:1 - it generally does not produce accurate results for thin plates and shells.

Traditionally, the optimization problem is cast as a minimization or maximization of an objective function subject to a set of constraints. A finite number of scalar variables are defined as design variables. However, if one needs to consider the geometry of a component as a design variable, then it no longer is a set of discrete variables. The geometry needs to be treated as a continuum. The problems of optimization dealing with continuum-type shape design variables are classified as shape optimization problems.

An extensive literature is available on numerical methods for optimization of structural and mechanical components whose shapes are defined by cross-section and thickness variables ([3], [41], [54]). Only limited literature has appeared in the area of shape optimization. The texts dedicated to this subject include: Pironneau ([39]), Haug, Choi and Komkov ([23]), Bennet and Botkin ([5]). The FEM has been applied extensively to shape optimal design of structures since 1973, while it is only in the last decade that BEM has been used in the field of shape optimization.

Mota Soares, Rodrigues, Oliveira Faria and Haug ([32]) developed models for the shape optimal design of solid and hollow shafts, based on constant, linear and quadratic boundary elements and non-linear programming techniques. The design objective is to choose a shaft with a given area, which has maximal torsional stiffness. The models are much more efficient and robust than the corresponding finite element discretization since the sensitivity information is more accurate.

Shape optimal design of shafts, based on the BEM, has also been developed by Burczynski and Adamczyk ([32]). Optimality conditions are generated and the Newton-Raphson method is used to solve a set of non-linear algebraic equations. The examples show that the number of analyses required is smaller than a corresponding finite element discretization.

Models for the shape optimal design of bidimensional elasticity based on the boundary element method and linear programming technique have been developed by Zychowski and Mizukami ([32]). The design objective is to minimize the area subject to displacement and geometrical constraints.

Mota Soares, Rodrigues and Choi ([32]) have developed models for the shape optimal design of bidimensional structures based on linear and quadratic boundary elements and the non-linear programming technique. The design objective is to minimize the compliance having a constraint of constant area. Applications show that the BEM is more accurate and efficient than the corresponding FEM. For general shapes, the technique used to calculate the stresses with the boundary was not accurate. This problem has been overcome by Leal who also has developed an automatic technique for mesh refinement ([32]).

Shape optimal design models for two and three-dimensional elasticity problems, based on BEM, have been developed by Burczynski and Adamczyk ([32]). The design objective is to maximize stiffness subjected to constant volume. The optimality conditions are derived for an optimal boundary. An iterative process, based on finite differences and Newton-Raphson method, is used to solve a set of non-linear algebraic equations, making it possible to determine the unknown optimal shape.

Eizadian and Trompette([32]) have also developed a model for shape optimal design of two-dimensional structures based on the BEM and NLP techniques. The design objective is to minimize the tangential stress subjected to geometrical constraints. The geometry is defined by linear and circular elements. Substructures are used to represent the fixed and moving boundaries. The multiplier method is employed to solve NLP problem. Several applications are presented including the shape design of connecting-rod and a rotor. Numerical instabilities are reported.

The BEM has been applied to the shape optimization of air-foils and wings by Pironneau ([39]). Furthermore, Fernand Ellyin ([18]) developed a methodology for shape optimization of intersecting pressure vessels. The methodology involves a profile of variable thickness which connects a spherical shell to a cylindrical one. The geometry of the mid-surface of the connecting shell of revolution is not known a priori, neither is the thickness variation. The profile and thickness is obtained based on minimum material volume and strength criterion. The optimum shape is obtained through a direct variation procedure of Rayleigh-Ritz method.

Esping and Holm ([15]) published a research work on structural optimization using OASIS. OASIS is a code for structural optimization. This paper demonstrates the capabilities in shape optimization. The CAD system ALADDIN is used for shape description and generation of finite element meshes. ALLADIN is a CAD system used to give meshes, loads, boundary conditions etc. to the finite element system, and to OASIS. It can also be used as a post-processor for stress, element errors etc.

Hajela and Jih ([22]) have published their research work on boundary element method in Optimal Shape Design - An integrated approach. This paper describes an implementation of BEM in optimal shape design. The computational advantages of the BEM over the more traditionally used FEM of analysis are examined in the context of the shape synthesis problem. An integrated analysis and optimization approach is also proposed for this problem. Numerical results are presented for shape design of torsional shafts and of structural components that can be characterized by a state of plane-stress.

Sandgren ([44]) has published a paper on shape optimiztion - Creating a Useful Design Tool. In this paper several new areas of research are presented which seek to eliminate some of the barriers to achieving a useful design optimization tool. These areas include consideration of geometrical and topological optimization as well as cross-sectional optimization, fundamental new approaches to combine analysis and optimization. Results for shape optimization using the boundary integral method with substructuring, zero-one integer programming for decision support and means of performing the analysis within the shape optimization formulations are presented.

Eschenaur ([14]) has published a paper on shape optimization of satellite tanks. The paper deals with the method of finding the optimal design of a thin walled satellite tank subject to constant internal pressure.

Hou ([24]) developed techniques and applications of shape optimal design. This research objective of Hou is to present a unified formulation and efficient numerical technique to perform shape optimum design. The numerical scheme consists of boundary parametrization, FEM and mathematical programming.

Shape optimization of two-dimensional elastic structures with optimal thickness for fixed parts, has also been developed by Ding ([12]). Shape optimization of two-dimensional elastic structures is treated in this paper. B-spline function is used as a shape function and design element technique is adapted simultaneously.

Boundary Integral Equation method for shape optimization of elastic structures has been published by Choi and Kwak ([9]). This work deals with a general method for shape design sensitivity analysis as applied to plane elasticity problems using a direct boundary integral formulation, material derivative concept and adjoint variable method. Among the several numerical implementations tested, the second order boundary elements with a cubic spline representation of the moving boundary have shown the best accuracy. Optimization as a philosophy of engineering structural design was reviewed by Schmit ([51]). There is now a collection of excellent titles reviewing optimization methods in engineering design ([3], [41], and [54]).

Shape optimization has attracted the attention of many researchers. Haftka and Grandhi have reviewed the work of several researchers in a review article ([21]). Vanderplaats has discussed the numerical problems associated with shape optimization. West and Sandgren ([56]) have used the variational approach to solve shape optimization problems.

The concept of shape optimization has been applied to the design of many mechanical components. Some applications are mentioned here.

As an application of optimization in automotive industry, Botkin([51]) used finite element analysis to design torque arm for an optimum shape which would minimize the weight subject to strength limitations. The optimum shape of rotating disks was studied by Bhavikatti and Ramakrishnan ([51]) using Non-Linear Programming (NLP) method. They used a 5th degree polynomial to define the shape of the cross-section. They also performed a stress analysis of the disk by FEM using isoparametric elements. They had satisfactory results which did not need any fairing process after the shape optimization.

The optimum shape of a gas turbine disk was obtained by Luchi, et al. ([30]). They used interactive procedure based on a method in which the disk profile was defined by spline

interpolation. Queue and Trompette ([40]) also worked on the design of an optimal shape of turbine blades. The weight of the rotating turbine blades was minimized in finding the optimal shapes of the cross-sections. They used polynomials to define the shape.

West and Sandgren ([56]) investigated the optimum shape for a ladle hook using BEM. Seventh order B-spline curve with nine control points were used to define the shape. As a second approach, the shape optimization problem was formulated as a variational statement. A fillet problem was studied by Wu ([51]). The design objective is to find the optimum shape of a fillet in order to minimize the total area of the fillet. A fourth-order B-spline was used to represent the design patch. Wu obtained optimum shapes by specifying different values of the permissible maximum stress. Mota Soares and Choi ([32]) have used boundary elements in shape optimal design of structures. They developed a technique for an automatic mesh refinement of the boundary elements. Tavakkoli and Dhande ([52]) have worked on the application of intrinsic geometry for shape synthesis and optimization to find a configurational design of a planar Variable Geometry Truss (VGT). However, this work is not enhanced to integrate with FEM/BEM analysis and first-order optimization methods and hence with the sensitivity analysis. This work was also not applied to the general application of engineering design problems involving weight or peak stress minimization.

BESHOP [Boundary Element Shape OPTimizer] - A Program Package for shape optimization in 2D-elasticity problems is developed by Farshi and Moradi ([16]). This work introduces a package which handles shape optimization in 2D-elasticity problems where BEM is used for analysis phase affording a large reduction in the problem dimensionality together with a variant of the method of center points for the optimization phase. Design variables in optimum shape determination consists of basic nodal co-ordinates for B-spline functions as the means to define smooth curves. Maximum stress and/or displacements at critical boundary points are considered as constraints in each cycle of the procedure.

Belegundu ([6]) has worked on optimizing the shapes of mechanical elements. According to his work, a set of basis shapes are generated using the pre- and post-processors. Then, an objective function such as weight or peak stress is minimized using a suitable optimization procedure.

Design optimization using BEM has been published by Tafreshi and Fenner ([50]). This work addresses the integration between numerical optimization techniques and the BEM in order to optimize the shape of machine elements and structural components subjected to static loading.

Design Sensitivity Analysis using the BEM has been published by Tafreshi and Fenner ([50]). This work deals with the application of boundary integral equations to design sensitivity analysis. Derivatives of displacement and stresses are calculated by implicit differentiation of the corresponding boundary element elasticity kernels.

A review of the current state-of-the-art shows that the geometrical description of a component is taken into account either as a set of auxiliary points or as a set of points lying on the geometry of the curve or surface. Auxiliary points may not lie on the curve or surface. For example, the control polygon points of a Bezier or B-spline curve or surface are the auxiliary points of a particular curve or surface being designed. They, however, do define the shape of the curve or the surface. The review of the current literature shows that introducing the concept of intrinsic shape definition will definitely provide a better foundation for solving shape optimization problems.

Among all the numerical techniques available for engineering analysis, Boundary Element Method is more suitable for shape optimization since one needs solutions only on the boundary. The shape optimization problems described above can also be formulated and solved using the shape optimization methodology based on intrinsic geometry proposed in this research work. The method of shape optimization, proposed here, consists of selecting a shape model, defining a set of intrinsic shape design variables (SDVs) and then evaluating cartesian co-ordinates of the curve. A shape model is conceived as a set of continuous piecewise linear segment of curvature (LINCEs), each segment defined as function of the arc length. The SDVs are the values of curvature and/or arc lengths at some of the Linear Curvature Elements. Then, mapping intrinsic space to cartesian space will be carried out. Thus, shape synthesis will be accomplished. The shape synthesis module thus obtained will be integrated through BEM analysis and an exhaustive search NLP (Non-Linear Programming) in one approach, and via first-order method of NLP in the other approach, to show how intrinsic geometry based shape definition can be used for engineering analysis and shape optimization. The proposed research also involves the method of calculating sensitivities of objectives like frontal-areas and the peak stress with respect to the intrinsic shape design variables.

The optimal shapes of a thick cylinder subjected to constant internal pressure, an elastic ring under diametral compression, a torque arm subjected to axial and transverse loading, a fillet under an axial load, and a ladle hook subjected to a tensile loading are obtained as an application of this proposed shape optimization methodology. The complete proposed methodology has successfully been implemented as a CAD tool by developing multi-window concept for cartesian and intrinsic space using SUN-view graphics on SUN-workstation in a UNIX-environment and also on HP 9000/800-series workstation using STARBASE graphics on a UNIX-platform. In addition, it can be said that the proposed approach requires fewer shape design variables as compared to the methods where shape is represented using spline-like functions.

## 1.4 Objectives and Scope of Work

The overall objective of this work is to develop a CAD (Computer Aided Design) approach to shape optimization using intrinsic geometry and Boundary Element Method and to show how this methodology can be applied to various structural and mechanical design problems. The specific objectives of this research work can be stated as follows.

(1). For the proposed methodology of shape optimization, it is required to develop and test a robust numerical scheme in order to solve Serret-Frenet equations. The Serret-Frenet equations play an important role in the curve synthesis. Since these are non-linear equations in intrinsic variables, to be solved simultaneously in order to satisfy geometric constraints during the first stage of shape synthesis, proper caution must be taken in deciding free and dependent design variables. Suitable attention also must be given to select a stable numerical scheme and its implementation. The robust numerical scheme eliminates the designer intervention during the design process. This involves selection and development of a numerical integration module from amongst various numerical integration schemes such as Trapezoidal rule, Simpson's rule and Gaussian quadrature etc. in order to develop a suitable scheme of shape synthesis and optimization. These numerical integration schemes will provide the necessary mapping from intrinsic domain to cartesian domain by solving the Serret-Frenet equations.

(2). It is also required to develop a generalized BEM analysis computer code based on existing sub-modules for 2D-elastostatic plane-stress, plane-strain, and axi-symmetric problems which take into account the geometrical definition of the boundary in the form of an intrinsic curve. Boundary Element Method for 2D-elastostatic problems will be applied as an analysis tool in the proposed shape optimization methodology and the problems considered are characterized by a state of either plane-stress or plane-strain.

(3). The key idea is to employ geometric modeling concepts of curve synthesis typical of the CAD technology in order to produce sensitivity analysis results. These sensitivities with respect to intrinsic shape design variables can then be used by an optimizer to generate an improved design. Presently, analysis of engineering problems requires either FEM/BEM approach or either algebraic or numerical analysis methods. All these techniques are carried out in cartesian domain. The intrinsic geometry should provide the information about the cartesian geometry and any change in the shape made through the intrinsic design variables should update the cartesian geometry. In short, it is necessary to develop a method in which intrinsic geometry along with the cartesian geometry will be used for engineering analysis. To study and develop the numerical aspects of sensitivity of the curve or boundary of the component and hence the frontal-area of the cross-section and the magnitude of the peak stress (Maximum Von-Mises stress) with respect to the intrinsic shape design variables. Determination of the sensitivity of the design to variations of the parameters is important in design and design optimization.

This seems particularly important since the intrinsic definition of the curve has been used to define the boundary of the component being designed in the present work. It is expected that changes in some of the intrinsic shape design variables will have a large impact on the resulting cartesian co-ordinates.

(4). The next objective is to develop an interactive redesign system that integrates optimization methods in order to have a flexible and efficient computational tool that can be used easily by design engineers. The interactive module is intended to create the missing link between BEM and CAD technologies and therefore it should constitute one of the key elements to computerize the shape optimization cycle. It has been found that the intrinsic definition of shape seems to suffer from a handicap that one doesn't get the feel of the geometry of a curve. This problem can be eliminated by creating a multi-window facility with provisions for cartesian space, intrinsic space and various option buttons and information. The shape optimization cycle is composed of non-linear equation solver, numerical integration solver for mapping from intrinsic domain to cartesian domain, BEM module and a non-linear programming optimizer.

(5). Illustrative examples are to be considered and solved in order to show the capabilities of the proposed shape optimization methodology. However, emphasis will be focused on structural and mechanical applications.

## 1.5 Organization

The present research work is aimed at developing a CAD-methodology for shape optimization using intrinsic geometry and Boundary Element Method (BEM). The organization of the dissertation can be outlined as follows:

Chapter 1 introduces the relevant background information pertaining to the present research work. This includes a state-of-the-art review of optimization methods, an introduction of shape optimization, review of the relevant literature of intrinsic geometry and shape optimization problems, the objectives and scope of work, and the organization of the presentation of the dissertation.

Chapter 2 deals with the shape synthesis using intrinsic geometry. The basic concepts of differential geometry are presented in this Chapter. The intrinsic geometrical aspects of the LINear Curvature Element model of a curve are introduced. Some fundamental definitions such as curvature, torsion, arc length are discussed. The Serret-Frenet equations which are the basis for curve synthesis are examined. For the case of planar curves, the differential equations relating to cartesian co-ordinates as a function of arc length are derived for the Serret-Frenet equations. The solution approach for synthesizing 2D-curves are introduced. Intrinsic definition of the 3D-surface is presented. Mapping

procedure from intrinsic to cartesian domain is discussed. Some illustrative examples are discussed to show the capabilities of intrinsic geometry based curve synthesis. Finally, some observation on 2D-curve synthesis have been discussed.

Chapter 3 addresses the concepts of BEM analysis using intrinsic geometry. Geometry, load, and restraints specifications have been discussed. BEM analysis formulation for 2D-elastostatic problems characterized by plane-stress, plane-strain, and axi-symmetric cases have been discussed. Sensitivity analysis aspects with respect to the SDVs are introduced. Finally, numerical example has been considered to show the numerical procedure of stress-sensitivity with respect to the shape design variables and the graphical plot of the same has been shown.

General approach of shape optimization methodology using intrinsic geometry and BEM has been addressed in Chapter 4. The integrating procedure between geometry, analysis and an exhaustive search NLP technique has been discussed. Similarly the procedure of linking between geometry, analysis, and first-order optimization method has also been discussed. Issues of sensitivities of objective function with respect to the shape design variables are addressed. The concepts of multi-window graphics environment to eliminate the handicap of intrinsic geometry has been discussed. Illustrative examples of some graphics environment have been presented. Finally, comparison and efficiency of the proposed shape optimization methodology is made with respect to the existing methods.

Case studies via zero-order method are illustrated in Chapter 5. The illustrative examples using 2-LINCEs model include: a thick cylinder subjected to constant internal pressure and an elastic ring under diametral compression are presented. The illustrative examples using 3-LINCEs model include: a torque arm subjected to axial and transverse loading, a fillet under an axial load, and a ladle hook subjected to a tensile load are presented. All these examples show how the intrinsic geometry based shape optimization can be used. An appreciable amount of reduction in the frontal area has been achieved depending upon the initial geometry of the component. Stress plots corresponding to the above examples are also presented.

Case studies via first-order method have been presented in Chapter 6. As an illustrative example the optimal shape of an elastic ring under diametral compression using 3-LINCEs model is obtained. The problem formulation and results have been discussed. The problem formulation include establishing the constrained optimization problem by imposing suitable geometric and stress constraints and transforming to an unconstrained optimization problem using interior penalty function method. The DFP (Davidon-Fletcher-Powell) method has been used as an unconstrained optimization solver.

Chapter 7 deals with the conclusions of the present work, which include a technical summary and the description concerning the scope for future work. The comparison and efficiency of the proposed shape optimization methodology has been made with the existing shape optimization procedures. Finally, the effectiveness of intrinsic geometry as a computer aided geometric design tool in shape optimization has been established.

---

# SHAPE SYNTHESIS USING INTRINSIC GEOMETRY

---

## 2.1 Basic Concepts of Differential Geometry

A few decades ago, researchers broke away from the main stream of research in computational geometry from using polynomials of one sort or another and turned their ideas to the task of **synthesizing** curves and surfaces via **differential geometry**. Differential geometry in its simplest form is the study of the shape of curves and surfaces using differential and integral calculus. Its origins lie in the writings of Euler and Monge 200 years ago, and the subject has an immense literature spanning many languages ([13], [26], and [34]). It provides a “study in the small or local study”, i.e. the properties of small piece of curves and surfaces. It can be explored that the intrinsic description of smooth curves as free curves in three-dimensional space. Arc length is denoted by  $s$ . At any point on a space curve there is infinity of normal vectors, but only one tangent vector. The **tangent vector** can be defined as the derivative of position vector  $\mathbf{t}(s) = \mathbf{r}'(s)$  and that it has **unit length**.

The derivative of the tangent vector defines both the **principal normal vector**  $\mathbf{n}$  and the curvature  $\kappa(s)$ . The vector cross product of the tangent vector and the normal vector defines the **binormal vector**  $\mathbf{b}(s)$ . The tangent vector, the normal vector, and the binormal vector are three unit vectors all mutually orthogonal and define a curve frame  $\mathbf{f}(s)$  (Figure 2.1) that moves along the curve as the arc length increases. The **torsion**  $\tau(s)$  to be introduced now should, roughly speaking, measure the magnitude and sense of deviation of a curve from the osculating plane in the neighbourhood of the corresponding point of the curve, or in other words, the rate of change of osculating plane (Figure 2.2).

The three unit vectors  $\mathbf{t}(s)$ ,  $\mathbf{n}(s)$ ,  $\mathbf{b}(s)$  form the space curve frame  $\mathbf{f}(s)$  (Figure 2.1).

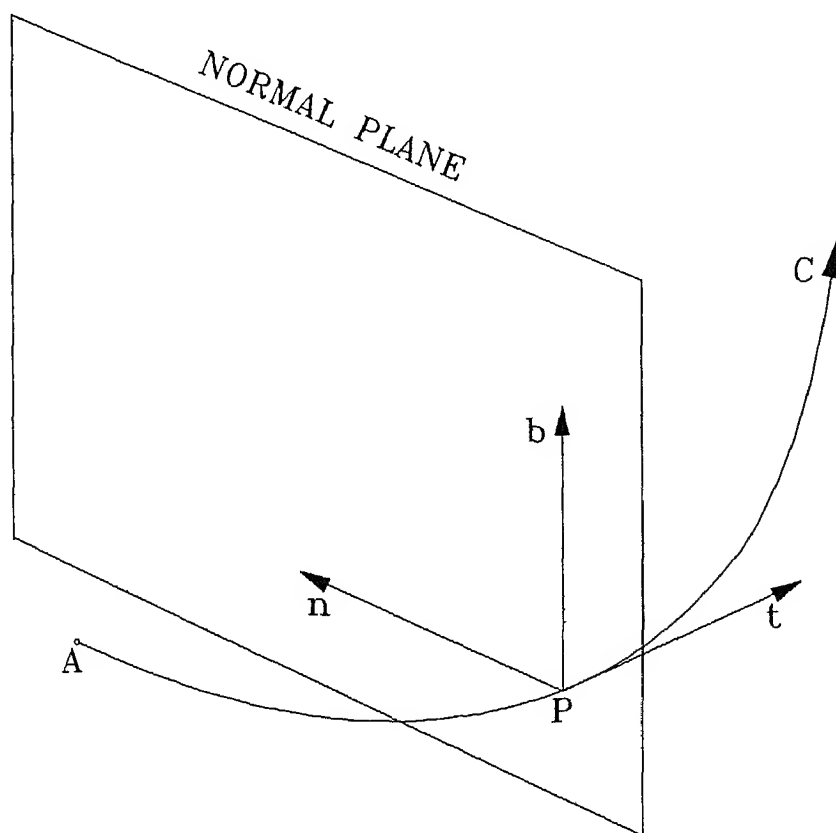


Figure 2.1 The Space Curve  $t$ - $n$ - $b$  Frame  $f(s)$ .

$$\mathbf{f}(s) = \begin{bmatrix} \mathbf{t}(s) \\ \mathbf{n}(s) \\ \mathbf{b}(s) \end{bmatrix} \quad (2.1)$$

The names given to the planes embraced by the vectors are as follows. The plane containing  $\mathbf{t}$  and  $\mathbf{n}$  is called the **osculating plane**. The plane containing  $\mathbf{n}$  and  $\mathbf{b}$  is called the **normal plane**. The plane containing  $\mathbf{b}$  and  $\mathbf{t}$  is called the **rectifying plane**. These planes are shown in Figure 2.2 ([13], [26], and [34]).

Geometric elements are represented by use of either parametric or non-parametric equations. For a plane curve, an explicit non-parametric equation takes the form  $y = f(x)$  which is not a convenient form to represent closed or multiple-valued curves. On the other hand, an implicit non-parametric equation takes the form  $f(x, y) = 0$  in which multiple-valued curves are possible. In either case both these forms are axis dependent. Moreover, the slope at a point may become infinitely large depending on the orientation of the curve with respect to the co-ordinate axes.

In parametric form, on the other hand, the slope values are computed in terms of the rate of change of the co-ordinates with respect to the parameter. For a plane curve, a set of two equations  $x = x(u)$ ,  $y = y(u)$ ,  $u_{min} \leq u \leq u_{max}$ , with the parameter  $u$ , represent its parametric form.

The formulation and application of Parametric Cubic (PC-curves), Bezier and B-spline curves have been thoroughly studied by Mortenson ([31]) and Rogers and Adams ([43]). Neither one of the geometrical forms have the ability to control explicitly the intrinsic properties such as, curvature ( $\kappa(s)$ ) and torsion ( $\tau(s)$ ) of a curve, which makes the shape synthesis using the intrinsic form more attractive.

A space curve requires two intrinsic equations  $\kappa = \kappa(s)$  and  $\tau = \tau(s)$  in order to determine its unique shape. For the case of a 2-D curve,  $\tau = 0$ . Torsion  $\tau = 0$  is a natural equation since it is a property of all 2-D curves. It suffices to claim that for any given function  $\kappa(s)$ , it is possible to solve the Serret-Frenet second-order equations for  $x(s)$  and  $y(s)$ . However, only ramp type curvature functions which correspond to spirals in the cartesian co-ordinates have been selected in the shape synthesis methodology presented in this research work. The selection of multi-ramp functions to represent the curvatures in the Serret-Frenet equations provides the designer with more free parameters and hence more flexibility of controlling the shape. The effects of second and higher order curvature equations is not studied fully in order to explore the results of shape synthesis by means of these higher order equations ([42]).

### Serret-Frenet Equations

Consider a curve  $C$  as shown in Figure 2.3. Let  $\mathbf{r}$  be the position vector of a generic

point  $P$  and let  $s$ , the arc length of  $P$  from a reference point  $A$ , be the parameter describing the curve as  $\mathbf{r}(s)$ . The unit tangent vector, the curvature, the torsion, the normal and the binormal of the curve  $C$  at the point  $P$  are given as follows:

$$\mathbf{t} = \frac{d\mathbf{r}}{ds} \quad (2.2)$$

$$\frac{d\mathbf{t}}{ds} = \kappa \mathbf{n} \quad (2.3)$$

$$\frac{d\mathbf{n}}{ds} = -\kappa \mathbf{t} + \tau \mathbf{b} \quad (2.4)$$

$$\frac{d\mathbf{b}}{ds} = -\tau \mathbf{n} \quad (2.5)$$

$$\mathbf{b} = \mathbf{t} \times \mathbf{n} \quad (2.6)$$

where  $\mathbf{t}$  is the unit tangent vector,  $\mathbf{n}$  is the unit normal vector,  $\mathbf{b}$  is the unit binormal vector,  $\kappa$  is the curvature, and  $\tau$  is the torsion. Equations (2.3), (2.4), and (2.5) are known as the formulae of Serret-Frenet([17], and [49]). These equations describe the location as well as the orientation of a moving trihedron consisting of unit vectors  $\mathbf{t}$ ,  $\mathbf{n}$ ,  $\mathbf{b}$  along the curve. These Serret-Frenet equations take a central part in the theory of curves. Furthermore, these equations can also be used as the basis for shape synthesis.

If a curve is planar then  $\tau = 0$  and the above equations can be written down as follows.

$$\mathbf{r} = \begin{bmatrix} x(s) \\ y(s) \end{bmatrix} \quad (2.7)$$

$$\mathbf{t} = \frac{d\mathbf{r}}{ds} \quad \text{and} \quad \mathbf{n} \cdot \mathbf{t} = 0 \quad (2.8)$$

$$\frac{d\mathbf{t}}{ds} = \kappa \mathbf{n} \quad (2.9)$$

$$\frac{d\mathbf{n}}{ds} = -\kappa \mathbf{t} \quad (2.10)$$

In general, the torsion and curvature of a space curve can be directly related to the position vector  $\mathbf{r}$  by the following equations ([17]).

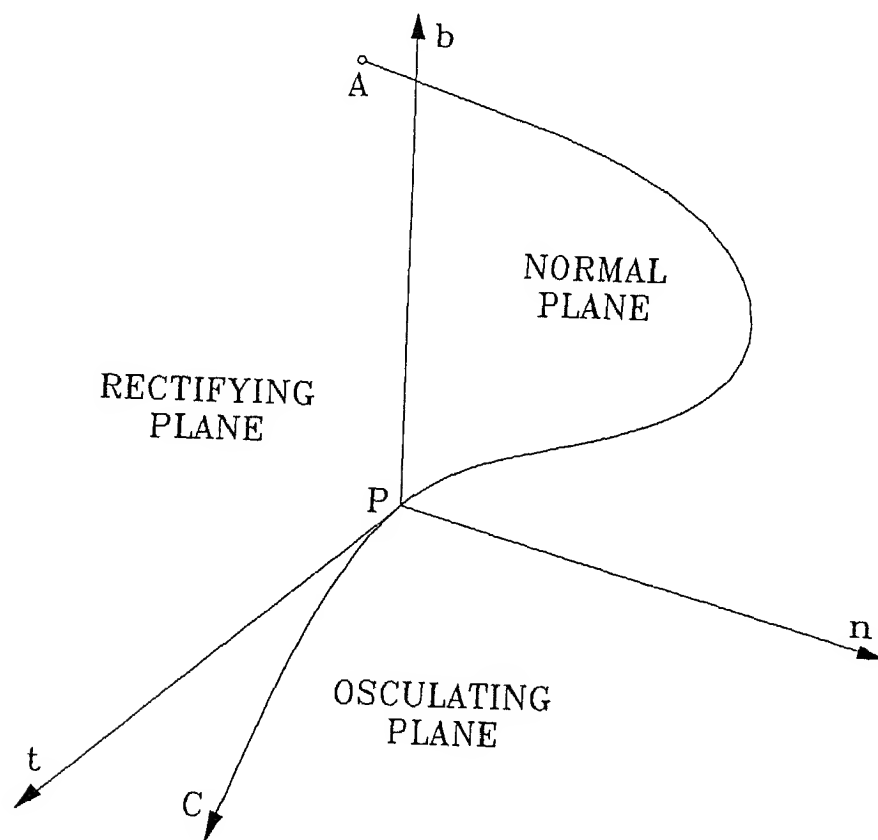


Figure 2.2 The Local Planes of Moving Trihedron of the Curve.

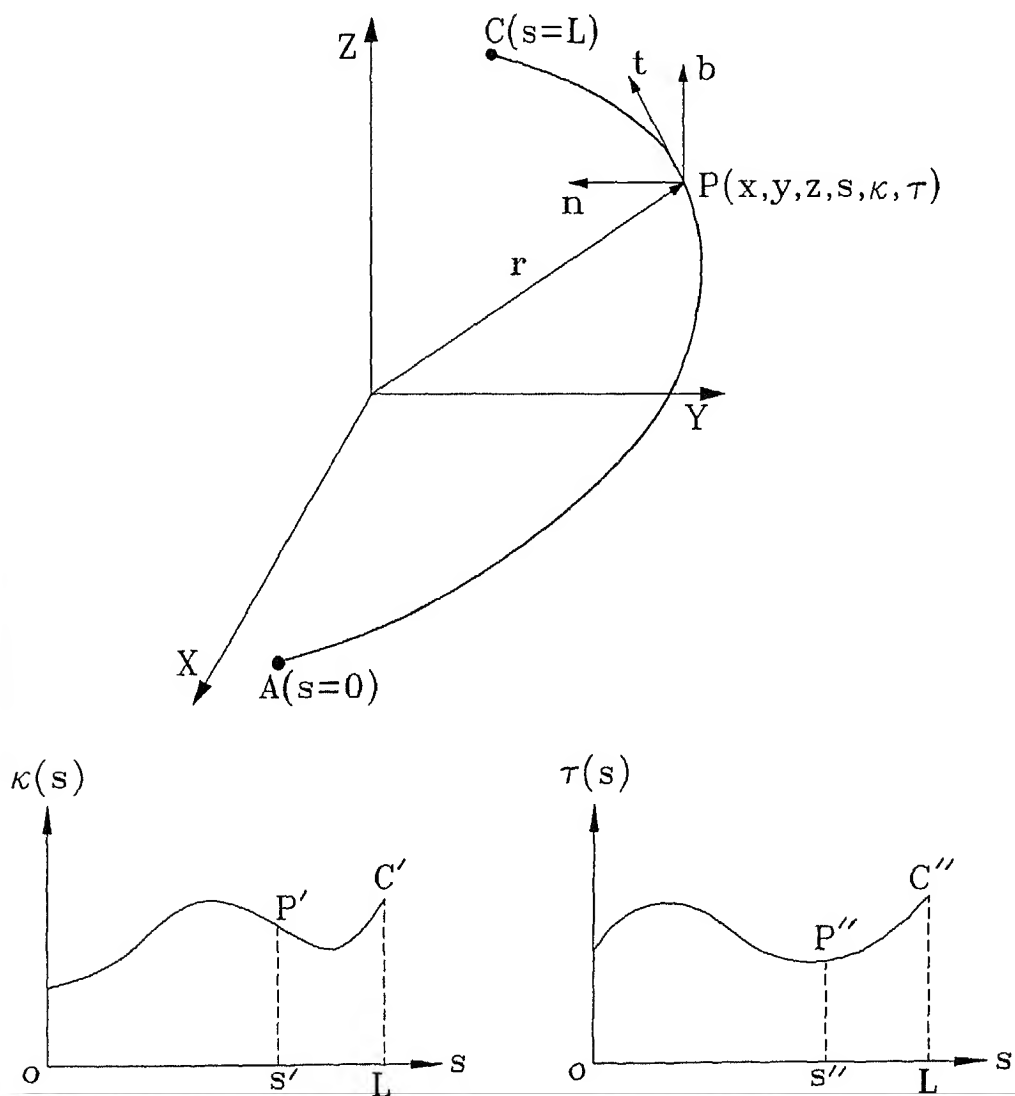


Figure 2.3 Intrinsic Geometry of 3D-Curve.

$$\kappa = \left| \frac{d\mathbf{r}}{ds} \times \frac{d^2\mathbf{r}}{ds^2} \right| \quad (2.11)$$

$$\tau \kappa^2 = \left| \frac{d\mathbf{r}}{ds} \cdot \left( \frac{d^2\mathbf{r}}{ds^2} \times \frac{d^3\mathbf{r}}{ds^3} \right) \right| \quad (2.12)$$

where

$$\frac{d\mathbf{r}}{ds} = \left[ \frac{dx}{ds} \quad \frac{dy}{ds} \quad \frac{dz}{ds} \right]^T \quad (2.13)$$

$$\frac{d^2\mathbf{r}}{ds^2} = \left[ \frac{d^2x}{ds^2} \quad \frac{d^2y}{ds^2} \quad \frac{d^2z}{ds^2} \right]^T \quad (2.14)$$

$$\text{and } \frac{d^3\mathbf{r}}{ds^3} = \left[ \frac{d^3x}{ds^3} \quad \frac{d^3y}{ds^3} \quad \frac{d^3z}{ds^3} \right]^T \quad (2.15)$$

### Solution Approach to 2-D Shape Synthesis

The problem of finding the co-ordinates  $x$  and  $y$  as a function of the arc length parameter  $s$  can be solved using Serret-Frenet equations (2.3) through (2.5). It should be remembered that the variation of the intrinsic property of curvature,  $\kappa$ , gives flexibility to shape synthesis.

To begin with, rewrite Eqn.(2.8) as follows:

$$\mathbf{t} = \frac{d\mathbf{r}}{ds} = \left[ \frac{dx(s)}{ds} \quad \frac{dy(s)}{ds} \right]^T \quad (2.16)$$

Since  $\mathbf{n} \cdot \mathbf{t} = 0$ , then

$$\mathbf{n} = \begin{bmatrix} -\frac{dy(s)}{ds} \\ \frac{dx(s)}{ds} \end{bmatrix} \quad (2.17)$$

On the other hand :

$$\frac{d\mathbf{t}}{ds} = \begin{bmatrix} \frac{d^2x(s)}{ds^2} \\ \frac{d^2y(s)}{ds^2} \end{bmatrix} \quad (2.18)$$

Substituting Equations (2.17) and (2.18) in Eqn.(2.3) yields :

$$\begin{bmatrix} \frac{d^2 x(s)}{ds^2} \\ \frac{d^2 y(s)}{ds^2} \end{bmatrix} = \kappa(s) \begin{bmatrix} -\frac{dy(s)}{ds} \\ \frac{dx(s)}{ds} \end{bmatrix} \quad (2.19)$$

Therefore,

$$\frac{d^2 x}{ds^2} + \kappa(s) \frac{dy}{ds} = 0 \quad (2.20)$$

$$\frac{d^2 y}{ds^2} - \kappa(s) \frac{dx}{ds} = 0 \quad (2.21)$$

where the boundary conditions at the starting point A are assumed to be known i.e., at  $s = s_0$ ,  $x = x_0$ ,  $y = y_0$ ,  $\psi = \psi_0$ .

Assume that  $\kappa(s)$  is defined as a piecewise linear function of  $s$ . Let

$$\eta' = x' + iy' \quad (2.22)$$

where  $\eta' = \frac{d\eta}{ds}$ ,  $x' = \frac{dx}{ds}$ , and  $y' = \frac{dy}{ds}$ .

The governing Equations (2.20) and (2.21) can now be written as follows:

$$(\eta') - i\kappa(s)(\eta') = 0 \quad (2.23)$$

$$\text{or} \quad \eta' = e^{i \int \kappa(s) ds} = e^{i\psi(s)} \quad (2.24)$$

where  $\int \kappa(s) ds = \psi(s)$ .

Separating the real and imaginary parts, we get

$$\frac{dx}{ds} = \cos[\psi(s)] \quad (2.25)$$

$$\frac{dy}{ds} = \sin[\psi(s)] \quad (2.26)$$

Integrating these equations with respect to the arc length  $s$  yields the parametric co-ordinates of the 2-D curve in terms of the parameter  $s$ .

$$x(s) = \int_{s_0}^s \cos[\psi(\sigma)] d\sigma + x_0 \quad (2.27)$$

$$y(s) = \int_{s_0}^s \sin[\psi(\sigma)] d\sigma + y_0 \quad (2.28)$$

where

$$\psi(\sigma) = \int_{s_0}^{\sigma} \kappa(s) ds + \psi_0 \quad (2.29)$$

Equations (2.27) through (2.29) could be solved using numerical integration and numerical nonlinear equation solving for the cartesian co-ordinates  $x(s)$  and  $y(s)$  and the change in the tangent angle  $\psi(s)$  along the 2-D curve once the curvature function  $\kappa(s)$  is known.

## 2.2 Intrinsic LINEar Curvature Element (LINCE) Model of a curve

Consider the problem of defining a curve passing through two points  $P_0(x_0, y_0)$  and  $P_n(x_n, y_n)$  in a two-dimensional space (Figure 2.4). It has also been assumed that the directions of tangents at  $P_0$  and  $P_n$  have been specified as  $\psi_0$  and  $\psi_n$  and the arc lengths from a reference point A as  $s_0$  and  $s_n$  respectively. If  $\kappa$  is the curvature at any point  $P$ , then it is assumed that the variation of  $\kappa$  as a function of the arc length as the parameter  $\kappa = \kappa(s)$  has been specified. It can be seen that  $\kappa(s)$  defines the shape of the curve. It should be remembered that the variation of the intrinsic property of curvature,  $\kappa$ , offers flexibility to shape synthesis.

In this section, linear equations are used as shape models. Let the curvature  $\kappa(s)$  be defined as a series of piecewise continuous linear functions with curvatures  $\kappa_0$  and  $\kappa_n$  at the initial and final points (Figure 2.5 and Figure 2.6). The intrinsic equation can be written as:

$$\begin{aligned} \kappa(s) &= \left( \frac{\kappa_1 - \kappa_0}{s_1 - s_0} \right) (s - s_0) + \kappa_0 & s_0 \leq s \leq s_1 \\ \kappa(s) &= \left( \frac{\kappa_2 - \kappa_1}{s_2 - s_1} \right) (s - s_1) + \kappa_1 & s_1 \leq s \leq s_2 \\ &\dots\dots\dots \\ \kappa(s) &= \left( \frac{\kappa_n - \kappa_{n-1}}{s_n - s_{n-1}} \right) (s - s_{n-1}) + \kappa_{n-1} & s_{n-1} \leq s \leq s_n \end{aligned} \quad (2.30)$$

Each linear segment corresponds to a spiral in cartesian co-ordinates. The area under the curvature equation represents the change in the tangent angles of the initial and final points of the 2-D curve. Therefore:

$$\psi_n - \psi_0 = \left(\frac{\kappa_0 + \kappa_1}{2}\right)(s_1 - s_0) + \left(\frac{\kappa_1 + \kappa_2}{2}\right)(s_2 - s_1) + \dots + \left(\frac{\kappa_{n-1} + \kappa_n}{2}\right)(s_n - s_{n-1}) \quad (2.31)$$

Upon substitution of the curvature Equation (2.30) in Equation (2.29) and subsequently in Equations (2.27) and (2.28) and considering the boundary conditions of the 2-D curve results in the following equations.

$$\begin{aligned} x_n - x_0 &= \int_{s_0}^{s_1} \cos \left[ \left( \frac{\kappa_1 - \kappa_0}{s_1 - s_0} \right) \left( \frac{\sigma^2}{2} - s_0 \sigma \right) + \kappa_0 \sigma + C_1 \right] d\sigma \\ &+ \int_{s_1}^{s_2} \cos \left[ \left( \frac{\kappa_2 - \kappa_1}{s_2 - s_1} \right) \left( \frac{\sigma^2}{2} - s_1 \sigma \right) + \kappa_1 \sigma + C_2 \right] d\sigma \\ &+ \dots \\ &+ \int_{s_{n-1}}^{s_n} \cos \left[ \left( \frac{\kappa_n - \kappa_{n-1}}{s_n - s_{n-1}} \right) \left( \frac{\sigma^2}{2} - s_{n-1} \sigma \right) + \kappa_{n-1} \sigma + C_n \right] d\sigma \end{aligned} \quad (2.32)$$

and

$$\begin{aligned} y_n - y_0 &= \int_{s_0}^{s_1} \sin \left[ \left( \frac{\kappa_1 - \kappa_0}{s_1 - s_0} \right) \left( \frac{\sigma^2}{2} - s_0 \sigma \right) + \kappa_0 \sigma + C_1 \right] d\sigma \\ &+ \int_{s_1}^{s_2} \sin \left[ \left( \frac{\kappa_2 - \kappa_1}{s_2 - s_1} \right) \left( \frac{\sigma^2}{2} - s_1 \sigma \right) + \kappa_1 \sigma + C_2 \right] d\sigma \\ &+ \dots \\ &+ \int_{s_{n-1}}^{s_n} \sin \left[ \left( \frac{\kappa_n - \kappa_{n-1}}{s_n - s_{n-1}} \right) \left( \frac{\sigma^2}{2} - s_{n-1} \sigma \right) + \kappa_{n-1} \sigma + C_n \right] d\sigma \end{aligned} \quad (2.33)$$

where  $C_1$  through  $C_n$  are constants of integration. Note that  $C_1 = \psi_0$ . The other constants can be expressed in terms of  $\kappa_i, s_i, i = 0, \dots, n$  and  $\psi_0$  using the following relation.

$$\begin{aligned} C_j = C_{j-1} &+ \frac{\kappa_{j-1} - \kappa_{j-2}}{s_{j-1} - s_{j-2}} \left( \frac{s_{j-1}^2}{2} - s_{j-1} s_{j-2} \right) + \kappa_{j-2} s_{j-1} \\ &+ \frac{\kappa_j - \kappa_{j-1}}{s_j - s_{j-1}} \left( \frac{s_{j-1}^2}{2} \right) - \kappa_{j-1} s_{j-1}, \quad j = 2, 3, \dots, n \end{aligned} \quad (2.33.a)$$

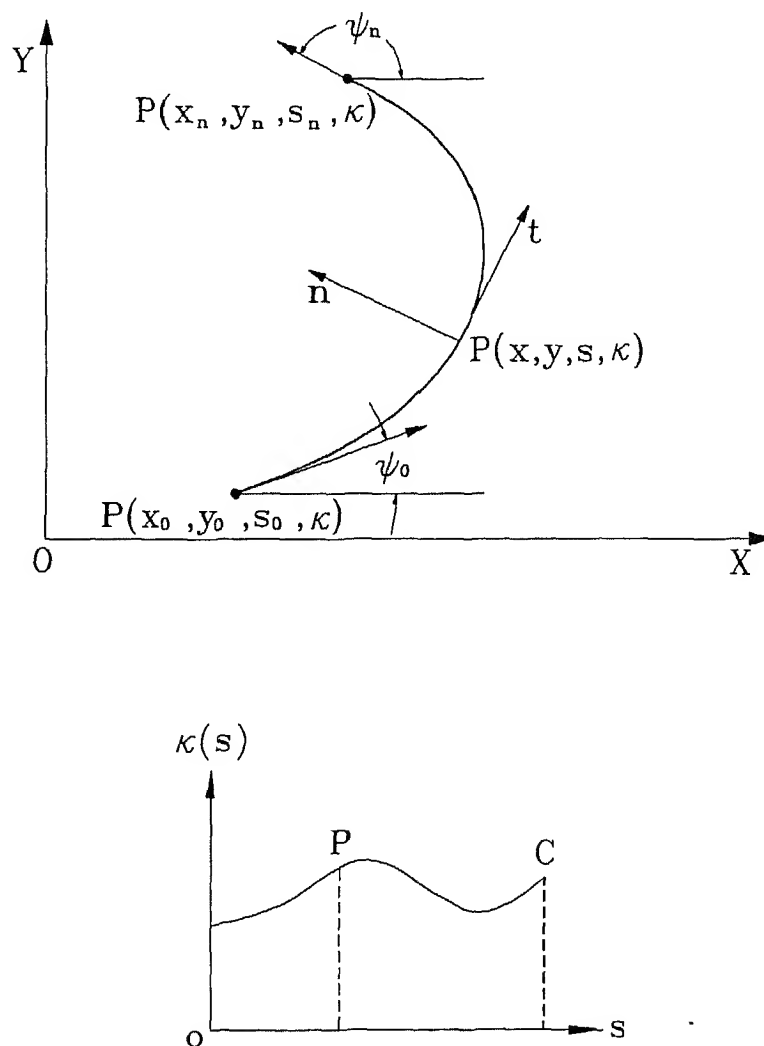


Figure 2.4 Plane Curve Definition Using Cartesian Coordinates and Tangent Angles.

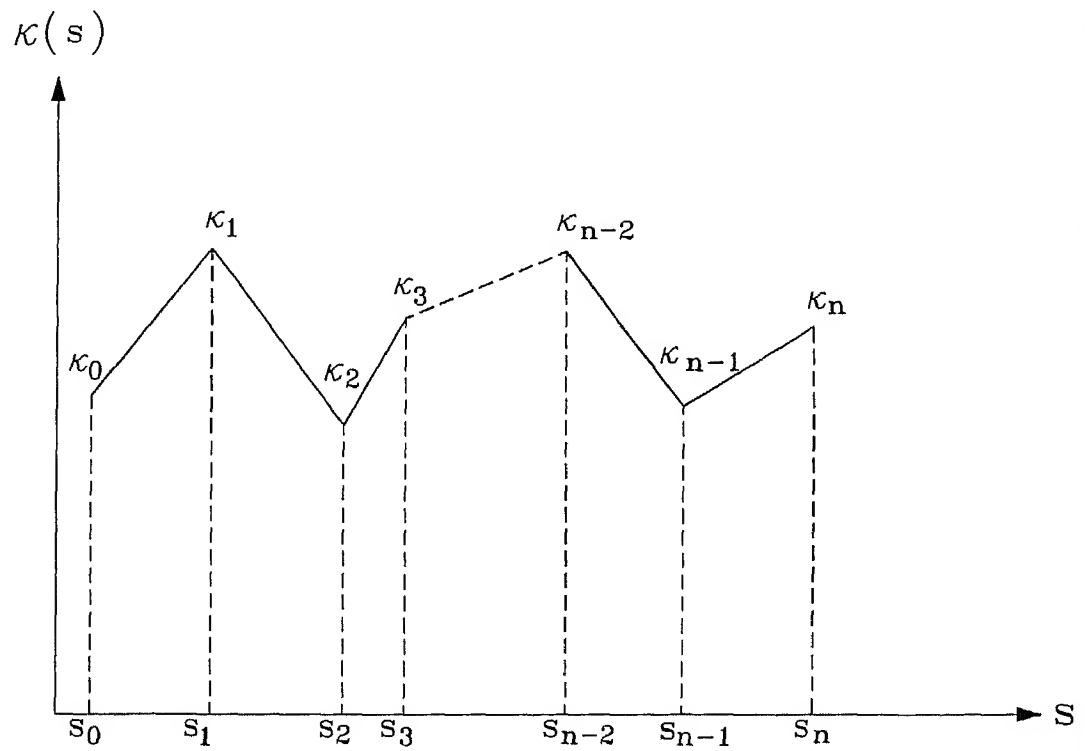


Figure 2.5 Generalized n-LINCEs Model.

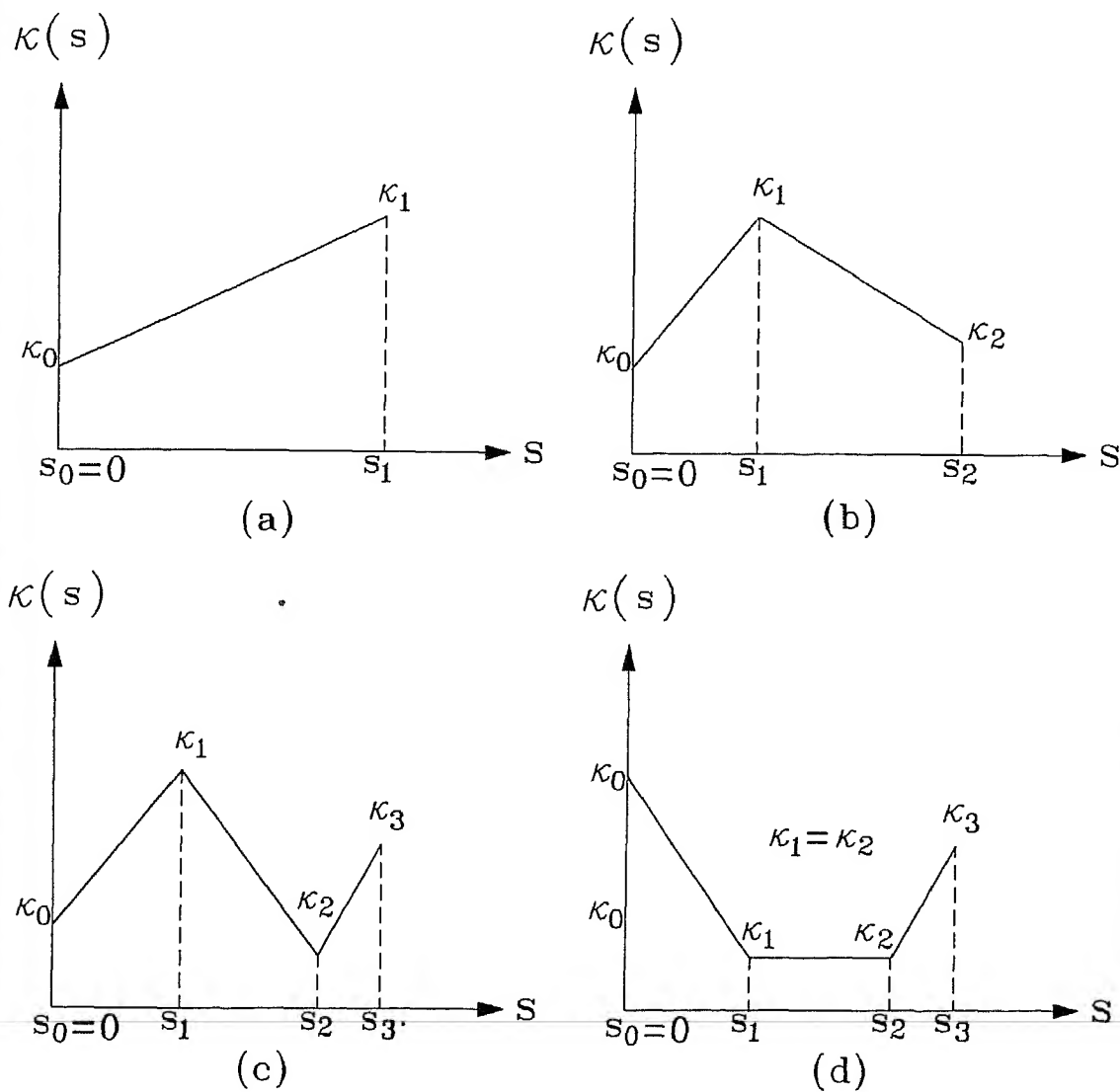


Figure 2.6 Shape Models :

- (a) 1-LINCE Model (R-Model  $n=1, l=0$ )
- (b) 2-LINCE Model (R-R Model  $n=2, l=0$ )
- (c) 3-LINCE Model (R-R-R Model  $n=3, l=0$ )
- (d) 3-LINCE Model (R-R-R Model  $n=3, l=1$ ).

Examination of the right-hand side of Equations (2.31) through (2.33) indicates the existence of  $(2n+2)$  variables  $s_0$  through  $s_n$  and  $\kappa_0$  through  $\kappa_n$ . Since there are only three non-linear simultaneous equations to be satisfied, the left over free design parameters will be  $(2n - 1)$ . Furthermore, if  $s_0$  is assumed to be zero, then the number of free design parameters reduces to  $(2n - 2)$ . These  $(2n - 2)$  parameters can be termed as Shape Design Variables (SDVs). If a feasible set of these  $(2n - 2)$  SDVs are selected, it is possible to evaluate the shape as well as the objective function. In order to find the optimal shape, it will be necessary to search the feasible domain of these  $(2n - 2)$  shape design variables.

The shape synthesis process can now be thought of as a two step process. The first step involves deciding the number  $n$ . Here, the selection of a shape model consisting of  $n$  linear curvature elements (LINCes) in the intrinsic plane. Examples of shape models for  $n = 1, 2$  and  $3$  are shown in Figure 2.6. These models will be termed as R model, R-R model and R-R-R model for  $n = 1, 2$ , and  $3$  respectively. The second step of shape definition involves establishing the set of shape design variables for a given shape model.

The total number of SDVs will be  $(2n - 2 - l)$  where  $l$  could be the additional constraints relating the intrinsic variables  $\kappa_i$ 's and  $s_i$ 's. Notice that for  $n = 1$  and  $l = 0$  the number of SDVs is zero and for  $n = 2$ ,  $l = 0$  and  $n = 3$ ,  $l = 0$ , the number of SDVs would be two and four respectively. Furthermore consider a R-R-R model with  $n = 3$ . If an additional constraint of  $\kappa_1 = \kappa_2$  is imposed, then the total number of SDVs would be 3 since  $l$  will be 1.

Once the total number of SDVs has been established, it is a matter of choice for the designer to select either all  $\kappa_i$ 's or  $s_i$ 's or a combination of some  $\kappa_i$ 's and some  $s_i$ 's as the shape design variables. It should be noted however, that there are two intricacies in choosing shape design variables. The first one is that, out of three dependent design variables which are usually obtained by solving three non-linear simultaneous equations, the number of  $s_i$ 's should not exceed one design variable, since the Eqns. (2.32) and (2.33) are too non-linear in terms of  $s_i$ 's than  $\kappa_i$ 's. Second difficulty is that, as the number  $n$  of LINCes increases, the feasible domain of SDVs may become smaller and difficult to evaluate. Computationally stable schemes are being selected for solving Eqns. (2.31) through (2.33) simultaneously as well as for evaluating integrals of Eqns. (2.32) and (2.33).

### 2.3 Intrinsic Definition of a Surface

Consider a biparametric surface  $\Sigma$  shown in Figure 2.7. A generic point  $P$  on this surface can be described by the radius vector  $\mathbf{r}(u, v)$  where the parameters  $u$  and  $v$  vary between 0 and 1.

$$\mathbf{r}(u, v) = \begin{bmatrix} x(u, v) \\ y(u, v) \\ z(u, v) \end{bmatrix} \quad 0 \leq u, v \leq 1 \quad (2.34)$$

The intrinsic properties of a surface patch can be described in terms of the unit normal vector at the point P, the tangent plane at the point P and the principal curvature at point P. The intrinsic quantities of a surface in the neighbourhood of a given point can also be described by the coefficients of the first and second fundamental forms denoted by Form I and Form II respectively ([31]). A brief description of these intrinsic properties of a surface are given below.

The unit normal vector to the surface at point P is defined as

$$\mathbf{n} = \frac{\mathbf{r}_u \times \mathbf{r}_v}{|\mathbf{r}_u \times \mathbf{r}_v|} \quad (2.35)$$

The tangent plane passing through the point P can be described by the following equation.

$$(\mathbf{q} - \mathbf{r}) \cdot (\mathbf{r}_u \times \mathbf{r}_v) = 0 \quad (2.36)$$

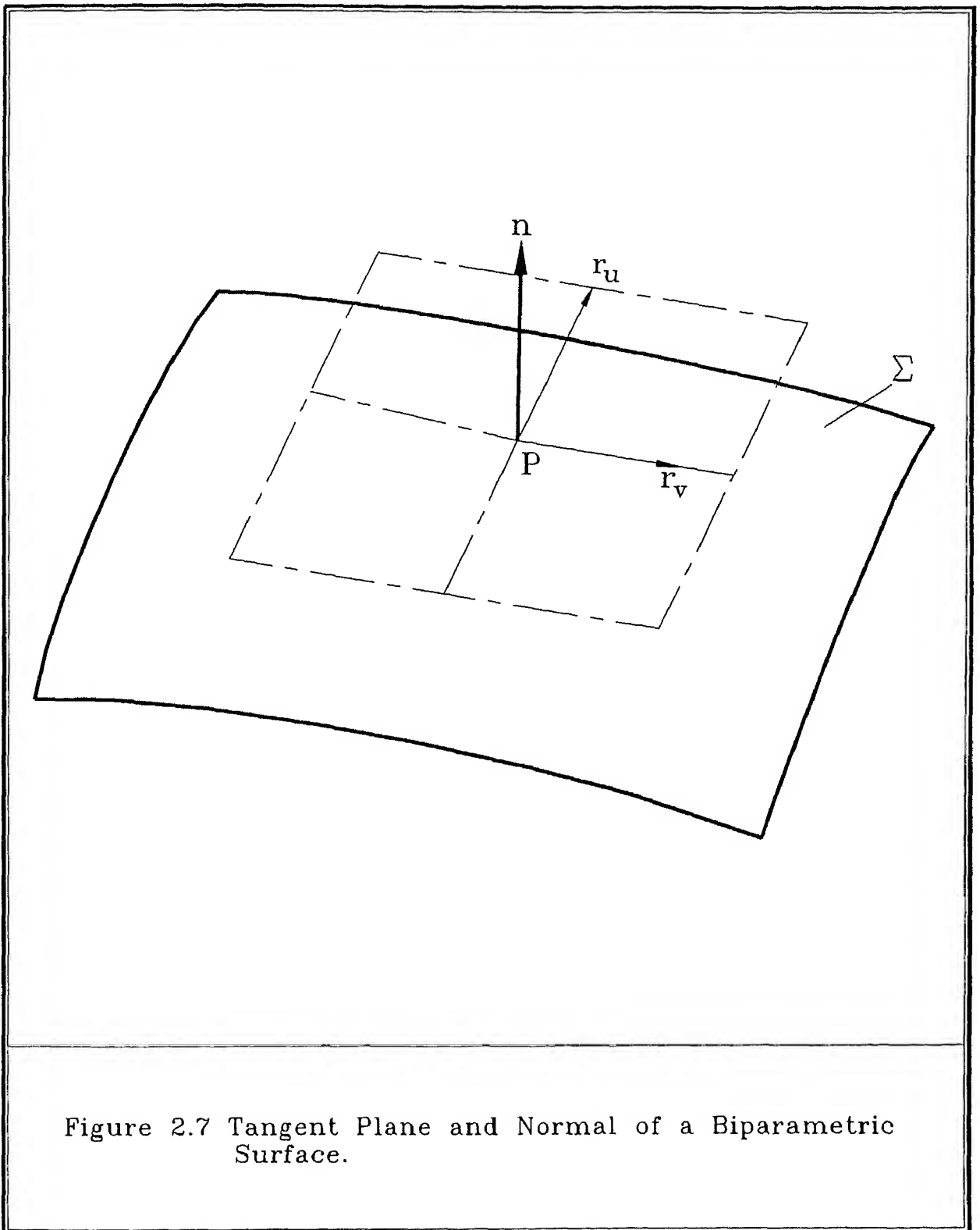
where  $\mathbf{q}$  is the radius vector of a generic point lying on the tangent plane.

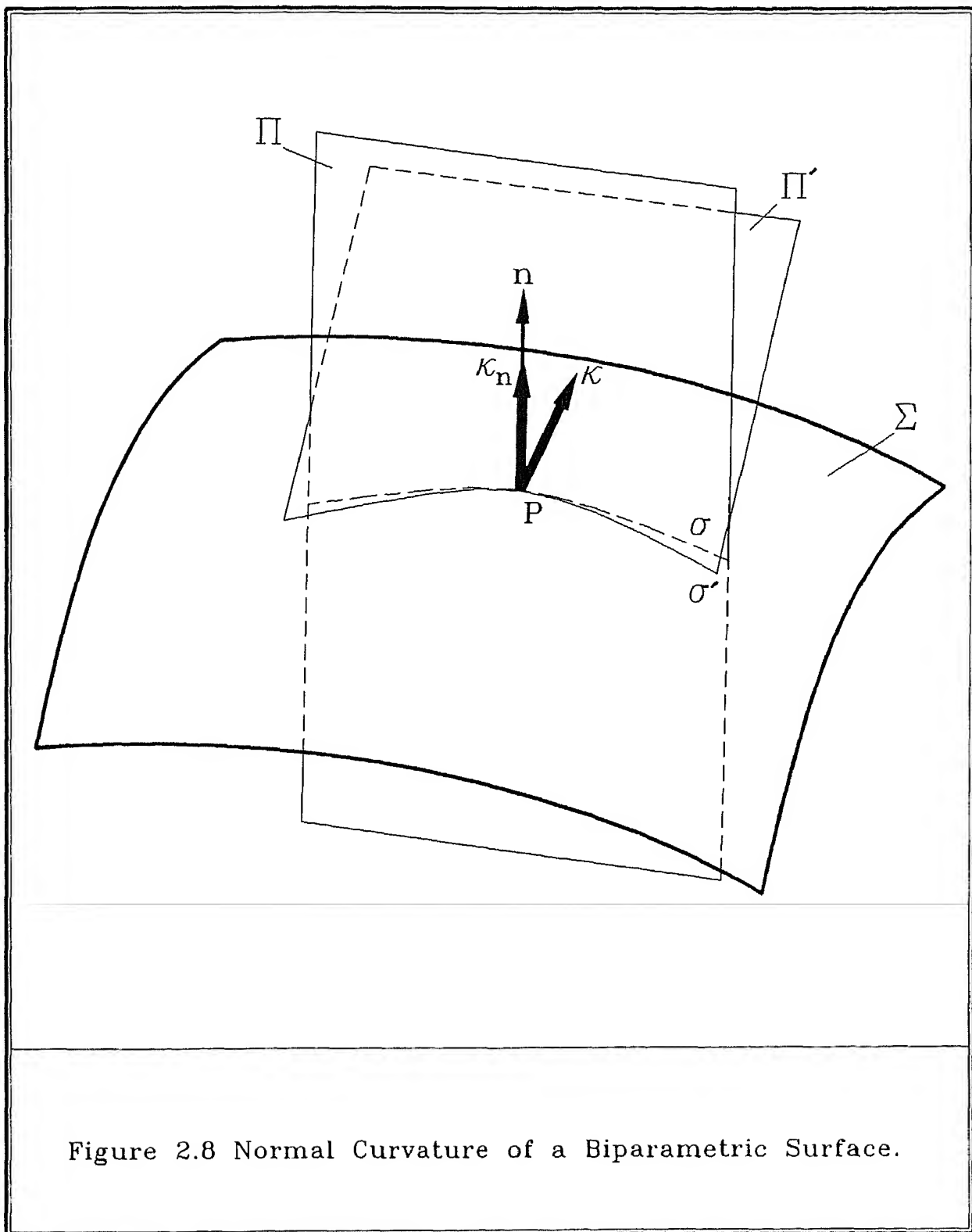
In order to define the curvature of a surface, it is necessary to define a specific curve lying on the surface and passing through the given point P. Consider a plane  $\Pi$  perpendicular to the tangent plane and passing through the normal  $\mathbf{n}$ . The curve of intersection between the surface  $\Sigma$  and the plane  $\Pi$  is denoted as  $\sigma$  as shown in Figure 2.8. The curvature of the curve  $\sigma$  at point P is defined as the normal curvature  $\kappa_n$  of the surface  $\Sigma$  at point P.

If there is a curve  $C'$  obtained as the curve of intersection of an inclined plane  $\Pi'$ , then the curvature of the curve  $\sigma'$  which is a curve of intersection between  $\Pi'$  and  $\Sigma$  is denoted by  $\kappa$ . The curvature  $\kappa_n$  and  $\kappa$  are related by the following equation.

$$\kappa_n = (\kappa \cdot \mathbf{n})\mathbf{n} \quad (2.37)$$

Now consider the effect of the variation of the curvature  $\kappa_n$  as the orientation of the normal plane changes. Let  $\alpha$  denote a reference angle in the tangent plane for describing the orientation of the plane  $\Pi$ . As  $\alpha$  varies from 0 to  $2\pi$ , the curvature  $\kappa_n$  changes its





magnitude. The direction of the curvature vector  $\kappa_n$  is along  $\mathbf{n}$  for all values of  $\alpha$ . It has been shown in the literature that within the range of 0 to  $2\pi$  the curvature  $\kappa_n$  has a maximum and minimum value at values of  $\alpha$ , say  $\alpha^*$  and  $\alpha^* + \frac{\pi}{2}$  ([49]). The extremum values of curvature are termed as the principal curvatures and the principal curvatures are denoted by  $\kappa_I$  and  $\kappa_{II}$ . It can also be mentioned that the curvature of a surface is a tensor and analogous to a quantity such as the stress at a point. In short, the properties such as the unit normal vector  $\mathbf{n}$ , the principal curvatures  $\kappa_I$ ,  $\kappa_{II}$  and the angle  $\alpha^*$  uniquely characterize the intrinsic geometry of the surface  $\Sigma$  at point P.

The intrinsic properties can also be described by means of coefficients E, F, G, and L, M, N where :

$$\begin{aligned} E &= \mathbf{r}_u \cdot \mathbf{r}_u \\ F &= \mathbf{r}_u \cdot \mathbf{r}_v \\ G &= \mathbf{r}_v \cdot \mathbf{r}_v \end{aligned} \quad (2.38)$$

and

$$\begin{aligned} L &= \mathbf{r}_{uu} \cdot \mathbf{n} \\ M &= \mathbf{r}_{uv} \cdot \mathbf{n} \\ N &= \mathbf{r}_{vv} \cdot \mathbf{n} \end{aligned} \quad (2.39)$$

These coefficients are used to express the well known first and second fundamental forms as follows:

$$\begin{aligned} \text{Form I} &= Edu^2 + 2Fdudv + Gdv^2 \\ \text{Form II} &= Ldu^2 + 2Mdudv + Ndv^2 \end{aligned} \quad (2.40)$$

Furthermore, it has been seen that the principal curvatures are the roots of the following equation.

$$(EG - F^2)\kappa^2 - (EN + GL - 2FM)\kappa + (LN - M^2) = 0 \quad (2.41)$$

where E, F, G and L, M, N are the coefficients described in Eqns. (2.38) and (2.39).

The foregoing description about the intrinsic properties of a surface needs to be taken in to account for designing or synthesizing the geometry using the intrinsic properties.

## 2.4 Intrinsic-Cartesian Mapping

Two numerical schemes have been used in the present work and these are described here as a ready reference. These robust numerical schemes are used for the numerical

integration and solving non-linear simultaneous equations (2.31), (2.32), and (2.33) in order to carry out intrinsic-cartesian mapping. The numerical schemes are as follows.

1. A Numerical Integration Scheme based on Simpson's  $\frac{1}{3}$  Rule.
2. A Nonlinear Equation Solver based on Newton-Raphson Iterative Scheme.

### Numerical Integration Based On Simpson's Rule

Let  $y = f(x)$ . In order to evaluate  $\int_a^b f(x)dx$ , it is required to follow the procedure described below.

Divide the interval from  $a$  to  $b$  into  $2n$  equal parts each of width  $h$ , and denote the ordinates

$$f(a), f(a+h), f(a+2h), \dots, f\{a+(2n-1)h\}, f(b)$$

as

$$y_0, y_1, y_2, \dots, y_{2n-1}, y_{2n}.$$

Then

$$\int_a^b f(x)dx = \frac{1}{3}h[y_0 + y_{2n} + 2(y_2 + y_4 + \dots + y_{2n-2}) + 4(y_1 + y_3 + \dots + y_{2n-1})]. \quad (2.42)$$

Consider, a typical integral term as given in Equation (2.32).

Let

$$I = \int_{s_0}^{s_1} \cos\left[\left(\frac{\kappa_1 - \kappa_0}{s_1 - s_0}\right)\left(\frac{\sigma^2}{2} - s_0\sigma\right) + \kappa_0\sigma + C_1\right]d\sigma$$

This integral can be evaluated using Equation (2.42). The pseudo-code of a procedure required for this purpose is given below. The Same procedure can be used to evaluate other integral terms of Equation (2.32) and (2.33).

---

```
double  int_cos( $\kappa_0, \kappa_1, s_0, s_1, n_1, c$ )
```

```
double   $\kappa_0, \kappa_1, s_0, s_1;$ 
```

```
int      $n_1;$ 
```

```
double   $*c;$ 
```

```
{
double  a, b, sum, temp, h1;
int     i;
```

```
a = s0;
```

```
b = s1;
```

```
h1 =  $\frac{(b-a)}{(2*n_1)}$ ;
```

```
sum = 0;
```

```
sum = sum  +  cos(((κ1 - κ0)/(s1 - s0)) * ((a * a/2) - s0 * a)
           +  κ0 * a + *(c + 1))
           +  cos(((κ1 - κ0)/(s1 - s0)) * ((b * b/2) - s0 * b)
           +  κ0 * b + *(c + 1));
```

```
for(i = 1; i <= (2 * n1 - 1); i+ = 2)
{
temp = a + i * h1;
```

```
sum = sum  +  4 * (cos(((κ1 - κ0)/(s1 - s0)) * ((temp * temp/2) - s0 * temp)
               +  κ0 * temp + *(c + 1)));
```

```
}
for(i = 2; i <= (2 * n1 - 2); i+ = 2)
{
temp = a + i * h1;
```

```
sum = sum  +  2 * (cos(((κ1 - κ0)/(s1 - s0)) * ((temp * temp/2) - s0 * temp)
               +  κ0 * temp + *(c + 1)));
```

```
}
sum = sum*(h1/3);
```

```

return (sum);
}

```

---

### Nonlinear Equation Solver Based On Newton-Raphson Iterative Scheme

It is frequently required to determine the value of  $x$  at which a function  $f(x)$  is zero. This value is called as the root of the function  $f$ . A commonly used method for determining the root is the Newton-Raphson scheme. It estimates the new value of the root by using the local tangent direction of the function evaluated at the assumed value of the root. Improvement in the estimates is carried out iteratively. This is shown in Figure 2.9.

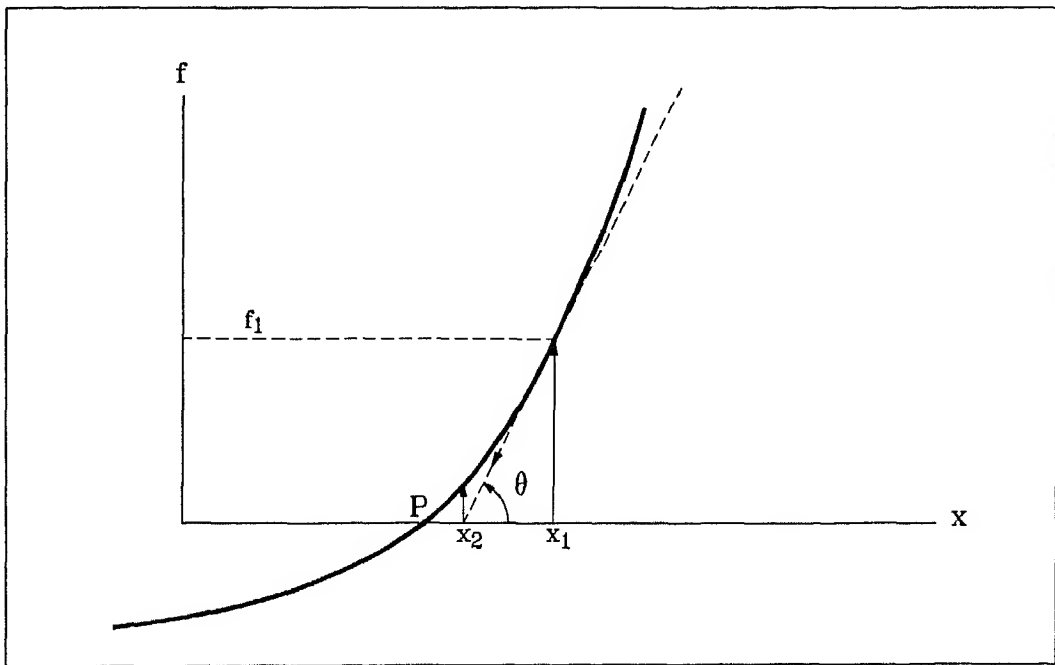


Figure 2.9 Newton-Raphson Iterative Scheme.

Let  $P$  be the point at which  $f$  is zero; let  $x_1$  be the initial guess for the root,  $f_1 = f(x_1)$

and  $f'_1 = \frac{df}{dx}$  at  $x = x_1$ . The improved value of the root ( $x_2$ ) is obtained from the formula,

$$\tan \theta = f'_1 = \frac{f_1}{(x_1 - x_2)}$$

Hence,

$$x_2 = x_1 - \left( \frac{f_1}{f'_1} \right). \quad (2.43)$$

Iterations continue till  $f$  calculated at  $x$ , is reasonably small. The procedure converges only if the initial guess for  $x$  at  $P$  satisfies the condition,  $f'_1 \neq 0$ . The above procedure converges rapidly as the root is approached.

If  $f(x)$  is known as an algebraic expression,  $f'(x)$  can be determined in closed form. If this expression is not available or is too complex being differentiated, the derivative is calculated as,

$$f'(x) = \frac{(f(x+\delta) - f(x))}{\delta}$$

where

$$\delta \simeq \frac{x}{1000}, \text{ a small value}$$

The roots of a pair of simultaneous equations,

$$\begin{aligned} f(x, y) &= 0 \\ g(x, y) &= 0 \end{aligned} \quad (2.44)$$

is determined as follows. Moving along the tangent direction in the one variable problem is equivalent to moving along a tangent plane (or surface) in a many variable problem. On this plane the tangent is represented by the total differential of the function. Using the rules of partial differentials we get,

$$\begin{aligned} df &\approx \Delta f = f_x \Delta x + f_y \Delta y \\ dg &\approx \Delta g = g_x \Delta x + g_y \Delta y \end{aligned} \quad (2.45)$$

where

$$f_x = \frac{\partial f}{\partial x}, f_y = \frac{\partial f}{\partial y} \text{ etc.}$$

If  $x$  and  $y$  are the present estimates of the roots, we need to find the corrections  $\Delta x$  and  $\Delta y$  such that  $x + \Delta x, y + \Delta y$  make  $f$  and  $g$  as zero. This gives  $\Delta f = f(x + \Delta x, y +$

$\Delta y) - f(x, y) = -f(x, y)$  and  $\Delta g = g(x + \Delta x, y + \Delta y) - g(x, y) = -g(x, y)$ . The two equations given above can be solved for  $\Delta x$  and  $\Delta y$  to yield,

$$\begin{aligned}\Delta x &= \frac{(fg_y - gf_y)}{\det} \\ \Delta y &= \frac{(gf_x - fg_x)}{\det}\end{aligned}\quad (2.46)$$

where

$$\det = (g_x f_y - f_x g_y).$$

Corrections  $\Delta x$  and  $\Delta y$  must be repeatedly applied to  $x$  and  $y$  till convergence is attained. This requires the magnitudes of  $x$  and  $y$  to become small or the values of  $f$  and  $g$  to be close to zero.

The above procedure can be generalized to  $n$ -simultaneous equations  $f_1 = f_2 = \dots = f_n = 0$ . The corrections to the roots  $x_1, x_2, \dots, x_n$  are calculated by inverting the matrix equation.

$$A \cdot [\Delta x_i] = -(f_1, f_2, \dots, f_n)^T$$

The  $A$  matrix is given as  $A = [f_{ij}]$ ,  $i, j = 1, 2, \dots, n$  where  $f_{ij} = \frac{\partial f_i}{\partial x_j}$ . Matrix inversion can be carried out using Gaussian Elimination method. As before, iterations continue till  $\Delta x_i$  is small and/or  $f_i$ 's are close to zero.

It is very important to note that, lot of care must be taken while selecting the design variables during Intrinsic-Cartesian mapping. It is due to the fact that the Eqn. (2.32) and (2.33) are too nonlinear in terms of  $s_i$ 's compared to  $\kappa_i$ 's. It has been tested through various non-linear equation solvers and Generalized Leibnitz rule ([35]) for partial derivatives of Eqns. (2.31), (2.32), and (2.33) and concluded that, out of three dependent design variables which would be obtained by solving above three equations simultaneously, the arc length variables ( $s_i$ 's) can not be more than one. In short, for example in a 2-LINCEs model select  $\kappa_1$ ,  $\kappa_2$ , and  $s_2$  as dependent design variables and hence  $\kappa_0$ ,  $s_1$  would be free shape design variables and  $s_0 = 0$  is always assumed. Instead, if  $\kappa_1$ ,  $s_1$ , and  $s_2$  are chosen as dependent design variables, then it is impossible to solve equations (2.32), (2.33), and (2.31) simultaneously and the numerical process will never converge at all.

In order to solve three non-linear Equations (2.31), (2.32) and (2.33), the Newton-Raphson method applied to 2-LINCEs model intrinsic-cartesian mapping can be seen as a detailed procedure described below.

Consider a 2-LINCEs model with the following shape design variables (SDVs),  $\kappa_0$ ,  $s_0$ ,  $\kappa_1$ ,  $s_1$ ,  $\kappa_2$ , and  $s_2$ . Out of these  $(2n + 2)$  SDVs, it has been assumed that  $s_0 = 0$ , and

$\kappa_0$  and  $s_1$  are selected as free SDVs, hence  $\kappa_1$ ,  $\kappa_2$ , and  $s_2$  would be dependent design variables. Then by applying the Newton-Raphson numerical scheme as explained above, we get the following.

Let

$$f = f(\kappa_1, s_2, \kappa_2) \text{ represent Eqn. (2.32)} \quad (2.47)$$

$$g = g(\kappa_1, s_2, \kappa_2) \text{ represent Eqn. (2.33)} \quad (2.48)$$

$$\text{and } w = w(\kappa_1, s_2, \kappa_2) \text{ represent Eqn. (2.31).} \quad (2.49)$$

Therefore,

$$f_{\kappa_1} \Delta \kappa_1 + f_{s_2} \Delta s_2 + f_{\kappa_2} \Delta \kappa_2 = 0 \quad (2.50)$$

$$g_{\kappa_1} \Delta \kappa_1 + g_{s_2} \Delta s_2 + g_{\kappa_2} \Delta \kappa_2 = 0 \quad (2.51)$$

$$w_{\kappa_1} \Delta \kappa_1 + w_{s_2} \Delta s_2 + w_{\kappa_2} \Delta \kappa_2 = 0 \quad (2.52)$$

where

$$\begin{aligned} f_{\kappa_1} &= \frac{\partial f}{\partial \kappa_1}, f_{s_2} = \frac{\partial f}{\partial s_2}, f_{\kappa_2} = \frac{\partial f}{\partial \kappa_2} \\ g_{\kappa_1} &= \frac{\partial g}{\partial \kappa_1}, g_{s_2} = \frac{\partial g}{\partial s_2}, g_{\kappa_2} = \frac{\partial g}{\partial \kappa_2} \\ w_{\kappa_1} &= \frac{\partial w}{\partial \kappa_1}, w_{s_2} = \frac{\partial w}{\partial s_2}, w_{\kappa_2} = \frac{\partial w}{\partial \kappa_2} \end{aligned}$$

For a 2-LINCEs model Eqns. (2.47) through (2.49) can be written as

$$\begin{aligned} f = x_2 - x_0 &= \int_{s_0}^{s_1} \cos\left[\left(\frac{\kappa_1 - \kappa_0}{s_1 - s_0}\right)\left(\frac{\sigma^2}{2} - s_0\sigma\right) + \kappa_0\sigma + C_1\right] d\sigma \\ &- \int_{s_1}^{s_2} \cos\left[\left(\frac{\kappa_2 - \kappa_1}{s_2 - s_1}\right)\left(\frac{\sigma^2}{2} - s_1\sigma\right) + \kappa_1\sigma + C_2\right] d\sigma = 0 \end{aligned} \quad (2.53)$$

$$\begin{aligned} g = y_2 - y_0 &= \int_{s_0}^{s_1} \sin\left[\left(\frac{\kappa_1 - \kappa_0}{s_1 - s_0}\right)\left(\frac{\sigma^2}{2} - s_0\sigma\right) + \kappa_0\sigma + C_1\right] d\sigma \\ &- \int_{s_1}^{s_2} \sin\left[\left(\frac{\kappa_2 - \kappa_1}{s_2 - s_1}\right)\left(\frac{\sigma^2}{2} - s_1\sigma\right) + \kappa_1\sigma + C_2\right] d\sigma = 0 \end{aligned} \quad (2.54)$$

$$w = \psi_2 - \psi_0 - \left(\frac{\kappa_0 + \kappa_1}{2}\right)(s_1 - s_0) - \left(\frac{\kappa_1 + \kappa_2}{2}\right)(s_2 - s_1) = 0 \quad (2.55)$$

The Eqns. (2.50) through (2.52) can be represented in matrix form as follows :

$$\begin{bmatrix} f_{\kappa_1} & f_{s_2} & f_{\kappa_2} \\ g_{\kappa_1} & g_{s_2} & g_{\kappa_2} \\ w_{\kappa_1} & w_{s_2} & w_{\kappa_2} \end{bmatrix} \begin{bmatrix} \Delta \kappa_1 \\ \Delta s_2 \\ \Delta \kappa_2 \end{bmatrix} = \begin{bmatrix} -f(\kappa_1, s_2, \kappa_2) \\ -g(\kappa_1, s_2, \kappa_2) \\ -w(\kappa_1, s_2, \kappa_2) \end{bmatrix} \quad (2.56)$$

$$\Delta\kappa_1 = (-A_1f - A_2g - A_3w)/\det A$$

$$\Delta s_2 = (-B_1f - B_2g - B_3w)/\det A$$

$$\Delta\kappa_2 = (-C_1f - C_2g - C_3w)/\det A$$

where

$$\begin{aligned} A_1 &= g_{s_2}w_{\kappa_2} - g_{\kappa_2}w_{s_2} \\ B_1 &= g_{\kappa_2}w_{\kappa_1} - g_{\kappa_1}w_{\kappa_2} \\ C_1 &= g_{\kappa_1}w_{s_2} - g_{s_2}w_{\kappa_1} \\ A_2 &= -f_{s_2}w_{\kappa_2} + f_{\kappa_2}w_{s_2} \\ B_2 &= -f_{\kappa_2}w_{\kappa_1} + f_{\kappa_1}w_{\kappa_2} \\ C_2 &= -f_{\kappa_1}w_{s_2} + f_{s_2}w_{\kappa_1} \\ A_3 &= f_{s_2}g_{\kappa_2} - f_{\kappa_2}g_{s_2} \\ B_3 &= f_{\kappa_2}g_{\kappa_1} - f_{\kappa_1}g_{\kappa_2} \\ C_3 &= f_{\kappa_1}g_{s_2} - f_{s_2}g_{\kappa_1} \end{aligned}$$

$$\det A = f_{\kappa_1}A_1 + f_{s_2}B_1 + f_{\kappa_2}C_1$$

The new values of design variable  $\kappa_i$ 's and/or  $s_i$ 's would be updated as follows.

$$\begin{aligned} \kappa_1 &\Leftarrow \kappa_1 + \Delta\kappa_1 \\ s_2 &\Leftarrow s_2 + \Delta s_2 \\ \kappa_2 &\Leftarrow \kappa_2 + \Delta\kappa_2. \end{aligned}$$

The iterative process is repeated till the convergence is obtained and/or function values are close to zero.

### Algorithm

Since the proposed methodology is a CAD approach to shape optimization, the shape synthesis and hence optimization module must be accompanied by an interactive graphics environment. This is an important issue since the intrinsic profile doesn't give the real feel of the geometry to the designer. In order to eliminate this handicap of the intrinsic geometry, the first step is a creation of multi-window interactive graphics environment that will include one window for the cartesian space, one window for the intrinsic space, the third one to have menu section buttons, and the fourth one to show the necessary written information or feed back within the graphics environment. To create this nature of graphics environment, computer program written in C has been developed based on SUN-view graphics on SUN-workstation with UNIX-platform. The next step in shape synthesis is to select the feasible shape model such as, 2-LINCEs,

3-LINCEs model etc. based on the geometry of the problem. Once, the shape model has been decided, the design variables can be specified as the input. A computer program has been developed in C using Simpson's  $\frac{1}{3}$  rule, Newton-Raphson non-linear equation solver as described above in order to solve Eqns. (2.31), (2.32), and (2.33) simultaneously and ensuring free and dependent design variables are selected properly. Thus, once all the shape design variables are established for a particular LINCE model, the next step will be to map from intrinsic to cartesian space. Thus, the intrinsic geometry based shape synthesis would be accomplished. This shape synthesis module would be used as a subroutine in any CAD based shape optimization cycle. The input being specified to this shape synthesis module in addition to the intrinsic variables  $\kappa_i$ 's and/or  $s_i$ 's would be, the initial and final co-ordinates (i.e.  $(x_0, y_0)$  and  $(x_n, y_n)$ ) of a curve and the initial and final tangent angles (i.e.  $\psi_0$  and  $\psi_n$ ) of the corresponding points. The final step of this intrinsic-cartesian mapping would be the displaying of the cartesian and intrinsic profiles of a particular component or structure. The effect of change in intrinsic design variables can be seen in cartesian space immediately through the multi-window graphics environment. The data files that are created for the display purpose have been developed as script files, so that they can be compatible with any graphics or plotting aids such as AutoCAD etc.

## 2.5 Illustrative Examples

When shape synthesis is carried out using intrinsic geometry, the designer has to select (i) appropriate end conditions, (ii) a suitable shape model, and (iii) an appropriate set of free and dependent shape design variables. This has been illustrated by means of 1-LINCE, 2-LINCEs, and 3-LINCEs model examples.

In Example 2.1, it is required to define a curve passing through points (0,0) and (12,10). The tangent angle at the first point ( $\psi_0$ ) is zero. The tangent angle at the end point ( $\psi_n$ ) is taken to be 120 degrees. In this case, 1-LINCE model (R-model) is selected as the shape model. The variation in intrinsic variables can be seen as dotted curves in both intrinsic and cartesian space. The result has been shown in Figure 2.10.

The selection of different free parameters can be illustrated with an example 2.2. A 2-LINCEs model (R-R model) is selected as the shape model in this example. The shape design variables for this model are  $\kappa_0$ ,  $\kappa_1$ ,  $\kappa_2$ ,  $s_1$  and  $s_2$ . The solid curve is designed by choosing  $\kappa_0$  and  $s_1$  as free SDVs and  $\kappa_1, s_2$ , and  $\kappa_2$  as dependent SDVs. The values chosen for  $\kappa_0$  and  $s_1$  are 0.6 and 12 respectively. The co-ordinates of end points are given as (0,0) and (12,10) and the tangent angles  $\psi_0 = 0$ ;  $\psi_2 = -70$  degrees. The Figure 2.11 shows the result of this curve design.

Example 2.3 is shown in Figure 2.12. The curvature model is selected being a 3-

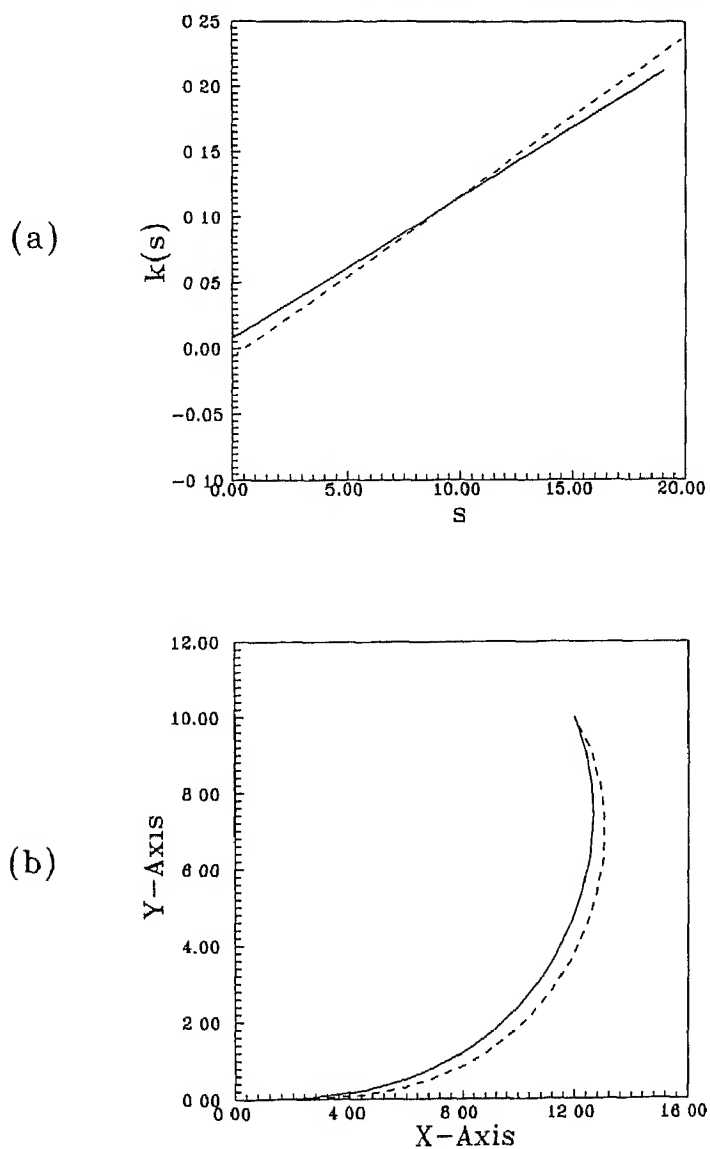


Figure 2.10 Graphical Output of  $\kappa$ - $s$  and  $x$ - $y$  Curves of Example 2.1.

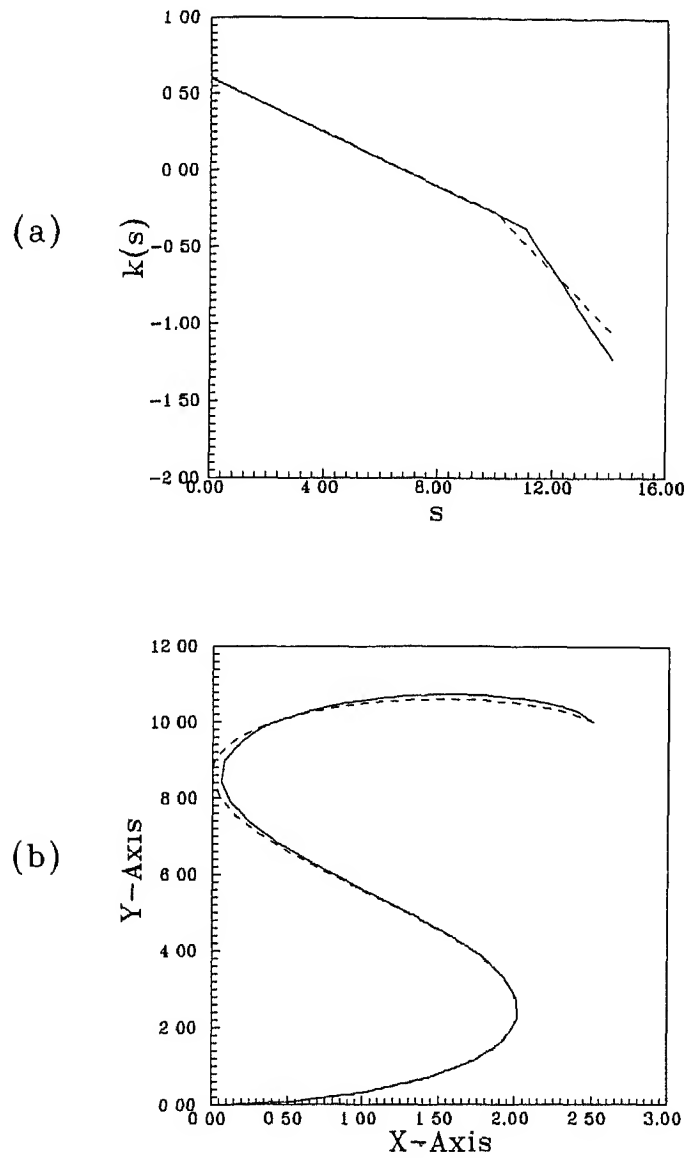


Figure 2.11 Graphical Output of Example 2.2.

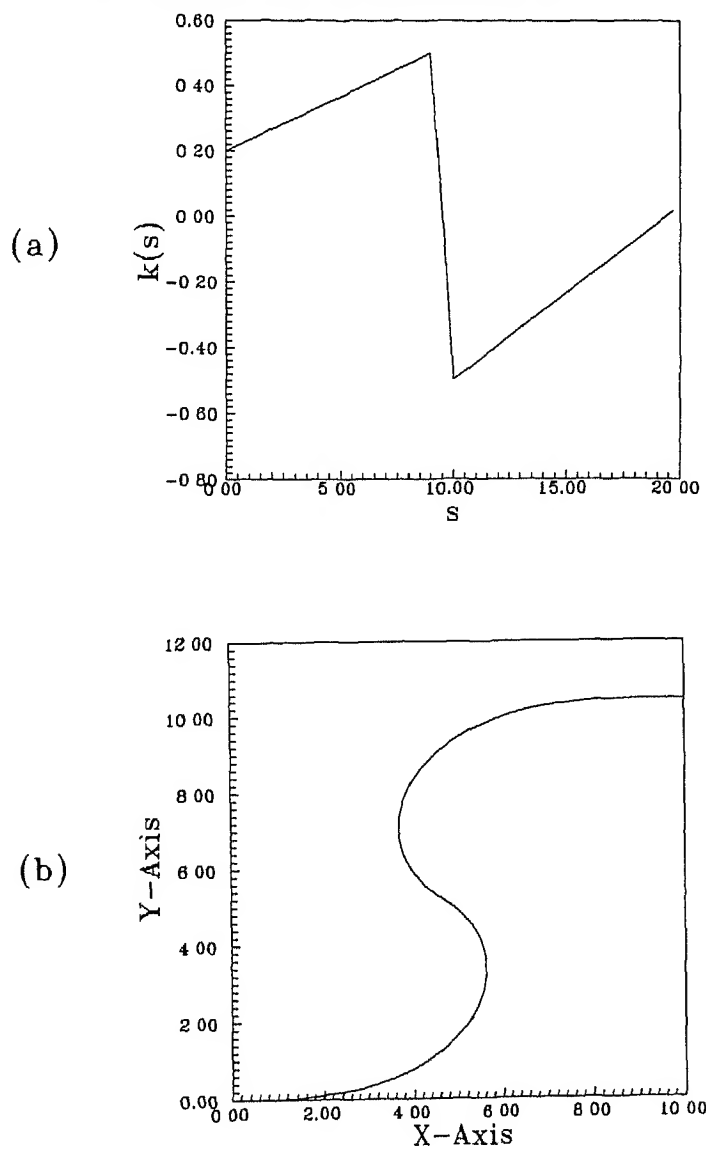


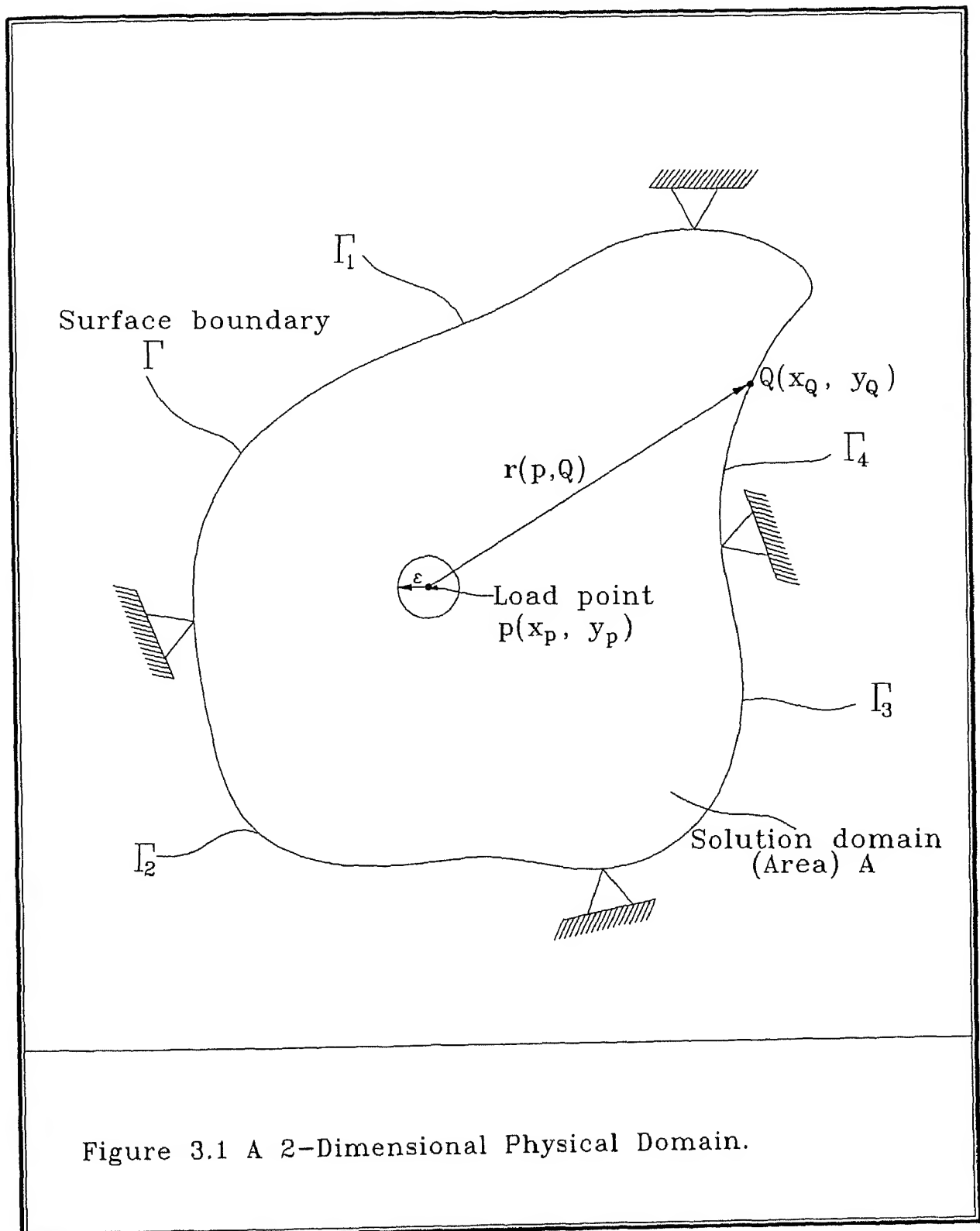
Figure 2.12 Graphical Output of Example 2.3.

LINCEs model (R-R-R model). The initial co-ordinates are at (0,0) with zero degree tangent angle ( $\psi_0 = 0$ ) and the final co-ordinates are (12,10) corresponding to the final tangent angle of zero degree. In this curve design problem, the SDVs include  $\kappa_0$ ,  $\kappa_1$ ,  $s_1$ ,  $\kappa_2$ ,  $s_2$ ,  $\kappa_3$  and  $s_3$ . Out of these SDVs,  $\kappa_2$ ,  $\kappa_3$  and  $s_3$  are chosen as dependent design variables and hence  $\kappa_0$ ,  $\kappa_1$  and  $s_1$  becomes free SDVs.

## 2.6 Some Observations

It should be noted that when a single ramp function (1-LINCE model) is selected as a shape model, no free shape design variables exists. In such a case, Equations (2.31) through (2.33) result in one unique answer. It has been found out that out of three dependent design variables, which are usually obtained by solving Serret-Frenet Equations (2.31) through (2.33) simultaneously, the number of arc length variables (i.e.  $s_i$ 's) can not be more than one. For example, in a 2-LINCEs model the selection of  $\kappa_1$ ,  $\kappa_2$  and  $s_2$  as dependent design variables would work perfectly. Instead,  $\kappa_2$ ,  $s_1$  and  $s_2$  or  $\kappa_1$ ,  $s_1$ ,  $s_2$  or  $\kappa_0$ ,  $s_1$  and  $s_2$  combination of dependent design variables would not be able to give converged solution by using any non-linear equation solver. It is owing to the fact that the Equations (2.32) and (2.33) are too non-linear in terms of  $s_i$ 's compared to  $\kappa_i$ 's. The situation will be similar in case of 3-LINCEs or n-LINCEs model.

The numerical schemes which have been selected for this shape synthesis are found to be more robust and stable. This eliminates the selection of specific input for shape synthesis as well as the intervention of the designer during the design process. Any mechanical and structural engineering shape optimization problem requires a shape synthesis module. Traditionally, this has been accomplished by using parametric spline functions. The co-ordinates of the control polygon vertices of the spline functions constitute the shape design variables. Such an approach invariably leads to a large number of design variables. In contrast, the intrinsic shape definition clearly indicates that the number of shape design variables is definitely less than the number of shape design variables in the parametric approach. This intrinsic geometry based shape synthesis module is an asset to the shape optimization cycle and will become an effective computer aided geometric modeling tool.



Since, there are  $2N$  unknowns, it need  $2N$  equations to solve the problem. Looking at it in a more general way, it requires  $N$  sets of equations where each set contains two equations. For example; a force (or traction) placed at node 1. Using the fundamental solution, it is possible to calculate displacements and tractions at every node from 1 to  $N$ . This yields a first set of linear equations (i.e. rows 1 and 2 of the matrix). To produce a second set of linear equations (i.e. rows 3 and 4 of the matrix), place the force at node2 and repeat the use of the fundamental solution to calculate the variables at the other nodes. This operation is repeated until the force is placed at the last node  $N$ , which will give the final set of equations (i.e. rows  $2N - 1$  and  $2N$  of the matrix). Therefore, we will end up with  $2N$  equations and  $2N$  unknowns which produces a unique solution.

The data required to fully define a given problem must include the following:

- (a) Data such as the number of Gaussian points, two-dimensional (plane-stress or plane-strain or axi-symmetric) geometry and material properties.
- (b) Mesh data such as the co-ordinates (in cartesian space) of the nodal points and the nodes on each element.
- (c) Boundary conditions such as prescribed displacements and/or stresses.
- (d) Co-ordinates of any internal points.

The description of the above mentioned data is shown below:

## ANALYSIS DATA

Geometry: This defines the type of geometry : either

- 1 (Axisymmetric)
- 2 (2-D plane stress) or
- 3 (2-D plane strain)

Gaussian: This defines the number of Gaussian integration points used for numerical integration. Either four or six Gaussian points are allowed. The use of four Gaussian points is sufficient for good accuracy. However, for thin structures better accuracy is obtained with a larger number of Gaussian points.

E : Young's modulus

$\nu$  : Poisson's ratio

NODAL CO-ORDINATES (Figure 3.2)

Node : Node number  
x : x - co-ordinate  
y : y - co-ordinate

#### ELEMENT DETAILS

Element : Element number  
Node 1 : First node of the element  
Node 2 : Second node of the element  
Node 3 : Third node of the element

#### DISPLACEMENT BOUNDARY CONDITIONS

Element : Element number  
Direction : The direction of the prescribed displacement : either  
1 (x - direction) or  
2 (y - direction)  
Disp 1 : Displacement of the first node of this element  
Disp 2 : Displacement of the second node of this element  
Disp 3 : Displacement of the third node of this element

#### STRESS BOUNDARY CONDITIONS

(  $\sigma_{xx}$ ,  $\sigma_{yy}$ ,  $\sigma_{xy}$  ) 1 : Prescribed stress on the first node of this element  
(  $\sigma_{xx}$ ,  $\sigma_{yy}$ ,  $\sigma_{xy}$  ) 2 : Prescribed stress on the second node of this element  
(  $\sigma_{xx}$ ,  $\sigma_{yy}$ ,  $\sigma_{xy}$  ) 3 : Prescribed stress on the third node of this element

(Note: Tensile stress is considered positive, while compressive stress such as pressure is considered negative. If a normal pressure, P, is prescribed on a curved surface, simply input  $\sigma_{xx} = \sigma_{yy} = -P$  and  $\sigma_{xy} = 0$ .)

#### INTERNAL POINTS

Point : Internal point number  
 $x_{int}$  : x - co-ordinate of the internal point  
 $y_{int}$  : y - co-ordinate of the internal point

### 3.2 BEM Analysis

Betti's reciprocal work theorem and the Somigliana's identity ([4]) for the displacements can be used to derive an integral equation for the displacements at a interior point  $p$  due to tractions and displacements on the surface at a boundary point  $Q$  (as discussed in Section 3.1). In the absence of body forces, the Boundary Integral Equation (BIE) can be written as follows:

$$\begin{aligned} \begin{bmatrix} u_x(p) \\ u_y(p) \end{bmatrix} + \int_{\Gamma} \begin{bmatrix} T_{xx}(p, Q) & T_{xy}(p, Q) \\ T_{yx}(p, Q) & T_{yy}(p, Q) \end{bmatrix} \begin{bmatrix} u_x(Q) \\ u_y(Q) \end{bmatrix} d\Gamma(Q) \\ = \int_{\Gamma} \begin{bmatrix} U_{xx}(p, Q) & U_{xy}(p, Q) \\ U_{yx}(p, Q) & U_{yy}(p, Q) \end{bmatrix} \begin{bmatrix} t_x(Q) \\ t_y(Q) \end{bmatrix} d\Gamma(Q) \end{aligned} \quad (3.1)$$

Using tensor notation, the above two BIE equations can be expressed as follows:

$$u_i(p) + \int_{\Gamma} T_{ij}(p, Q) u_j(Q) d\Gamma(Q) = \int_{\Gamma} U_{ij}(p, Q) t_j(Q) d\Gamma(Q) \quad (3.2)$$

Before attempting the numerical implementation of BIE, it is necessary to examine its physical significance. The fundamental solution (represented by the kernels  $U_{ij}$  and  $T_{ij}$ ) simply works out the "influence" of a concentrated point force at a given point  $p$  on any other point  $Q$  (except when  $p$  coincides with  $Q$  then it becomes singular). This fundamental solution is valid for any elastostatic problem regardless of its geometry. The BIE of Eqn. (3.1) effectively relates two distinct problems: the first is the fundamental solution of a point force (the kernels  $U_{ij}$  and  $T_{ij}$ ) and the second is the problem of solving the unknown variables  $u_i$  and  $t_j$ .

#### Numerical Implementation

In order to solve the BIE numerically, the steps required are as follows:

##### STEP 1 : Division of the Boundary into Elements

The boundary of the solution domain must be divided into a number of connected elements. Over each element, the variation of the geometry and the variables (displacements and tractions) must be described. These variations can be constant, linear, quadratic, cubic or higher order. Furthermore, it is possible to allow the geometry variation to be different from the variation of the variables (for example a linear geometry description but with a quadratic variation of displacement). The literature review on BEM and FEM shows that, in most stress analysis applications, isoparametric quadratic elements provide the best compromise between accuracy and efficiency. Isoparametric

elements are elements that use the same order of variation for both the geometry and unknown variables. The elements which are used in the stress analysis of this research are of isoparametric quadratic elements, but the change in the order of variation can be made by prescribing a new 'shape function'.

Shape functions are the most convenient way of describing the behaviour of any element because they use number of points on each element ( called 'nodes' or 'nodal points' ) where the variable value is given. Therefore, for a quadratic element, it requires three nodes on each element: one at the mid point and one at either end. It can be defined a new co-ordinate system that is local to the element using a variable,  $\xi$ , with its origin at the mid point of the element and values of -1 to +1 at the end node (Figure 3.2).

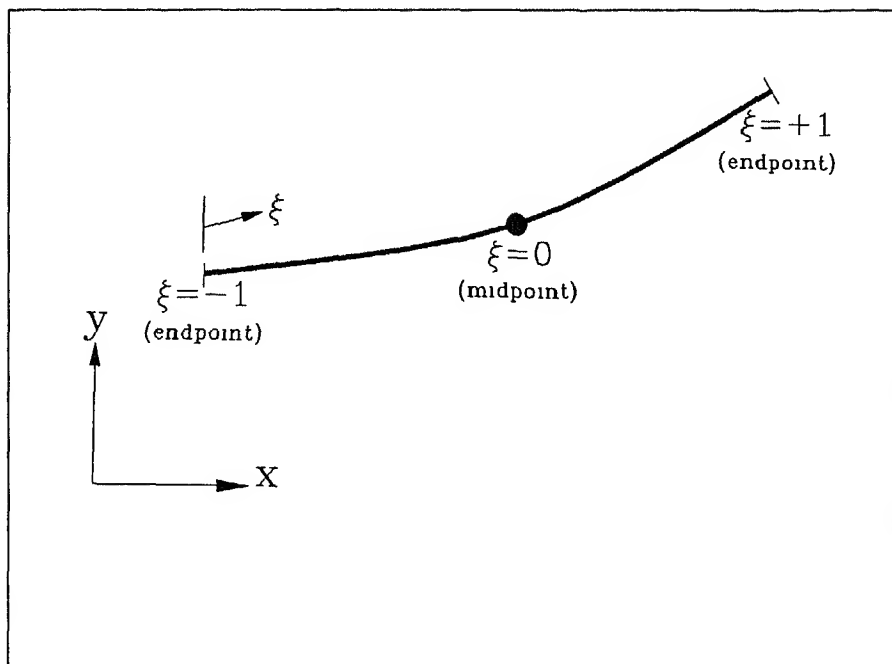


Figure 3.2 An Isoparametric Quadratic Element.

Therefore, the geometry of an element can be described by the co-ordinates of its three nodes and the shape function as follows:

$$\begin{aligned}
x(\xi) &= \sum_{c=1}^3 N_c(\xi) x_c = N_1(\xi) x_1 + N_2(\xi) x_2 + N_3(\xi) x_3 \\
y(\xi) &= \sum_{c=1}^3 N_c(\xi) y_c = N_1(\xi) y_1 + N_2(\xi) y_2 + N_3(\xi) y_3
\end{aligned} \tag{3.3}$$

where the shape functions  $N_c(\xi)$  are quadratic functions that must satisfy two conditions:

1.  $N_c(\xi) = 1$  at the node  $c$  and
2.  $N_c(\xi) = 0$  at the other two nodes.

The explicit expressions for the shape functions are as follows:

$$\begin{aligned}
N_1(\xi) &= \frac{-\xi}{2}(1 - \xi) \\
N_2(\xi) &= (1 + \xi)(1 - \xi) \\
N_3(\xi) &= \frac{\xi}{2}(1 + \xi)
\end{aligned} \tag{3.4}$$

Similarly, because the elements are isoparametric, the shape functions are used for the solution variables, as follows:

$$\begin{aligned}
u_x(\xi) &= \sum_{c=1}^3 N_c(\xi) (u_x)_c \\
&= N_1(\xi) (u_x)_1 + N_2(\xi) (u_x)_2 + N_3(\xi) (u_x)_3 \\
u_y(\xi) &= \sum_{c=1}^3 N_c(\xi) (u_y)_c \\
&= N_1(\xi) (u_y)_1 + N_2(\xi) (u_y)_2 + N_3(\xi) (u_y)_3 \\
t_x(\xi) &= \sum_{c=1}^3 N_c(\xi) (t_x)_c \\
&= N_1(\xi) (t_x)_1 + N_2(\xi) (t_x)_2 + N_3(\xi) (t_x)_3 \\
t_y(\xi) &= \sum_{c=1}^3 N_c(\xi) (t_y)_c \\
&= N_1(\xi) (t_y)_1 + N_2(\xi) (t_y)_2 + N_3(\xi) (t_y)_3
\end{aligned} \tag{3.5}$$

The explicit expressions for the shape functions in terms of  $\xi$  are given in Eqns. (3.4).

### STEP 2 : Numerical Integration of the Kernels

The numerical integration is now performed over each element using the local co-ordinate  $\xi$  rather than the boundary curve parameter  $\Gamma$ .

Because of the transformation of the variable from the boundary curve  $\Gamma$  to the local co-ordinate  $\xi$ , the Jacobian of transformation  $J$  must be calculated as follows:

$$J(\xi) = \frac{d\Gamma}{d\xi} = \sqrt{\left[\frac{dx(\xi)}{d\xi}\right]^2 + \left[\frac{dy(\xi)}{d\xi}\right]^2} \quad (3.6)$$

In order to determine the components of the unit outward normal, the unit tangential vector,  $\mathbf{m}$  can be defined as follows:

$$\text{Unit Vector } \mathbf{m} = \frac{m_x}{|\mathbf{m}|} \mathbf{e}_x + \frac{m_y}{|\mathbf{m}|} \mathbf{e}_y \quad (3.7)$$

where the magnitude of the vector  $\mathbf{m}$  is given by

$$|\mathbf{m}| = \sqrt{(m_x)^2 + (m_y)^2} = \sqrt{\left[\frac{dx(\xi)}{d\xi}\right]^2 + \left[\frac{dy(\xi)}{d\xi}\right]^2} \quad (3.8)$$

and  $\mathbf{e}_x$ ,  $\mathbf{e}_y$  are the unit vectors along the  $x$  and  $y$  axes respectively.

The magnitude of the vector  $\mathbf{m}$  is equal to the Jacobian  $J(\xi)$ , defined in Eqn. (3.6). Therefore, the components of the unit tangential vector can be written as follows:

$$\begin{aligned} m_x &= \frac{1}{J(\xi)} \left[ \frac{dx(\xi)}{d\xi} \right] \\ m_y &= \frac{1}{J(\xi)} \left[ \frac{dy(\xi)}{d\xi} \right] \end{aligned} \quad (3.9)$$

Consider now the unit vector in the  $z$ -direction,  $\mathbf{e}_z$  (normal to the two-dimensional  $xy$  plane). The unit normal vector is, therefore, equal to the vector product (cross product) of the vectors  $\mathbf{m}$  and  $\mathbf{e}_z$  as follows:

$$\mathbf{n} = \mathbf{m} \times \mathbf{e}_z \quad (3.10)$$

where  $\mathbf{e}_z$  is the unit vector along the  $z$ -axis. The component of the unit outward normal (of unit length) are given by

$$\begin{aligned} n_x &= \frac{1}{\mathbf{J}(\xi)} \left[ \frac{dy(\xi)}{d\xi} \right] \\ n_y &= \frac{-1}{\mathbf{J}(\xi)} \left[ \frac{dx(\xi)}{d\xi} \right] \end{aligned} \quad (3.11)$$

The differentials of the co-ordinates  $x(\xi)$  and  $y(\xi)$  with respect to  $\xi$  are given by

$$\begin{aligned} \frac{dx(\xi)}{d\xi} &= \frac{dN_1(\xi)}{d\xi} x_1 + \frac{dN_2(\xi)}{d\xi} x_2 + \frac{dN_3(\xi)}{d\xi} x_3 \\ \frac{dy(\xi)}{d\xi} &= \frac{dN_1(\xi)}{d\xi} y_1 + \frac{dN_2(\xi)}{d\xi} y_2 + \frac{dN_3(\xi)}{d\xi} y_3 \end{aligned} \quad (3.12)$$

where the differentials of the shape functions are given by

$$\begin{aligned} \frac{dN_1(\xi)}{d\xi} &= \xi - \frac{1}{2} \\ \frac{dN_2(\xi)}{d\xi} &= -2\xi \\ \frac{dN_3(\xi)}{d\xi} &= \xi + \frac{1}{2} \end{aligned} \quad (3.13)$$

The BIE of Eqn.(3.1) can now be written as in terms of the local co-ordinate  $\xi$  as follows:

$$\begin{aligned} & \begin{bmatrix} C_{xx}(p) & C_{xy}(p) \\ C_{yx}(p) & C_{yy}(p) \end{bmatrix} \begin{bmatrix} u_x(p) \\ u_y(p) \end{bmatrix} \\ & + \sum_{m=1}^M \sum_{c=1}^3 \left( \int_{-1}^{+1} \begin{bmatrix} T_{xx}(p, Q) & T_{xy}(p, Q) \\ T_{yx}(p, Q) & T_{yy}(p, Q) \end{bmatrix} N_c(\xi) \mathbf{J}(\xi) d\xi \right) \begin{bmatrix} u_x(Q) \\ u_y(Q) \end{bmatrix} \\ & = \sum_{m=1}^M \sum_{c=1}^3 \left( \int_{-1}^{+1} \begin{bmatrix} U_{xx}(p, Q) & U_{xy}(p, Q) \\ U_{yx}(p, Q) & U_{yy}(p, Q) \end{bmatrix} N_c(\xi) \mathbf{J}(\xi) d\xi \right) \begin{bmatrix} t_x(Q) \\ t_y(Q) \end{bmatrix} \end{aligned} \quad (3.14)$$

where  $M$  is the total number of elements. The integrals in the above equations can be placed in new functions  $[A]$  and  $[B]$  as follows:

$$\begin{aligned} & \begin{bmatrix} C_{xx}(p) & C_{xy}(p) \\ C_{yx}(p) & C_{yy}(p) \end{bmatrix} \begin{bmatrix} u_x(p) \\ u_y(p) \end{bmatrix} + \begin{bmatrix} A_{xx} & A_{xy} \\ A_{yx} & A_{yy} \end{bmatrix}_{m,c} \begin{bmatrix} u_x(Q) \\ u_y(Q) \end{bmatrix} \\ & = \begin{bmatrix} B_{xx} & B_{xy} \\ B_{yx} & B_{yy} \end{bmatrix}_{m,c} \begin{bmatrix} t_x(Q) \\ t_y(Q) \end{bmatrix} \end{aligned} \quad (3.15)$$

Taking each node in turn as the load point  $p$  and performing the integrations indicated in the above equation, a set of algebraic equations emerges as follows:

$$[A][u] = [B][t] \quad (3.16)$$

where the matrices  $[A]$  and  $[B]$  contains the integrals of the kernels  $T_{ij}$  and  $U_{ij}$ , respectively. Note that the parameter  $C_{ij}(p)$  contributes only to the diagonal coefficients of the  $[A]$  matrix (when  $p$  is equal to  $Q$ ). The formation of the matrices  $[A]$  and  $[B]$  can be seen as

$$= \begin{bmatrix} [A]_{11} & [A]_{12} & [A]_{13} & [A]_{14} & \dots \\ [A]_{21} & [A]_{22} & [A]_{23} & [A]_{24} & \dots \\ [A]_{31} & [A]_{32} & [A]_{33} & [A]_{34} & \dots \\ [A]_{41} & [A]_{42} & [A]_{43} & [A]_{44} & \dots \\ \dots & \dots & \dots & \dots & \dots \end{bmatrix} \begin{bmatrix} [u]_1 \\ [u]_2 \\ [u]_3 \\ [u]_4 \\ \dots \end{bmatrix} = \begin{bmatrix} [B]_{11} & [B]_{12} & [B]_{13} & [B]_{14} & \dots \\ [B]_{21} & [B]_{22} & [B]_{23} & [B]_{24} & \dots \\ [B]_{31} & [B]_{32} & [B]_{33} & [B]_{34} & \dots \\ [B]_{41} & [B]_{42} & [B]_{43} & [B]_{44} & \dots \\ \dots & \dots & \dots & \dots & \dots \end{bmatrix} \begin{bmatrix} [t]_1 \\ [t]_2 \\ [t]_3 \\ [t]_4 \\ \dots \end{bmatrix} \quad (3.17)$$

where the submatrices of  $[A]$  and  $[B]$  are defined as follows:

$$[A]_{ij} = \begin{bmatrix} A_{xx}A_{xy} \\ A_{yx}A_{yy} \end{bmatrix}; \quad [B]_{ij} = \begin{bmatrix} B_{xx}B_{xy} \\ B_{yx}B_{yy} \end{bmatrix} \quad (3.18)$$

Note that vectors  $[u]$  and  $[t]$  represent displacements and tractions in  $x$  and  $y$  direction as follows:

$$[u]_i = \begin{bmatrix} u_x \\ u_y \end{bmatrix}_i; \quad [t]_i = \begin{bmatrix} t_x \\ t_y \end{bmatrix}_i \quad (3.19)$$

It is to be noted that the fundamental solution is 'singular'. This singularity means that the kernels contains terms of the order  $\frac{1}{\eta}$  and  $\ln(\frac{1}{\eta})$  as  $\eta \rightarrow 0$ . Since the kernels are dependent on the distance between  $p$  and  $Q$ , the three possibilities of the positions of  $p$  and  $Q$  can be examined as follows:

**$p$  and  $Q$  in different elements:** The standard Gaussian quadrature can be easily applied to the  $U_{ij}$  and  $T_{ij}$  kernels because they are not singular in this case:

$$\int_{-1}^{+1} f(\xi) d\xi = \sum_{g=1}^G f(\xi_g) w_g \quad (3.20)$$

where  $G$  is the total number of Gaussian integration points (usually 4) and the Gaussian co-ordinates with an associated weighting function  $w_g$ .

**$p$  and  $Q$  are in the same element but  $p \neq Q$ :** In this case, the  $U_{ij}$  and  $T_{ij}$  kernels are singular but the shape function  $N_c(\xi)$  in the vicinity of  $p$  is of the order  $r(p, Q)$ . Therefore, the product of the kernels and the shape function is not singular and the integrals can be evaluated using the standard Gaussian quadrature.

**$p$  and  $Q$  are in the same element and  $p = Q$ :** In this case, the standard Gaussian quadrature can not be used because of the singularity of the kernels. Dealing with the  $U_{ij}$  kernels first, it is clear that as  $p$  coincides with  $Q$ , the singularity is of the form  $\ln(\frac{1}{\eta})$  as  $\eta \rightarrow 0$ . This form of integral can be calculated by using the special logarithmic Gaussian quadrature and changing the limits of integration to become 0 to 1, as follows:

$$\int_0^1 f(\eta) \ln\left(\frac{1}{\eta}\right) d\eta = \sum_{gl=1}^{G_l} f(\eta_{gl}) w_{gl} \quad (3.21)$$

where  $G_l$  is the total number of logarithmic Gaussian integration points (usually 4) and  $\eta_{gl}$  is the Gaussian co-ordinate with an associated weighting function  $w_{gl}$ . A simple linear transformation can be used to accommodate the 0 to 1 integration limits as follows:

1. If  $p$  is the first node of the element,  $\eta = 0.5(1 + \xi)$ .
2. If  $p$  is the second node of the element, the element is divided in to two sub-elements:  $\eta = -\xi$  (for  $-1 < \xi < 1$ ).
3. If  $p$  is the third node of the element,  $\eta = 0.5(1 - \xi)$ .

### STEP 3: Application of the Boundary Conditions

So far, calculation of all the coefficients of the  $[A]$  and the  $[B]$  matrices have been, discussed, but the problem is not unique until all the boundary conditions are applied. In a typical elastostatic problem, three types of boundary conditions are possible:

1. Prescribed displacement.
2. Prescribed traction (or stress).
3. Linear relationship between traction and displacement.

In a given problem, because there are  $2N$  equations, it require  $2N$  prescribed values. In other words, each node must have two of the four variables ( $u_x$ ,  $u_y$ ,  $t_x$ , and  $t_y$ ) prescribed.

If a node has no prescribed value of any kind then it is assumed to have  $t_x = t_y = 0$  (i.e. stress free).

To be able to use standard solvers, the  $[A]$  and  $[B]$  matrices must be rearranged such that all the known variables are on the right-hand side and all the unknown variables on the left-hand side which will result in the following system of algebraic equations:

$$[A^*][x] = [B^*][y] \quad (3.22)$$

where  $[x]$  contains all unknown variables (whether displacement or traction), whereas  $[y]$  contains all known variables prescribed as boundary conditions (whether displacement or traction). The matrices  $[A^*]$  and  $[B^*]$  are the modified forms of  $[A]$  and  $[B]$ , respectively. Therefore, the final system of linear algebraic equations can be written as follows:

$$[A^*][x] = [c] \quad (3.23)$$

where  $[c]$  now contains known coefficients.

To perform this arrangement of the  $[A]$  and  $[B]$  matrices, all the prescribed tractions are multiplied by the relevant  $[B]$  coefficients and added together to form the relevant elements of vector  $[c]$ . If a node has a prescribed displacement then its  $[A]$  coefficient is multiplied by the prescribed displacement value and moved to the right-hand side after reversing its sign. In its place, the  $[B]$  coefficient is moved to the left-hand side after reversing its sign.

After solving the system of linear equations, the variables contained in the unknown vector  $[x]$  of Eqn. (3.25) have to be sorted into displacements and tractions for computer output purposes. The above procedure can be easily applied to any size of mesh.

Before solving the equations, it is worth noting that in practical elastostatic problems the displacement values are usually several orders of magnitude less than the traction magnitudes (because of the very high value of Young's modulus, e.g.  $200 \times 10^9$  GPa for steel). This means that the typical value of the  $[A]$  coefficients are several orders of magnitude larger than the typical  $[B]$  coefficients. Since the  $[A]$  and  $[B]$  coefficients are placed together in the  $[A^*]$  matrix before solving the equations, they should be roughly of the same order of magnitude (otherwise, the solution may suffer from some inaccuracies). This can be easily achieved by multiplying the right-hand side of Eqn. (3.16) by a suitable scaling factor, as follows:

$$[A][u] = S[B] \times \frac{1}{S}[t] \quad (3.24)$$

where the scaling factor,  $S$ , is defined as follows:

$$S = \frac{E}{L_{max}} \quad (3.25)$$

where  $E$  is Young's modulus and  $L_{max}$  is the maximum distance between any two nodes. Therefore, the traction values are effectively normalized, and after solving the equations can be simply multiplied by  $S$  to yield absolute (un-normalized) tractions.

#### STEP 4: Solution of Algebraic Equation

The solution matrix  $[A^*]$  resulting after the application of the boundary conditions is not symmetric and fully populated with non-zero coefficients. Because of this, the choice of solution solver is clear: Gaussian eliminations or any other direct technique. It should be noted that all properly defined elastostatic problems must result in properly conditioned matrices (particularly if the scaling factor is used correctly) and they only become ill conditioned or singular if there is a mistake some where ( such as two nodes having the same co-ordinates ). It is a good practice to check for ill-conditioning when BE formulation is implemented in a computer program.

#### STEP 5: Calculation of the Boundary Stresses

There are two alternative methods of calculating the boundary stresses. In the first method, the BIEs for the stresses at  $p$  are used together with the appropriate third-order kernels. In the second method, the stresses are calculated directly from the computed displacements and tractions by simple differentiation using the shape functions.

In Eqn. (3.7), it has been defined the unit tangential vector  $\mathbf{m}$ , which has two components  $m_x$  and  $m_y$  in the  $x$  and  $y$  directions, respectively. Now define the local directions 1 and 2 as tangential and normal directions, respectively. Therefore, the local tangential component of the displacement vector  $u_1$  can be written in terms of the cartesian displacements as follows:

$$u_1(\xi) = u_x(\xi)m_x + u_y(\xi)m_y \quad (3.26)$$

Using the shape functions from Eqn. (3.5) this becomes

$$u_1(\xi) = \left[ \sum_{c=1}^3 N_c(\xi)(u_x)_c \right] m_x + \left[ \sum_{c=1}^3 N_c(\xi)(u_y)_c \right] m_y \quad (3.27)$$

To obtain the tangential strain  $\epsilon_{11}$ , the above equation is differentiated with respect to the tangential direction as follows:

$$\epsilon_{11}(\xi) = \frac{1}{J(\xi)} \left\{ \left[ \sum_{c=1}^3 \frac{\partial N_c(\xi)}{\partial \xi} (u_x)_c \right] m_x + \left[ \sum_{c=1}^3 \frac{\partial N_c(\xi)}{\partial \xi} (u_y)_c \right] m_y \right\} \quad (3.28)$$

Note that the Jacobian,  $J(\xi)$ , is used in the above equation because of the relationship between the local co-ordinate  $\xi$  and the boundary path .

The local components of the traction vector,  $t_1$  and  $t_2$ , can be defined as the tangential and normal tractions to the surface, respectively as shown in Figure 3.3. Note that the convention used here is that positive tangential traction should point to the left of the outward normal. If  $\alpha$  is the angle between the normal traction and the global  $x$ -direction, then the local tractions can be written in terms of the cartesian global tractions as follows:

$$\begin{aligned} t_1 &= -t_x \sin \alpha + t_y \cos \alpha \\ t_2 &= t_x \cos \alpha + t_y \sin \alpha \end{aligned} \quad (3.29)$$

To obtain the stresses in the local directions 1 and 2, the stress-strain are used as follows:

$$\begin{aligned} \sigma_{11} &= \left( \frac{E}{1-\nu^2} \right) \epsilon_{11} + \left( \frac{\nu}{1-\nu} \right) t_2 \\ \sigma_{22} &= t_2 \\ \sigma_{12} &= t_1 \end{aligned} \quad (3.30)$$

Note that plane-strain conditions have been used in the above expressions for the stress. Provided that the 'effective' material properties of Eqn. (3.35) are used, the Eqns. (3.34) are also valid for plane-stress conditions. To transform local stresses into global stresses, the transformation matrix is to be used. The direction cosines of the local co-ordinates are easily obtained as

$$\begin{aligned} E^* &= E; \quad \nu^* = \nu; \quad \mu^* = \mu \text{ (plane - strain)} \\ E^* &= \frac{E(1+2\nu)}{(1+\nu)^2}; \quad \nu^* = \frac{\nu}{1+\nu}; \quad \mu^* = \mu \text{ (plane - stress)} \end{aligned} \quad (3.31)$$

$$\begin{aligned} \text{Direction cosines of tangential direction 1} &= (-\sin \alpha); (\cos \alpha) \\ \text{Direction cosines of normal direction 2} &= (\cos \alpha); (\sin \alpha) \end{aligned} \quad (3.32)$$

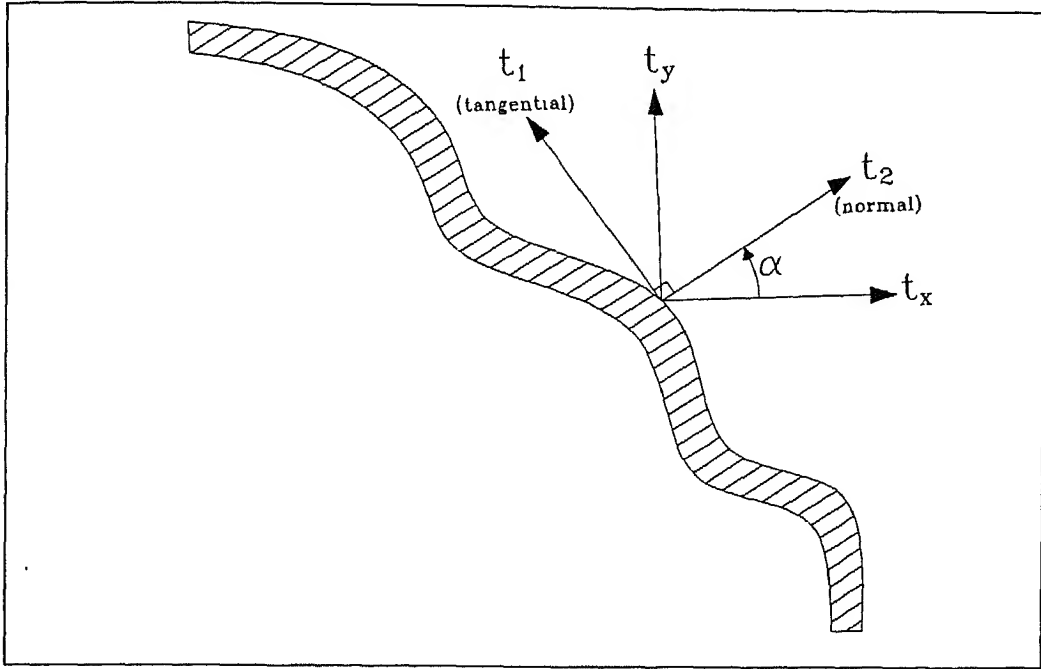


Figure 3.3 Local and Cartesian components of the traction vector.

Therefore, using the transformation matrix ([4]), the global cartesian stresses are given by

$$\begin{bmatrix} \sigma_{xx} \\ \sigma_{yy} \\ \sigma_{xy} \end{bmatrix} = \begin{bmatrix} \sin^2\alpha & \cos^2\alpha & -2\sin\alpha\cos\alpha \\ \cos^2\alpha & \sin^2\alpha & 2\sin\alpha\cos\alpha \\ -\sin\alpha\cos\alpha & \sin\alpha\cos\alpha & (\cos^2\alpha - \sin^2\alpha) \end{bmatrix} \begin{bmatrix} \sigma_{11} \\ \sigma_{22} \\ \sigma_{12} \end{bmatrix} \quad (3.33)$$

The angle can be written in terms of the unit normal components,  $n_x$  and  $n_y$ , as follows:

$$\alpha = \tan^{-1}\left(\frac{n_y}{n_x}\right) \quad (3.34)$$

#### STEP 6: Calculation of Internal Variables

After solving the equations, all of the values of displacements and tractions are determined at all the nodal points on the boundary. It is now a straightforward matter to determine the displacements at any interior point by substituting all of the boundary values in the BIE for displacements in Eqn. (3.1) and assuming the interior point to be the load point  $p$ . Similarly, the internal stresses can be determined by using the BIE for the stresses ([4]).

### 3.3 Sensitivity Analysis

In this Section the sensitivity analysis has been carried out, in general, for any function with respect to the intrinsic shape design variables. The function may represent either an objective function or behavioural constraint of an optimization problem. For example, the objective function in case of shape optimization problems using BEM stress analysis could be the peak value of the Von-Mises equivalent stress at a particular node or it could be the weight of the component. The nature of the behavioural constraint will depend on the formulation of the optimization problem. Since the objective function or the constraint function is expressed in the cartesian domain, the sensitivity analysis requires the use of chain rule and change of variables concepts of partial differentiation.

Consider a function  $g$ . It is assumed that the function  $g$  is explicitly related to the cartesian co-ordinates of the nodes,  $x_i, y_i, i = 1, 2, \dots, m$ . Each of these cartesian co-ordinates in turn related to the intrinsic parameters  $\kappa_j, s_j, j = 0, 1, 2, \dots, n$ . The rate of change of function  $g$  with respect to any intrinsic parameter can now be written as

$$\frac{\partial g}{\partial \kappa_1} = \sum_{i=1}^m \left( \frac{\partial g}{\partial x_i} \right) \left( \frac{\partial x_i}{\partial \kappa_1} \right) + \sum_{i=1}^m \left( \frac{\partial g}{\partial y_i} \right) \left( \frac{\partial y_i}{\partial \kappa_1} \right) \quad (3.35)$$

$$\frac{\partial g}{\partial s_1} = \sum_{i=1}^m \left( \frac{\partial g}{\partial x_i} \right) \left( \frac{\partial x_i}{\partial s_1} \right) + \sum_{i=1}^m \left( \frac{\partial g}{\partial y_i} \right) \left( \frac{\partial y_i}{\partial s_1} \right) \quad (3.36)$$

in general,

$$\begin{aligned} \frac{\partial g}{\partial \kappa_n} &= \sum_{i=1}^m \left( \frac{\partial g}{\partial x_i} \right) \left( \frac{\partial x_i}{\partial \kappa_n} \right) + \sum_{i=1}^m \left( \frac{\partial g}{\partial y_i} \right) \left( \frac{\partial y_i}{\partial \kappa_n} \right) \\ \frac{\partial g}{\partial s_n} &= \sum_{i=1}^m \left( \frac{\partial g}{\partial x_i} \right) \left( \frac{\partial x_i}{\partial s_n} \right) + \sum_{i=1}^m \left( \frac{\partial g}{\partial y_i} \right) \left( \frac{\partial y_i}{\partial s_n} \right) \end{aligned} \quad (3.37)$$

The equations given above provide derivation of the function  $g$  can be estimated as follows.

$$dg = \sum_{j=0}^n \left( \frac{\partial g}{\partial \kappa_j} \right) \Delta \kappa_j + \sum_{j=0}^n \left( \frac{\partial g}{\partial s_j} \right) \Delta s_j \quad (3.38)$$

The foregoing procedure can be used to compute the sensitivity coefficients of any function  $g$  with respect to shape design variable. Also, Equation (3.42) can be used to compute the total change in a function  $g$  due to simultaneous changes in the SDVs.

In the present work, the partial derivatives have been computed using the forward finite difference scheme. Some typical cases are given below.

$$\begin{aligned}
\frac{\partial g}{\partial x_1} &\simeq \frac{g(x_1 + \Delta x_1, x_2, \dots, x_m, y_1, y_2, \dots, y_m) - g(x_1, x_2, \dots, x_m, y_1, y_2, \dots, y_m)}{\Delta x_1} \\
\frac{\partial g}{\partial y_1} &\simeq \frac{g(x_1, x_2, \dots, x_m, y_1 + \Delta y_1, y_2, \dots, y_m) - g(x_1, x_2, \dots, x_m, y_1, y_2, \dots, y_m)}{\Delta y_1}
\end{aligned}
\tag{3.39}$$

$$\begin{aligned}
\frac{\partial x_1}{\partial \kappa_1} &\simeq \frac{x_1(\kappa_0, \kappa_1 + \Delta \kappa_1, \kappa_2, \dots, \kappa_n, s_0, s_1, s_2, \dots, s_n) - x_1(\kappa_0, \kappa_1, \kappa_2, \dots, \kappa_n, s_0, s_1, s_2, \dots, s_n)}{\Delta \kappa_1} \\
\frac{\partial x_1}{\partial s_1} &\simeq \frac{x_1(\kappa_0, \kappa_1, \kappa_2, \dots, \kappa_n, s_0, s_1 + \Delta s_1, s_2, \dots, s_n) - x_1(\kappa_0, \kappa_1, \kappa_2, \dots, \kappa_n, s_0, s_1, s_2, \dots, s_n)}{\Delta s_1}
\end{aligned}
\tag{3.40}$$

$$\begin{aligned}
\frac{\partial y_1}{\partial \kappa_1} &\simeq \frac{y_1(\kappa_0, \kappa_1 + \Delta \kappa_1, \kappa_2, \dots, \kappa_n, s_0, s_1, s_2, \dots, s_n) - y_1(\kappa_0, \kappa_1, \kappa_2, \dots, \kappa_n, s_0, s_1, s_2, \dots, s_n)}{\Delta \kappa_1} \\
\frac{\partial y_1}{\partial s_1} &\simeq \frac{y_1(\kappa_0, \kappa_1, \kappa_2, \dots, \kappa_n, s_0, s_1 + \Delta s_1, s_2, \dots, s_n) - y_1(\kappa_0, \kappa_1, \kappa_2, \dots, \kappa_n, s_0, s_1, s_2, \dots, s_n)}{\Delta s_1}
\end{aligned}
\tag{3.41}$$

It should be noted that appropriate values of  $\Delta x_1$ ,  $\Delta y_1$ ,  $\Delta \kappa_1$ , and  $\Delta s_1$  should be chosen while computing the partial derivatives. In the present case a range of 0.1% to 1.0% has been used to select a suitable value for the change of all these parameters. Computer programs have been developed in C on UNIX-platform to compute the sensitivity coefficients with respect to the intrinsic shape design variables. An illustrative example has been considered and the results obtained are given in the following Section.

### 3.4 Numerical Examples

A number of computer programs have been developed in both C and FORTRAN 77 and integrated through system calls on SUN-workstation with UNIX-platform for shape synthesis, automatic mesh refinement of boundary elements, BEM analysis, NLP optimization and sensitivity analysis as explained in the foregoing Chapters. With the help of these computer programs the intermediate shape of an elastic ring under diametral compression problem has successfully been implemented. Once, the intermediate shape is achieved, a small perturbation on intermediate shape design variables has been applied and the resultant stress sensitivities are plotted as shown in Figure 3.7.

#### Example:

This example shows an elastic ring under diametral compression. Taking an advantage of symmetry, one quarter of the ring is modelled, as shown in Figure 3.4(a). Young's

modulus, Poisson's ratio and the allowable stress are 2338 MPa, 0.38 and 18 MPa respectively. It is a case of plane-strain, and the object is to minimize the weight, while keeping the outer boundaries defining the exterior shape of the ring unchanged. For a shape optimization,  $\Gamma_3$  and  $\Gamma_4$  are assumed to be fixed,  $\Gamma_2$  is allowed to move horizontally, and  $\Gamma_1$  is allowed to move freely. The boundary  $\Gamma_1$  is being varied by selecting a feasible shape model such that stress constraints are satisfied.

Figure 3.4(b) shows quadratic boundary element model with 100 nodes and 50 elements. The cartesian and intrinsic profiles for an initial geometry of the ring as shown in Figure 3.5. A 2-LINCEs model (R-R model) has been chosen in order to define each boundary  $\Gamma_1$ ,  $\Gamma_2$ ,  $\Gamma_3$ , and  $\Gamma_4$ . The intrinsic variables of the boundary  $\Gamma_1$  (i.e. curve A-B) corresponding to the initial geometry are given by

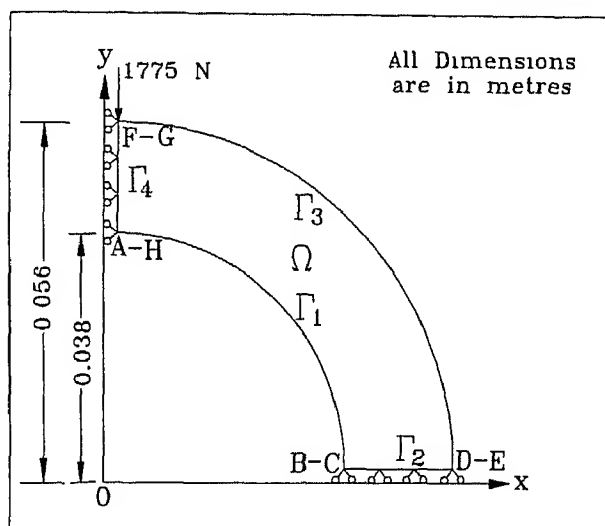
$$\kappa_0 = -26.315789; s_0 = 0.0; \kappa_1 = -26.315789; s_1 = 0.0298451; \kappa_2 = -26.315789; s_2 = 0.0596902$$

The Figure 3.6 shows the cartesian and intrinsic profiles for an intermediate shape of an elastic ring. The intrinsic shape design variables of the boundary  $\Gamma_1$  corresponding to an intermediate shape are given below:

$$\kappa_0 = -26.315789; s_0 = 0.0; \kappa_1 = -19.614253; s_1 = 0.029845; \kappa_2 = -35.08690; s_2 = 0.062217$$

In order to calculate the stress sensitivity with respect to  $\kappa_1$ , a set of 20 different magnitudes of perturbed values (i.e.  $\Delta\kappa_1$ ) have been applied to the intermediate value of  $\kappa_1$ . The Figure 3.7 shows the stress sensitivity Vs change in curvature according to the stress sensitivity procedure described in Section 3.3. This stress sensitivity study gives an information that a small change in intrinsic variables (i.e. curvature or arc length) caused a large variation in stress magnitude.

(a)



(b)

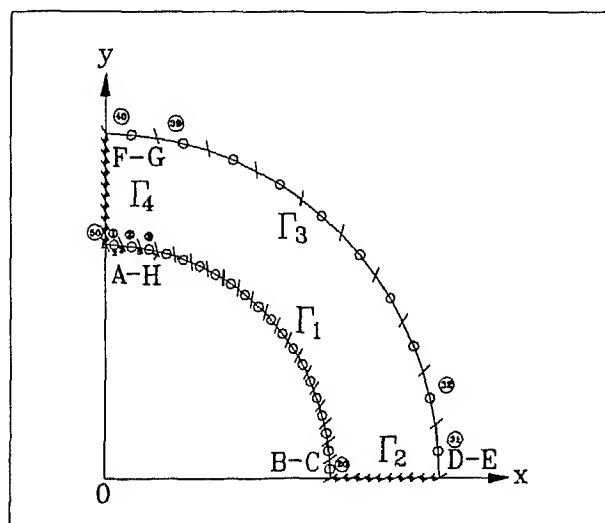
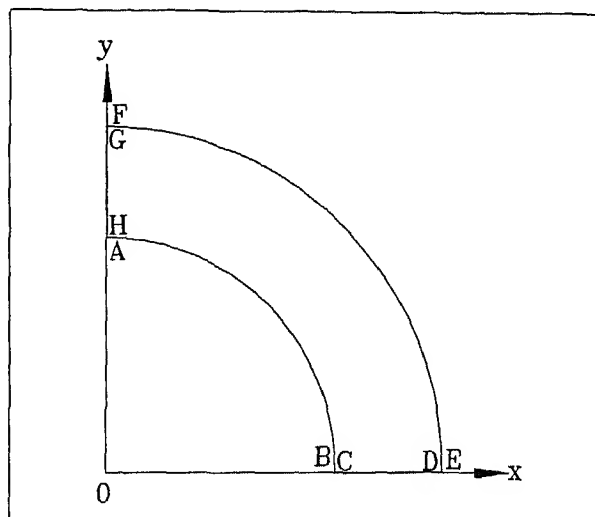


Figure 3.4 (a) Definition of An Elastic Ring Problem.  
(b) BEM Mesh for the Elastic Ring Problem.

(a)



(b)

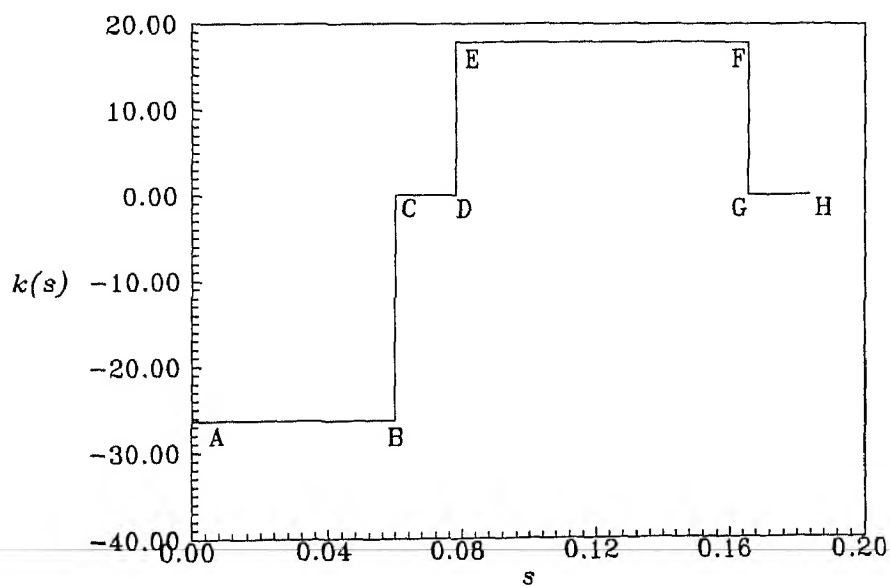
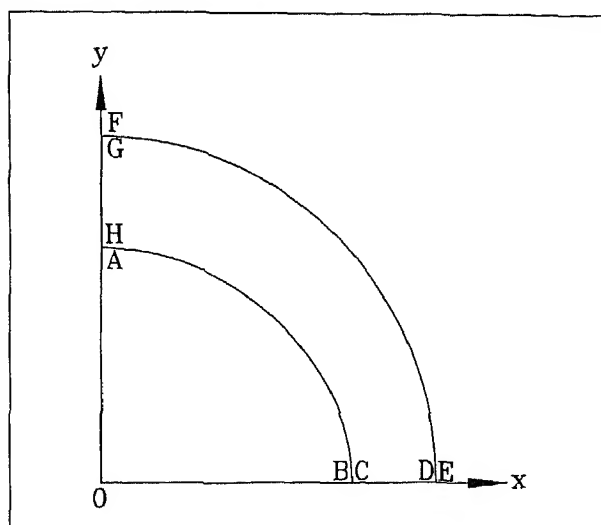


Figure 3.5 (a) Cartesian Profile for An Initial Shape of An Elastic Ring.  
 (b) Intrinsic Profile for An Initial Shape of An Elastic Ring.

(a)



(b)

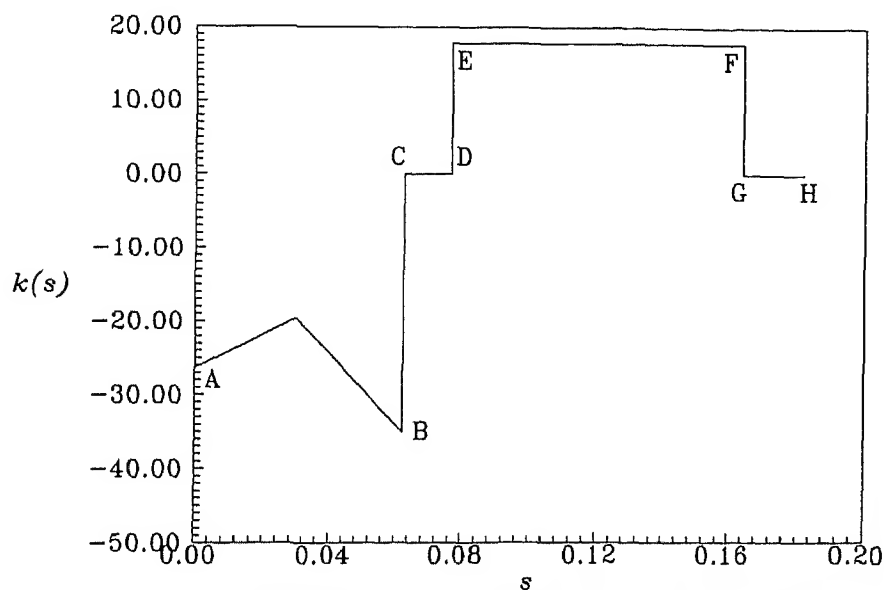


Figure 3.6 (a) Cartesian Profile for An Intermediate Shape of An Elastic Ring.  
 (b) Intrinsic Profile for An Intermediate Shape of An Elastic Ring.

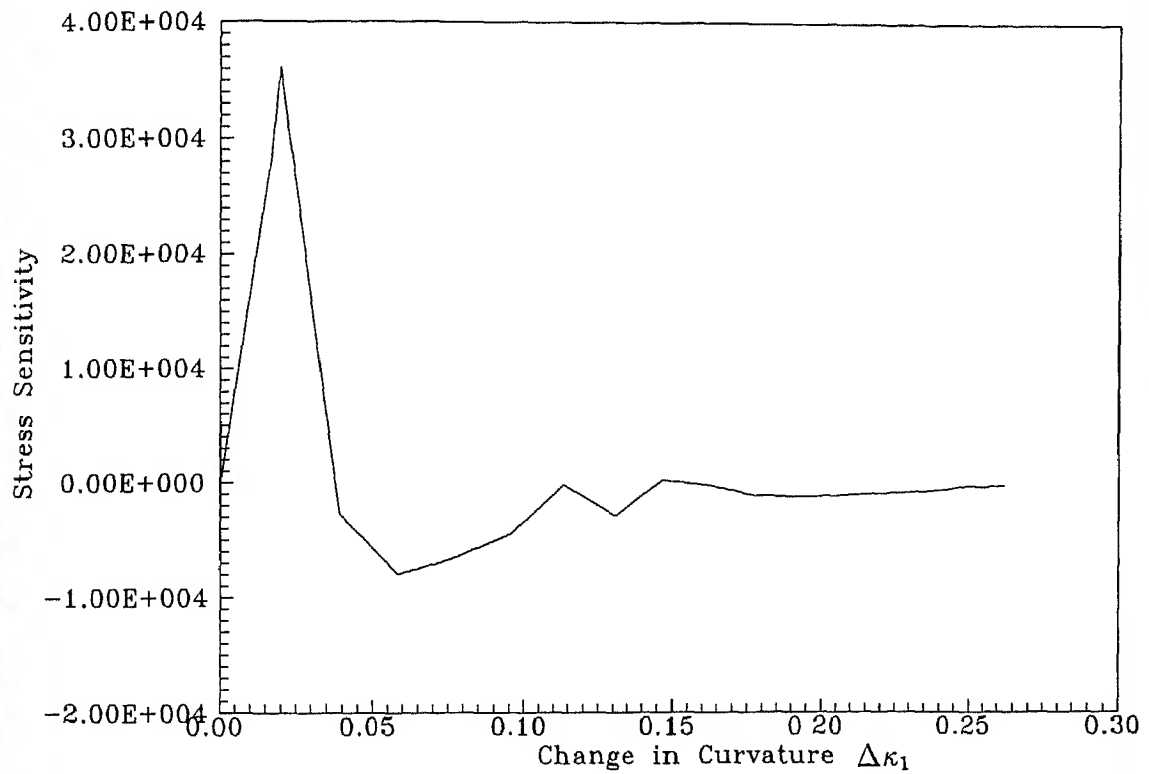


Figure 3.7 Graph shows Stress Sensitivity Vs Change in Curvature Plot.

# SHAPE OPTIMIZATION METHODOLOGY

---

## 4.1 General Approach

The first and foremost step towards shape optimization based on a CAD approach is the creation of a multi-window interactive graphics environment in order to facilitate clear visualization of the design history of the optimal design process. To fulfil this requirement, a computer program has been developed in C language and implemented on a SUN-workstation with UNIX-platform based on SUN-view graphics. The graphics environment is comprised of multi-windows; one for the cartesian space, one for the intrinsic space and one for the selection menu and the last one for the graphics manipulation during the design process. Figure 4.1 shows such a graphics environment. Once, such a graphics environment is ready, then the shape optimization methodology can be described as follows.

The problem of shape optimization can be described as a problem of synthesizing the geometry of the surface boundary of a component cross-section that will maximize or minimize an objective function as well as satisfy a set of behavioural and side constraints. In general, the equation of the objective function and constraints require the geometry of a component surface boundary in terms of cartesian co-ordinates. However, as proposed in this research, the shape definition is described most suitably in terms of intrinsic geometry of the component. The structural and mechanical components considered for this research use BEM analysis for 2-D plane-stress, plane-strain and axi-symmetric problems in order to satisfy the stress constraints during optimization cycle. In order to avoid the intervention of the designer during shape optimization cycle, an automatic mesh refinement of boundary elements has been introduced. The automatic mesh refinement module acts as a mediator between the synthesizer and the BEM analyzer.

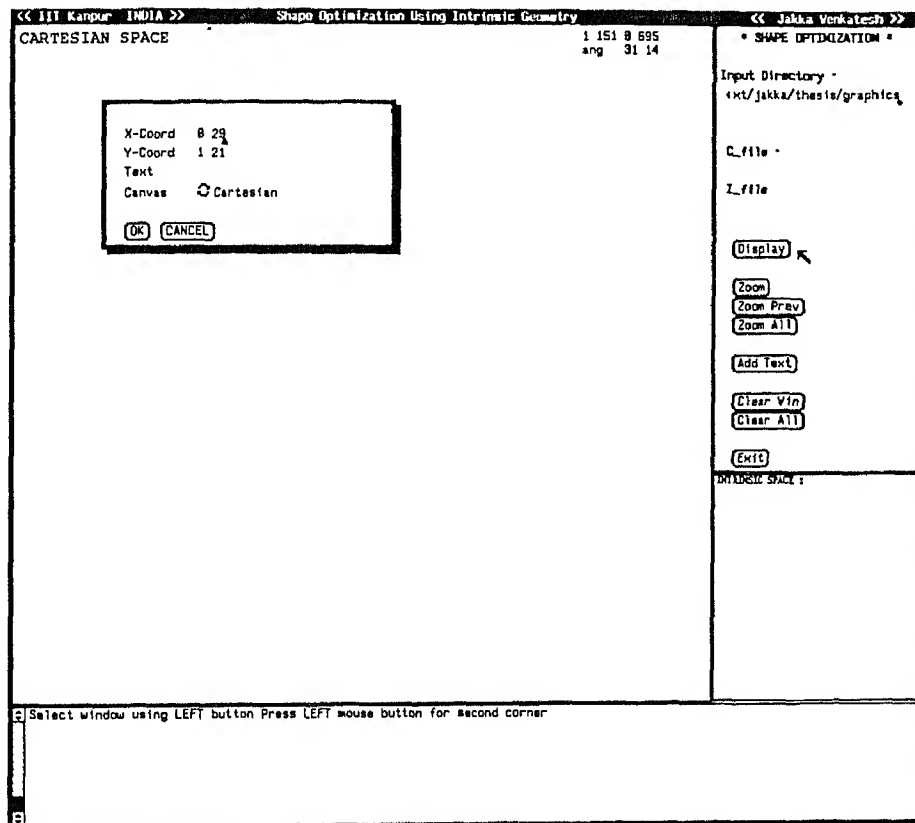


Figure 4.1 Multi-Window Graphics Environment Designed on SUN-workstation via SUN-view Graphics.

Consider a given component  $\Gamma$  (surface boundary)  $= \Gamma_1 \cup \Gamma_2 \cup \Gamma_3 \cup \Gamma_4$  as shown in Figure 4.2. It is required to find a set of optimal shape curves between successive pairs of points such as  $\Gamma_1, \Gamma_2, \Gamma_3$ , and  $\Gamma_4$ . Let  $(i_1, i_2, \dots, i_n)$  be a set of  $n$  shape design variables (SDVs). These are considered to be intrinsic geometry parameters. Let  $(c_1, c_2, \dots, c_m)$  be a set of  $m$  variables representing the cartesian geometry of the component. Let  $M$  be a mapping relation that enables us to find the set  $(c_1, c_2, \dots, c_m)$  from a given values of  $(i_1, i_2, \dots, i_n)$ .

$$(c_1, c_2, \dots, c_m) = [M](i_1, i_2, \dots, i_n) \quad (4.1)$$

Let  $W$  be the objective function and  $g_j$ 's be the set of constraints. The optimization problem formulation can be stated as follows.

Minimize

$$W(i_1, i_2, \dots, i_n) \quad (4.2)$$

subject to

$$g_j(c_1, c_2, \dots, c_m(i_1, i_2, \dots, i_n)) \leq 0 \quad (4.3)$$

where  $j = 1, 2, \dots, k$ .

At this point, it is necessary to point out that  $c_1, c_2, \dots, c_m$  are not the design variables for the present problem. Any change of the shape is effected by changing the vector  $(i_1, i_2, \dots, i_n)$ .

The design problem, in turn, now is to select a shape model for  $\Gamma_1, \Gamma_2, \Gamma_3$ , and  $\Gamma_4$  etc. individually or collectively and their shape design variables such that  $W$  is minimized. The 2-LINCEs model (R-R model) and 3-LINCEs model (R-R-R model) have been considered in this research work, but the same procedure can be extended to  $n$ -LINCEs model depending upon the problem situation. In general, the R-R-R model (3-LINCEs model) has been found to be suitable having a minimum number of shape design variables. The solution procedures via zero-order and first-order NLP optimization methods outlined in Sections 4.2 and 4.3. The sensitivity aspects have been discussed in Section 4.4. Before outlining the zero-order method, it is necessary to understand how the frontal-area of the surface boundary can be evaluated, if the geometry is available in  $R^2$ -Euclidean space. The following equation has been used for evaluating the frontal-area of the closed boundary in a 2-Dimensional space. The weight of a component can be evaluated once the cross-sectional area is available.

$$Area = \sum_{i=0}^n \frac{(y_i + y_{i+1})}{2} (x_i - x_{i+1}) \quad (4.4)$$

where the vertices of the closed polygon are marked as  $0, 1, 2, \dots, (n-1)$ . The starting point is also designated as  $n$ .

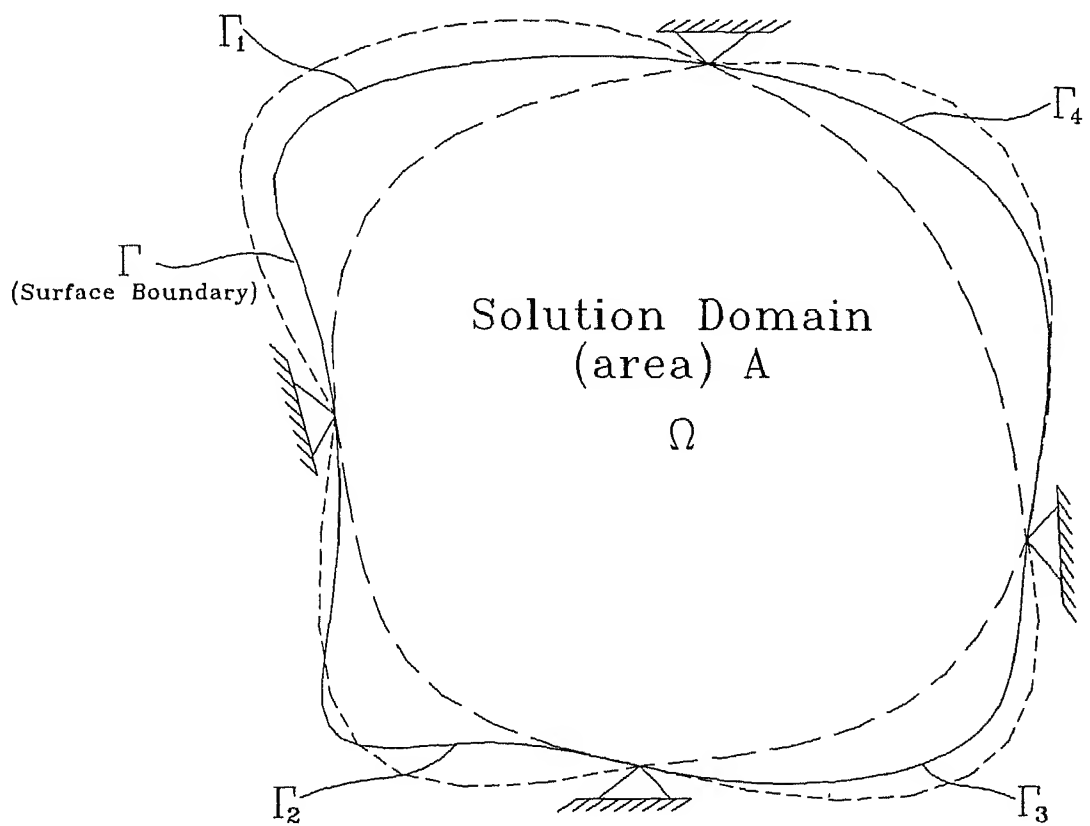


Figure 4.2 General Definition of the Shape Optimization Problem Using Intrinsic Geometry and BEM.

## 4.2 Zero-order Method (Exhaustive Search Method)

It is convenient to categorize algorithms according to the type of information that must be provided in searching for the minimum of the function.

The simplest approach to minimizing  $W(\mathbf{X})$  is to select either randomly or in some logical manner, a large number of candidate  $\mathbf{X}$  vectors and evaluate the objective for each of them. The  $\mathbf{X}$  corresponding to the minimum  $W(\mathbf{X})$  obtained from this set is called the optimum,  $\mathbf{X}^*$ . Obviously, if a precise solution to the problem is to be found, a great many  $\mathbf{X}$  vectors may have to be considered. Methods such as this, which require only function values in searching for the optimum, are referred to as zero-order methods.

These methods are usually reliable and easy to program, often can deal effectively with nonconvex and discontinuous functions, and in many cases can work with discrete values of design variables. The price paid for this generality is that these methods often require thousands of function evaluations to achieve the optimum, even for the simplest problems. Therefore, these methods are considered most useful for the problems in which the function evaluation is not computationally expensive. Used in appropriate fashion, zero-order methods are a useful and powerful design tool for many common applications.

Exhaustive Search method, in particular can be used to solve problems where the interval in which the optimum known to lie is finite. Let  $x_s$  and  $x_f$  denote, the starting and final points of the interval of uncertainty. The exhaustive search method consists of evaluating the objective function at predetermined number of equally spaced points in the interval  $(x_s, x_f)$ , and reducing the interval of uncertainty, assuming that the objective function is a unimodal function. In general, if the function is evaluated at  $n$  equally spaced points in the original interval of length  $L_0 = x_f - x_s$ , and if the optimum value of the function (among the  $n$  function values) turns out to be at the point  $x_j$ , then the final interval of uncertainty is given by ([41])

$$L_n = x_{j+1} - x_{j-1} = \left(\frac{2}{n+1}\right)L_0 \quad (4.5)$$

It is to be noted that the objective function may be defined in terms of intrinsic variables explicitly or in terms of cartesian co-ordinates of some specific interpolating points. For the applications dealt in the present work the objective function involves in many cases the computation of the frontal-area. The frontal-area in turn, can be calculated using the formula given under Equation (4.4) earlier. Moreover, the geometry or the curve is synthesized using a 2-LINCEs or 3-LINCEs model.

The shape optimization methodology via a zero-order method can be described as follows.

Minimize

$$\Phi = \Phi[c_1, c_2, \dots, c_m(i_1, i_2, \dots, i_n)] \quad (4.6)$$

subject to

$$g_j[c_1, c_2, \dots, c_m(i_1, i_2, \dots, i_n)] - g_{all} \leq 0 \quad (4.7)$$

where  $j = 1, 2, \dots, k$ .

The description of the terms involved in the above two equations include:  $\Phi$  defines the frontal-area of cross-section of the component, the outer boundary of the component, and  $g_j$  defines the peak value of Von-Mises stress corresponding to the  $j$ th iteration, and  $g_{all}$  defines the maximum allowable stress of the component. The solution procedure can be outlined as follows.

STEP 1. Define the surface boundary ( $\Gamma = \Gamma_1 \cup \Gamma_2 \cup \Gamma_3 \cup \Gamma_4$  etc.) in terms of intrinsic parameters by selecting a shape model depending on the physical nature of the problem. In general, the 3-LINCEs model (R-R-R model) has been found to be suitable having a minimized number of shape design variables (SDVs).

STEP 2. Once a particular model is chosen, the SDVs are selected depending on the number of free parameters for that particular model. It has been found that  $\kappa_i$ 's serve as a better choice for shape design variables than  $s_i$ 's.

STEP 3. Define cartesian-intrinsic mapping for a feasible set of SDVs, find cartesian co-ordinates using equations (2.31) through (2.33).

STEP 4. Once the cartesian co-ordinates are available, it is possible to analyze stress constraints ( $g_j$ 's -  $g_{all} \leq 0$ ) for maximum Equivalent stress (Von-Mises stress), maximum deflection etc. using Boundary Element Method. If any constraint is violated then the design is discarded. The process now resumes at step 3 with a new set of shape design variables. This step also involves the automatic mesh refinement of boundary elements through an automatic mesh refinement module.

STEP 5. Check how stress and deflection situation changes by altering  $\Gamma_1$ , and hence  $\Gamma_2, \Gamma_3$ , and  $\Gamma_4$  individually or simultaneously.

STEP 6. Evaluate objective function (i.e. frontal-area  $\Phi$  in this case) and optimal shapes using values of shape design variables and the cartesian co-ordinates that satisfy all the constraints. If the value of  $\Phi$  is minimum then the process terminates. Otherwise

an improved feasible design is required. This will be accomplished by an exhaustive search NLP (Non-Linear Programming) technique.

The exhaustive search NLP technique which has been used in this method can be summarized as follows. Initially the interval of uncertainty of free SDVs is assumed to lie in between  $\kappa_{max}$  and  $\kappa_{min}$  corresponding to inner and outer boundaries of the frontal-area of component being minimized respectively. The interval of uncertainty will be reduced with the assumption of unimodal function and the accuracy with which the optimum value is required. This decides the number of iterations. Once the number of intervals is decided based on the above procedure, it is possible to select a set of values of shape design variables - some  $s_i$ 's and  $\kappa_i$ 's. The values of remaining  $\kappa_i$ 's and  $s_i$ 's are obtained from the geometric constraint equations. The SDVs thus obtained will be used in establishing the shape model and hence the objective function  $\Phi$ .

The shapes which satisfy all the stress constraints can only undergo the frontal-area evaluation whereas the shapes which are not able to fulfil any of the stress constraints will be discarded. The value of  $\Phi$  which will be obtained in every iteration of the optimization cycle is compared to the existing or preceding one for the condition of minimization. Thus the shape corresponding to an optimal frontal-area can be obtained.

### 4.3 First-order Method

Let  $W(\mathbf{X})$  be the objective function, then a more difficult but usually more efficient approach to the minimization problem is to use gradient information in seeking the optimum. For example, it can be said that calculate the gradient of  $W(\mathbf{X})$  and then search in the negative, or  $-\nabla W(\mathbf{X})$ , direction. Now because this is the direction of steepest descent at  $\mathbf{X}$ , then it may be expected that choosing a new  $\mathbf{X}$  vector using this information will lead to move to a solution of the problem rapidly. That is, a new  $\mathbf{X}$  vector will be chosen by

$$\mathbf{X}^1 = \mathbf{X}^0 - \alpha \nabla W(\mathbf{X}^0) \quad (4.8)$$

If several values are tried for the scalar parameter  $\alpha$ , and for each resulting  $\mathbf{X}$  vector evaluate  $W(\mathbf{X}) = W(\alpha)$ , then some value  $\alpha^*$  will provide a minimum  $W(\mathbf{X})$  for this search direction. By using the gradient of  $W(\mathbf{X})$ , it will be possible to limit our search to a specific direction, rather than randomly searching the entire space. Of course, because  $W(\mathbf{X})$  may be highly non-linear, then it will be necessary to calculate a new gradient at  $\mathbf{X}$  and repeat the process. Methods such as this which use gradient, or first derivative, information are called first-order methods. It is to be noted that the objective function and geometric and stress or behavioural constraints must be expressed in terms of intrinsic shape design variables either explicitly or implicitly. The formulation has been done for the problems which are characterized 2-D plane-stress or plane-strain case.

A 2-LINCEs model (R-R model) and a 3-LINCEs model (R-R-R model) have been used for modeling the surface boundary of the component.

The problem formulation (for 3-LINCEs model) can be stated as follows.

Minimize

$$\Phi = \Phi[c_1, c_2, \dots, c_m(i_1, i_2, \dots, i_n)] \quad (4.9)$$

subject to

(i) Geometric Equivalency constraints ( $h_i$ 's) include :

$$\begin{aligned} x_3 - x_0 &= \int_{s_0}^{s_1} \cos\left[\left(\frac{\kappa_1 - \kappa_0}{s_1 - s_0}\right)\left(\frac{\sigma^2}{2} - s_0\sigma\right) + \kappa_0\sigma + C_1\right] d\sigma \\ &- \int_{s_1}^{s_2} \cos\left[\left(\frac{\kappa_2 - \kappa_1}{s_2 - s_1}\right)\left(\frac{\sigma^2}{2} - s_1\sigma\right) + \kappa_1\sigma + C_2\right] d\sigma \\ &- \int_{s_2}^{s_3} \cos\left[\left(\frac{\kappa_3 - \kappa_2}{s_3 - s_2}\right)\left(\frac{\sigma^2}{2} - s_2\sigma\right) + \kappa_2\sigma + C_3\right] d\sigma = 0 \end{aligned} \quad (4.10)$$

$$\begin{aligned} y_3 - y_0 &= \int_{s_0}^{s_1} \sin\left[\left(\frac{\kappa_1 - \kappa_0}{s_1 - s_0}\right)\left(\frac{\sigma^2}{2} - s_0\sigma\right) + \kappa_0\sigma + C_1\right] d\sigma \\ &- \int_{s_1}^{s_2} \sin\left[\left(\frac{\kappa_2 - \kappa_1}{s_2 - s_1}\right)\left(\frac{\sigma^2}{2} - s_1\sigma\right) + \kappa_1\sigma + C_2\right] d\sigma \\ &- \int_{s_2}^{s_3} \sin\left[\left(\frac{\kappa_3 - \kappa_2}{s_3 - s_2}\right)\left(\frac{\sigma^2}{2} - s_2\sigma\right) + \kappa_2\sigma + C_3\right] d\sigma = 0 \end{aligned} \quad (4.11)$$

$$\psi_n - \psi_0 - \left(\frac{\kappa_0 + \kappa_1}{2}\right)(s_1 - s_0) - \left(\frac{\kappa_1 + \kappa_2}{2}\right)(s_2 - s_1) - \left(\frac{\kappa_2 + \kappa_3}{2}\right)(s_3 - s_2) = 0 \quad (4.12)$$

(ii) Inequality stress constraint  $[(g_j - g_{all})'$ s] and other geometric constraints include :

$$(\tau_{max} - \tau_{all}) \leq 0$$

$$\text{or } \frac{\tau_{max}}{\tau_{all}} - 1 \leq 0 \quad (4.13)$$

$$x_3 \geq x_{min}$$

$$\text{or} \quad -x_3 - x_{min} \leq 0 \quad (4.14)$$

$$x_3 \leq x_{max}$$

$$\text{or} \quad x_3 - x_{max} \leq 0 \quad (4.14 \text{ a})$$

(iii) Constant values include :

If  $\psi_{start}$  and  $\psi_{end}$  = specified tangent conditions at the start and end of boundary curve,

$$\begin{aligned} \text{then } \psi_0 &= \psi_{start} \\ \psi_3 &= \psi_{end} \\ x_0 &= 0 \\ y_3 &= 0 \\ \text{and } s_0 &= 0 \end{aligned} \quad (4.15)$$

The terms involved in Eqns. (4.9) through (4.15) have got their own meaning as described in Chapter 2 and Chapter 3.  $\tau_{max}$  corresponds to the peak value of Von-Mises equivalent stress at the boundary and  $\tau_{all}$  defines maximum allowable stress of the component.

In order to convert the above constrained non-linear optimization into unconstrained optimization problem, the following SUMT (Sequential Unconstrained Minimization Technique) has been used.

If  $W(\mathbf{X})$  is an objective function, then

minimize

$$W(\mathbf{X}) \quad (4.16)$$

subject to

$$g_j(\mathbf{X}) \leq 0 \quad \text{where } j = 1, 2, \dots, m \quad (4.17)$$

$$\text{and } h_i(\mathbf{X}) = 0 \quad \text{where } i = 1, 2, \dots, p. \quad (4.18)$$

Using interior penalty function method, the above constrained optimization problem can be converted into unconstrained minimization problem by adding suitable penalty terms. The pseudo-objective function after adding suitable penalty terms using interior penalty function can be written as follows ([41]).

Pseudo-objective function include :

$$\begin{aligned} \Phi_k &= \Phi(\mathbf{X}, r_k) \\ &= W(\mathbf{X}) - r_k \sum_{j=1}^m \frac{1}{g_j(\mathbf{X})} + \frac{1}{\sqrt{r_k}} \sum_{i=1}^p h_i^2(\mathbf{X}) \end{aligned} \quad (4.19)$$

where  $r_k$  is called the penalty parameter.

The solution procedure for the proposed first-order shape optimization methodology can be outline as follows.

STEP 1. Define the surface boundary ( $\Gamma = \Gamma_1 \cup \Gamma_2 \cup \Gamma_3 \cup \Gamma_4$  etc.) of the initial geometry in terms of intrinsic parameters by selecting a shape model depending on the physical nature of the problem. In general, the R-R-R model has been found to be more suitable having less number of shape design variables.

STEP 2. Once a particular shape model is chosen, the SDVs are selected depending on the initial geometry of the problem.

STEP3. Define intrinsic-cartesian mapping for a feasible set of SDVs, find the cartesian co-ordinates using shape synthesis procedure explained in Chapter 2.

STEP 4. An automatic mesh generation of boundary elements will be obtained using an automatic mesh refinement module, once the cartesian co-ordinates of geometry, displacement and stress boundary conditions and material properties are available.

STEP 5. Evaluate the maximum Von-Mises equivalent stress ( $\tau_{max}$ ) at the surface boundary using Boundary Element Method.

STEP 6. Since the maximum allowable stress ( $\tau_{all}$ ) of the component is given, then the first-order constrained optimization problem can be formulated using Equations (4.9) through (4.15) and then normalizing the necessary constraints.

STEP 7. Once the Non-linear constrained optimization problem is formulated as stated in STEP 6, then the non-linear constrained optimization problem will be converted in to a non-linear unconstrained optimization using interior penalty function

method of Sequential Unconstrained Minimization Technique (SUMT) according to the Equation 4.19. Thus, the non-linear constrained problem becomes non-linear unconstrained optimization problem with suitable penalty parameters added to the objective function, called pseudo-objective function.

STEP 8. Once the non-linear unconstrained optimization problem is formulated, then the optimization solution can be obtained using Davidon-Fletcher-Powell (DFP) method of unconstrained minimization technique. The gradient information about the objective function required to be used may utilize concepts of chain rule and change of variables for partial differentiation depending upon the objective function is defined either explicitly or implicitly in terms of the SDVs.

STEP 9. The optimal shape of the component can be visualized using the graphics environment created on SUN-workstation as mentioned at the outset of this Chapter with the help of cartesian geometry produced in STEP 8.

STEP 10. Using the cartesian geometry corresponds to an optimal shape evaluate the objective function (i.e. the frontal-area of the cross-section) of the problem. Thus, the shape optimization cycle will be accomplished.

#### 4.4 Issues of Sensitivity Analysis

The sensitivity analysis is an approach to indicate how a constraint behaves owing to small perturbations in the values of the design variables. In an intrinsic geometry based shape optimization, the effects of small changes in intrinsic shape design variables,  $\kappa_1, s_1$  etc. on the behaviour of constraints will be studied in this section. For example Figure 4.3(a) and 4.3(b) shows cartesian and intrinsic geometries respectively. The sensitivity analysis concept based on intrinsic geometry can be explained with the help of these Figures.

If there is a change in the value of, say  $\kappa_1$  to  $\kappa_1 + \Delta\kappa_1$  then the effect on the  $x$ - $y$  curve (curve A-B) can be studied.

Suppose there is function such as an area ( $A$ ) which depends on the  $x$ - $y$  (and hence on  $\kappa$ - $s$  shape) (of the) curve, then the change

$\Delta A$  in the area ( $A$ ) due to a change in the variable  $\kappa_1$  as  $\Delta\kappa_1$ .

If  $\kappa_1$  is a shape design variable and area ( $A$ ) is a constraint then the ratio ( $\frac{\Delta A}{\Delta\kappa_1}$ ) is the sensitivity of the area with respect to a shape design variable; in this case  $\kappa_1$ .

If it is case for  $\kappa_1$  then the same logic could be used to evaluate for any other SDVs such as  $\kappa_0, \kappa_2, \dots, \kappa_n$  or  $s_0, s_1, \dots, s_n$ . The solution procedure for sensitivity computations can

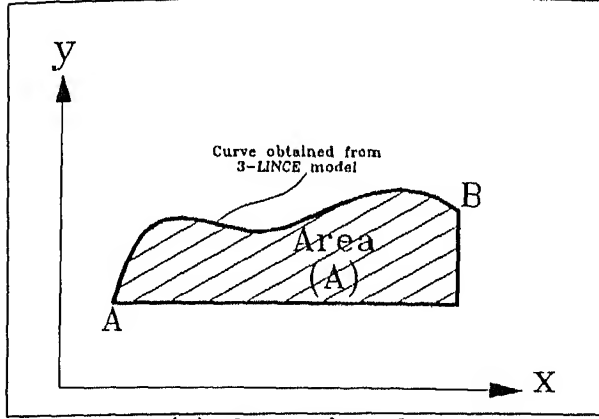


Figure 4.3(a) Cartesian Geometry.

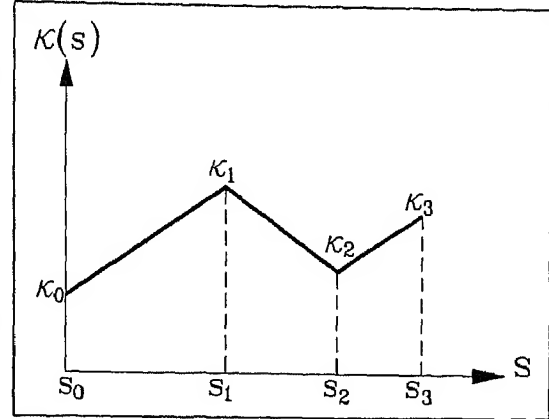


Figure 4.3(b) Intrinsic Geometry.

be described using chain rule and change of variables concept of partial differentiation and finite difference approximations.

If  $\Phi = \Phi(\kappa_0, s_0, \kappa_1, s_1, \dots, \kappa_n, s_n) = \Phi(\mathbf{I})$  defines the frontal-area of the surface boundary, then the rate of change of  $\Phi$  w.r.t  $\kappa_1$  can be defined as follows.

Where

$$\mathbf{I} = \begin{Bmatrix} \kappa_0 \\ s_0 \\ \kappa_1 \\ s_1 \\ \kappa_2 \\ s_2 \\ \vdots \\ \kappa_n \\ s_n \end{Bmatrix}$$

then

$$\frac{\partial \Phi(\mathbf{I})}{\partial \kappa_1} = \frac{\Phi(\mathbf{I}(\kappa_1 + \Delta \kappa_1)) - \Phi(\mathbf{I})}{\Delta \kappa_1} \quad (4.20)$$

where  $\Delta \kappa_1$  denotes a small perturbation in  $\kappa_1$ . Similarly, for other SDVs  $\kappa_0, s_0, \kappa_2, s_2$  etc. can be defined.

Suppose  $\Phi = \Phi(c_1, c_2, \dots, c_m(i_1, i_2, \dots, i_n)) = \Phi(\mathbf{C}(\mathbf{I}))$  define the frontal-area of the surface boundary, then the sensitivity computations will be carried out as follows:

$$C = \begin{Bmatrix} x_1 \\ y_1 \\ x_2 \\ y_2 \\ \vdots \\ x_m \\ y_m \end{Bmatrix}$$

Where  $(c_1, c_2, \dots, c_m)$  defines cartesian variables such as  $(x_1, y_1), (x_2, y_2), \dots, (x_m, y_m)$  and  $(i_1, i_2, \dots, i_n)$  defines intrinsic variables such as  $\kappa_0, s_0, \kappa_1, s_1, \dots, \kappa_n, s_n$ .

Then

$$\frac{\partial \Phi}{\partial \kappa_1} = \sum_{i=1}^m \left( \frac{\partial \Phi}{\partial x_i} \right) \left( \frac{\partial x_i}{\partial \kappa_1} \right) + \sum_{i=1}^m \left( \frac{\partial \Phi}{\partial y_i} \right) \left( \frac{\partial y_i}{\partial \kappa_1} \right) \quad (4.21)$$

$$\text{but } \frac{\partial \Phi}{\partial x_1} \simeq \frac{\Phi(x_1 + \Delta x_1, x_2, \dots, x_m, y_1, y_2, \dots, y_m) - \Phi(x_1, x_2, \dots, x_m, y_1, y_2, \dots, y_m)}{\Delta x_1} \quad (4.22)$$

$$\frac{\partial \Phi}{\partial y_1} \simeq \frac{\Phi(x_1, x_2, \dots, x_m, y_1 + \Delta y_1, y_2, \dots, y_m) - \Phi(x_1, x_2, \dots, x_m, y_1, y_2, \dots, y_m)}{\Delta y_1} \quad (4.23)$$

$$\frac{\partial x_1}{\partial \kappa_1} \simeq \frac{x_1(\kappa_0, \kappa_1 + \Delta \kappa_1, \kappa_2, \dots, \kappa_n, s_0, s_1, s_2, \dots, s_n) - x_1(\kappa_0, \kappa_1, \kappa_2, \dots, \kappa_n, s_0, s_1, s_2, \dots, s_n)}{\Delta \kappa_1} \quad (4.24)$$

$$\text{and } \frac{\partial y_1}{\partial \kappa_1} \simeq \frac{y_1(\kappa_0, \kappa_1 + \Delta \kappa_1, \kappa_2, \dots, \kappa_n, s_0, s_1, s_2, \dots, s_n) - y_1(\kappa_0, \kappa_1, \kappa_2, \dots, \kappa_n, s_0, s_1, s_2, \dots, s_n)}{\Delta \kappa_1} \quad (4.25)$$

Similarly, the same concept could be used for the other shape design variables.

If more than one shape design variable is perturbed simultaneously, for example  $\kappa_1$  and  $s_1$  then the net effect on the frontal-area (i.e. objective function) would be determined as follows.

$$d\Phi = \sum_{j=0}^n \left( \frac{\partial \Phi}{\partial \kappa_j} \right) \Delta \kappa_j + \sum_{j=0}^n \left( \frac{\partial \Phi}{\partial s_j} \right) \Delta s_j. \quad (4.26)$$

The value of  $d\Phi$  gives the total change of  $\Phi$  w.r.t the simultaneous variation of  $\kappa_1$  and  $s_1$ . The same concept could be extended to  $n$ -shape design variables. This sensitivity procedure has been implemented on a numerical example of an elastic ring under diametral compression in Chapter 5.

#### 4.5 Comparison and Efficiency of Proposed Method

As mentioned at the outset of this Chapter, the interactive graphics capabilities integrated with the proposed shape optimization cycle is prudent to allow designer interaction in the Computer Aided Design (CAD) process. Such a dialogue can be very beneficial, saving computer and human resources.

In general purpose design optimization methodology needs the following information about the problem to be solved : (i) input data such as number of design variables, number of constraints, etc. (ii) the cost and constraint functions (iii) gradient of cost and constraint functions. If the gradients are not available system should automatically approximate them by a finite difference method. If there is a mistake in the input data or problem definition, error will occur in the problem-solving procedure. The optimization system should take care of such mistakes as much as possible. In contrast, the interactive graphics capabilities developed on SUN-workstation and HP 9000/800-series workstation with UNIX-platform together with intrinsic geometry based shape synthesis, automatic boundary element mesh generation and refinement, BEM analysis, and numerical optimization programming modules makes the shape optimization cycle more attractive. The introduction of multi-window concept makes the intrinsic shape definition more versatile. This is due to the fact that the effect of changes in the intrinsic space can be seen immediately in the cartesian space, thus it gives real feeling of the shape to the designer. In addition, the interactive capabilities include : Design history of cost function, constraint functions, design variables, maximum constraint violation, convergence parameter would be monitored. Since, the interactive environment developed in this approach, especially graphical display can be of great help in certain decision making during design process.

Since the computational cost of shape optimization is very sensitive to the number of shape design variables needed to define the boundary geometry, the number of SDVs can be kept to a minimum using intrinsic shape synthesis approach compared to Bezier or B-spline and Hermitian cubic spline functions. Hence, it can be said that intrinsic form provides flexible and compact geometric capability to the designer.

The strategy that has been adopted in this research involves mapping the geometry from intrinsic to cartesian domain and then interpolating to quadratic boundary elements for BEM stress analysis purpose. There is no direct relation between cartesian co-ordinates obtained after intrinsic-cartesian mapping and the boundary element nodes, although in some cases they may happen to coincide.

The number of iterations required via zero-order method in the proposed shape optimization cycle is slightly more than the number of iterations required in the reviewed methods of shape optimization using B-spline or Hermitian geometric representation

and BEM analysis. Whereas, the first-order proposed method requires less number of iterations when compared to the methods based on B-spline or Hermitian geometric representation and BEM analysis. The present methodology tackles the linear and non-linear objective functions and side and behavioural constraints.

The total computational (CPU) time required for the proposed shape optimization cycle vary from six to seven hours on SUN-workstation depending upon the nature of the problem and the initial geometry.

The proposed shape optimization methodology can be applied to a broad range of applications in order to show its effectiveness over the parametric approach. The computer programs developed based on the above mentioned shape optimization methodology include: Non-linear Equation solver, Numerical Integration module, An Automatic Boundary Element Mesh generation and refinement module, Boundary Element Analysis for Design (BEAD), and Zero-order (or First-order) NLP optimizer makes the software elegant for 2-D elastostatic problems characterized by plane-stress, plane-strain, and axisymmetric cases. It deserves particular acclaim in its ability to get results in low number of cycles, few analyses of small dimensionality, and proper use of reliable optimization algorithms, capable of making best use of approximation concepts in minimizing the per step optimization problem size.

Aside from the above built in efficiency properties, it is however, to be noted, that the proposed separation of shape synthesis module from the analysis model, allows the designer to make a judicious choice in defining the shape via simple intrinsic forms and low number of design variables, while at the same time using a highly refined analysis model for sufficient accuracy of the performance of the end results. Therefore, the matter of overall efficiency of the performance of the proposed CAD approach, remains to a great extent in the hands of the designer.

---

## CASE STUDIES VIA ZERO-ORDER METHOD

---

### 5.1 Computer Software Development

The intrinsic definition of a curve or a surface seems to suffer from a handicap that one doesn't get the feel of the geometry explicitly. In order to eliminate this drawback of intrinsic geometry a multi-window platform has been developed using SUN-view graphics on SUN-workstation and STARBASE graphics on HP 9000/800-series workstation. The programs have been written in C-language. In addition to the graphics environment created as said above, number of programs for non-linear equation solver, numerical integration, shape synthesizer, automatic boundary element mesh generation and refinement, Boundary Element Analysis for Design (BEAD), and NLP optimizer have been developed in C and FORTRAN 77 languages. The linking between C and FORTRAN 77 has been carried out via system calls in Unix-environment. The illustrative examples described in this Chapter are modelled using either 2-LINCEs model (R-R model) or 3-LINCEs model (R-R-R model) and are characterized by 2-D elastostatic plane-stress or plane-strain case. Shape optimization is carried out for minimum weight design problems. Grapher and ANSYS/FEM packages have been used for plotting stress versus node number graphs and colour stress plots respectively. Also, number of C-programs have been developed based on sensitivity procedures explained in Chapter 3 and Chapter 4.

### 5.2 Illustrative Examples

Based on the proposed shape optimization methodology via zero-order method (exhaustive search method) practical engineering problems include: (i) A thick cylinder subjected to a constant internal pressure, (ii) an elastic ring under diametral compression, (iii) a torque arm subjected to an axial and transverse loading, (iv) a fillet under an axial load, and (v) a ladle hook subjected to a tensile load have successfully been implemented. The sensitivity analysis has been carried out for an elastic ring problem.

$\Phi_1$  - Area bounded by the outer curve E-F (for a quadrant section) =  $\frac{\pi}{4}(\text{radius of the outer boundary})^2$ .

$\tau_{max}$  - Peak value of Von-Mises stress at the surface boundary.

$\tau_{all}$  - Allowable stress or Yield stress of the component.

Optimal shape has been obtained using shape optimization algorithm explained in Section 4.2. From Figure 5.3(b) the shape design variables related to initial shape including:  $\kappa_0 = -13.3333$ ;  $s_0 = 0.0$ ;  $\kappa_1 = -13.3333$ ;  $s_1 = 0.0589048$ ;  $\kappa_2 = -13.3333$ ; and  $s_2 = 0.1178097$ . The Figure 5.4(b) shows optimal shape related to SDVs including:  $\kappa_0 = -13.3333$ ;  $s_0 = 0.0$ ;  $\kappa_1 = -10.405382$ ;  $s_1 = 0.04$ ;  $\kappa_2 = -16.134596$ ; and  $s_2 = 0.122595$ . The frontal-area (i.e. objective function) has been reduced 10.34% from the uniform thick cylinder, with the inner radius the same as the smallest in optimum.

### 5.2.2 An Elastic Ring Problem

This example shows an elastic ring under diametral compression. Taking the advantage of symmetry, one quarter of the ring is modelled, as shown in Figure 5.9(a). Young's modulus, Poisson's ratio and the allowable stress are 2338 MPa, 0.38, and 18 MPa respectively. The boundary  $\Gamma_1$  (i.e. curve A-B) is varied in the search direction by selecting a suitable shape model such that stress constraints are satisfied. The point B or C is assumed to be free to move horizontally in this problem, as shown in Figure 5.9. The other boundaries  $\Gamma_3$  (i.e. curve E-F) and  $\Gamma_4$  (i.e. curve F-G) are assumed to be fixed. The stress analysis is done for the plane-strain condition. Figure 5.9(b) shows quadratic boundary element model with 100 nodes and 50 elements.

The shape model chosen in order to vary the curve A-B to be of 2-LINCEs model (R-R model) with  $\kappa_1$  and  $s_1$  as free shape design variables. The formulation of the above problem can be stated as follows.

Minimize

$$\Phi = \Phi_1 - \frac{1}{2} \left[ \int_{s_0}^{s_1} \frac{1}{\left\{ \left( \frac{\kappa_1 - \kappa_0}{s_1 - s_0} \right) (s - s_0) + \kappa_0 \right\}} ds + \int_{s_1}^{s_2} \frac{1}{\left\{ \left( \frac{\kappa_2 - \kappa_1}{s_2 - s_1} \right) (s - s_1) + \kappa_1 \right\}} ds \right] \quad (5.3)$$

subject to

$$\tau_{max} - \tau_{all} \leq 0 \quad (5.4)$$

where

$\Phi$  - Defines the frontal-area of the surface boundary of a component (for quadrant section).

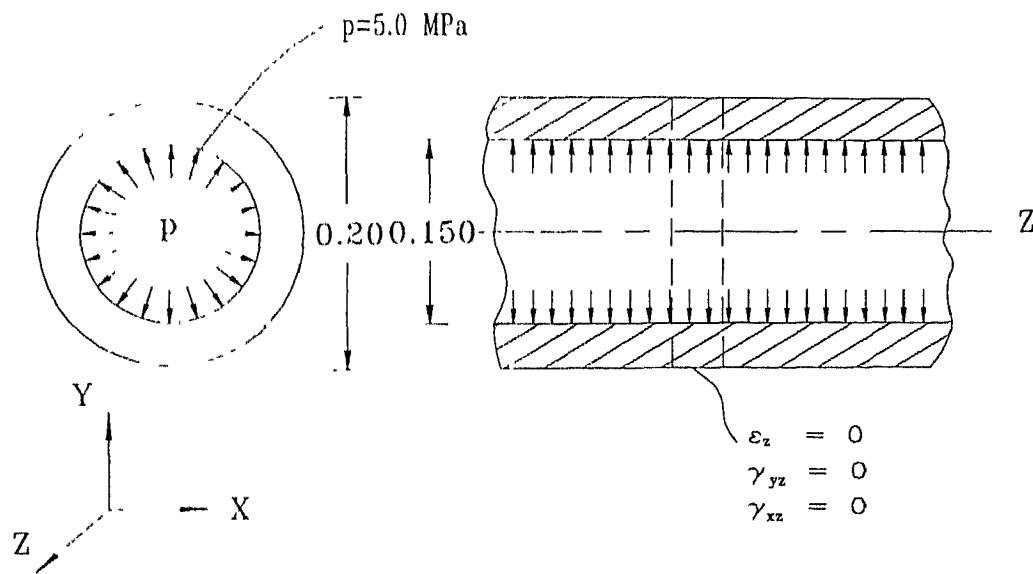
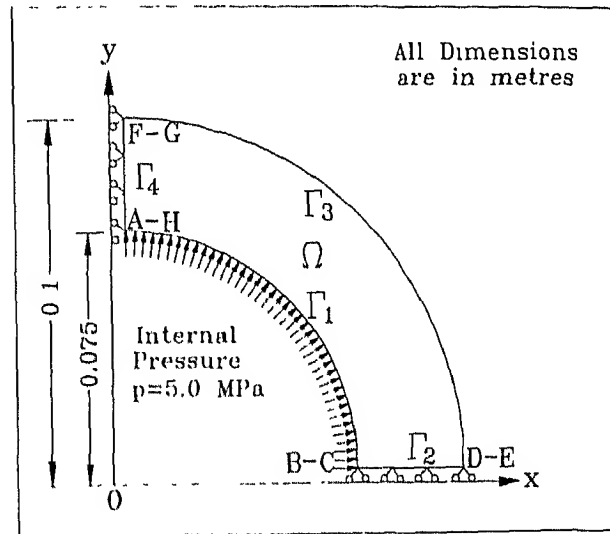


Figure 5.1 Thick Cylinder Subjected to an Internal Pressure.

(a)



(b)

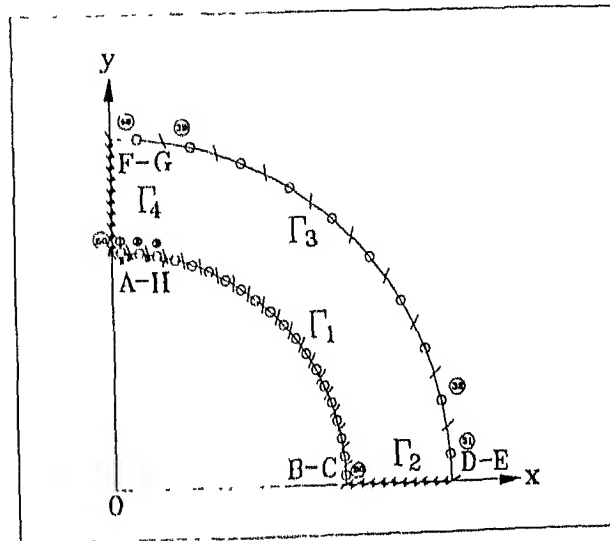
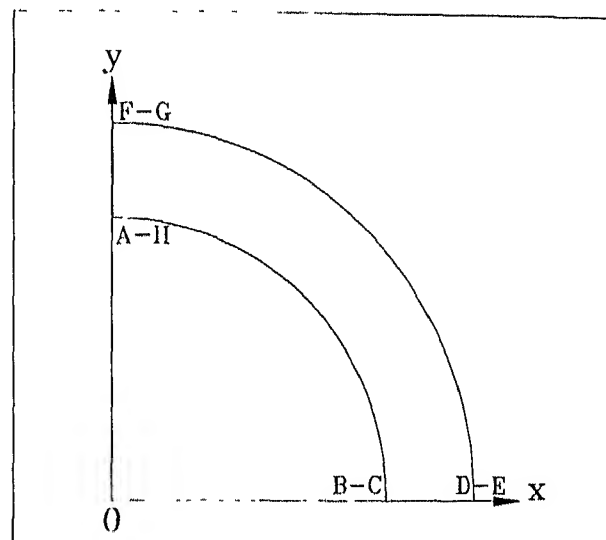


Figure 5.2 (a) Definition of a Thick Cylinder Problem with Displacement and Stress Boundary Conditions.  
 (b) Boundary Element Mesh for a Thick Cylinder Problem.

(a)



(b)

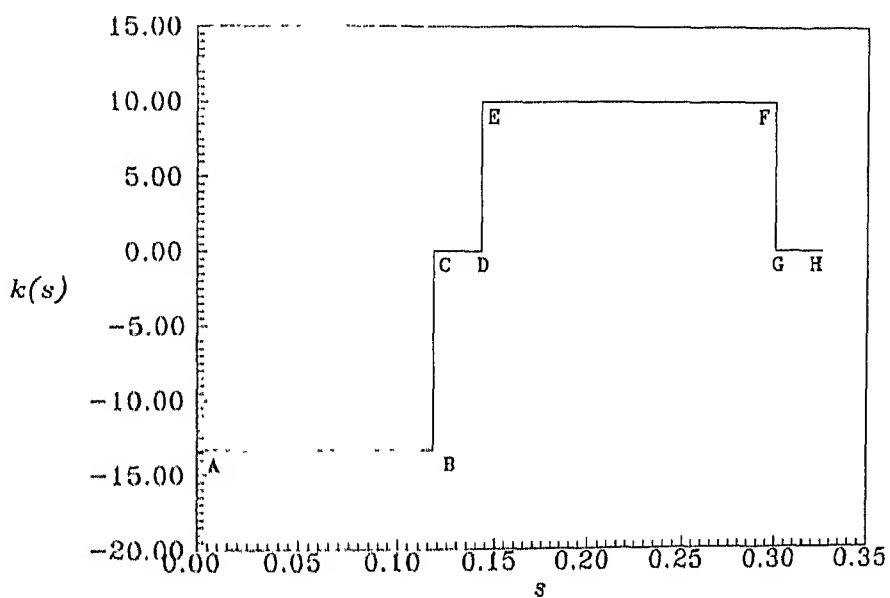
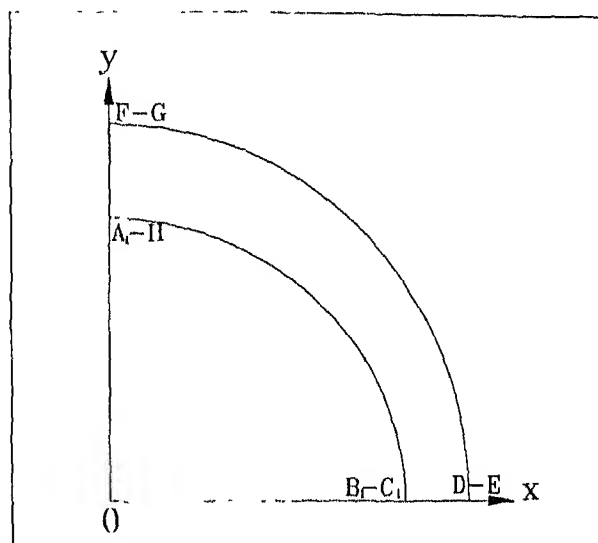


Figure 5.3 (a) Cartesian Profile for the Initial Shape of a Thick Cylinder.

(b) Intrinsic Profile for the Initial Shape of a Thick Cylinder.

(a)



(b)

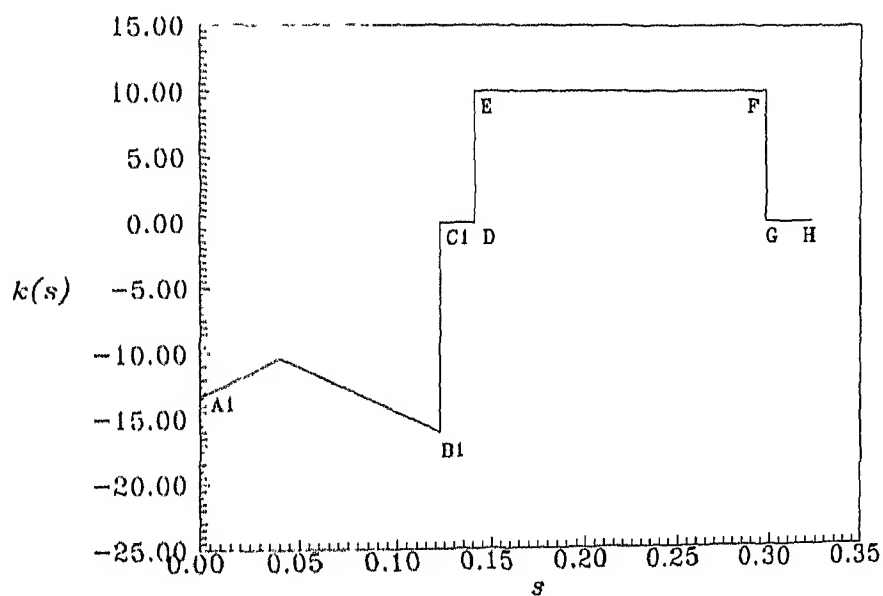


Figure 5.4 (a) Cartesian Profile for the Optimal Shape of a Thick Cylinder.

(b) Intrinsic Profile for the Optimal Shape of a Thick Cylinder.

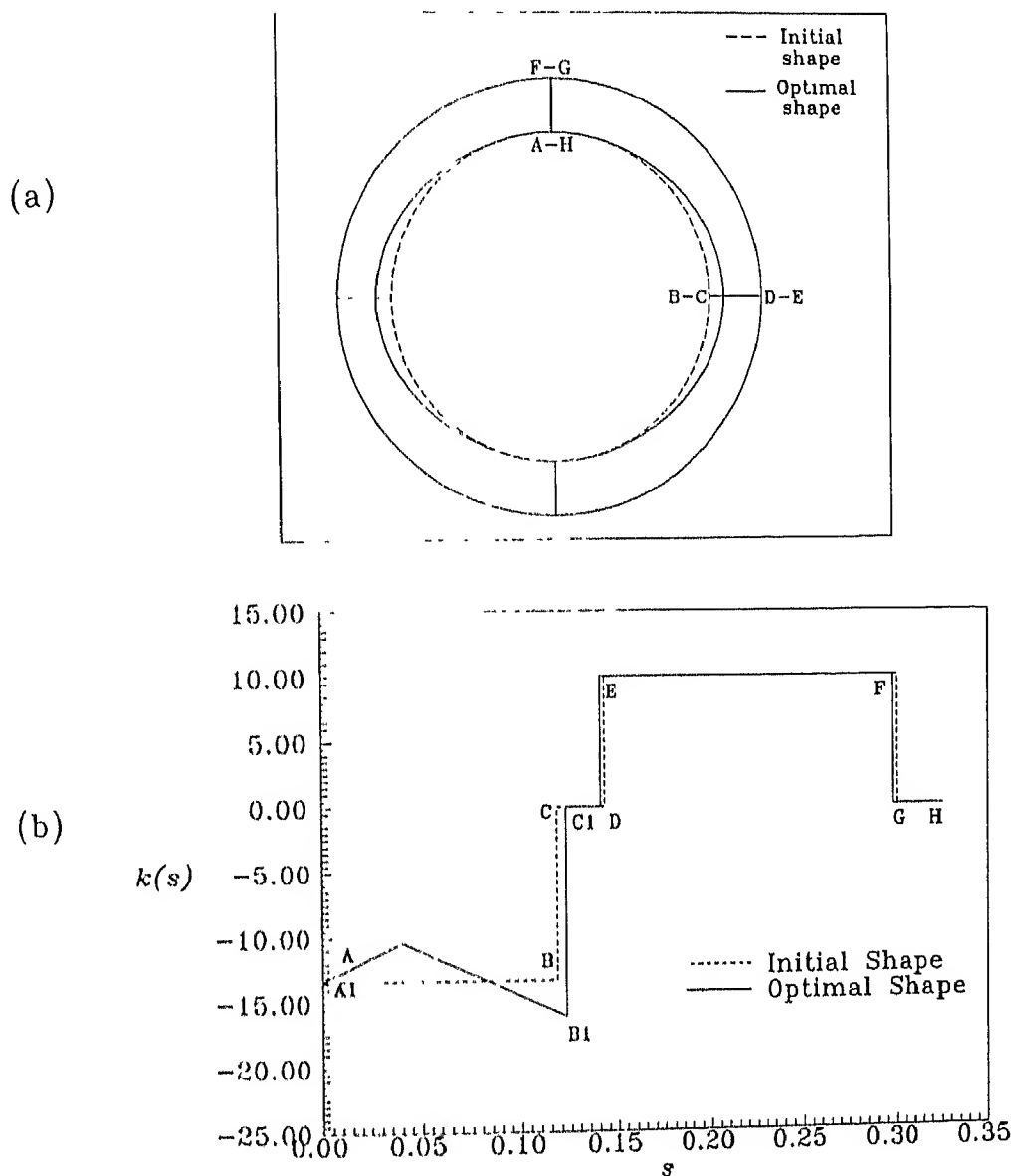


Figure 5.5 (a) Cartesian Profiles of Initial and Optimal Shapes of a Thick Cylinder.  
 (b) Intrinsic Profiles of Initial and Optimal Shapes of a Thick Cylinder.

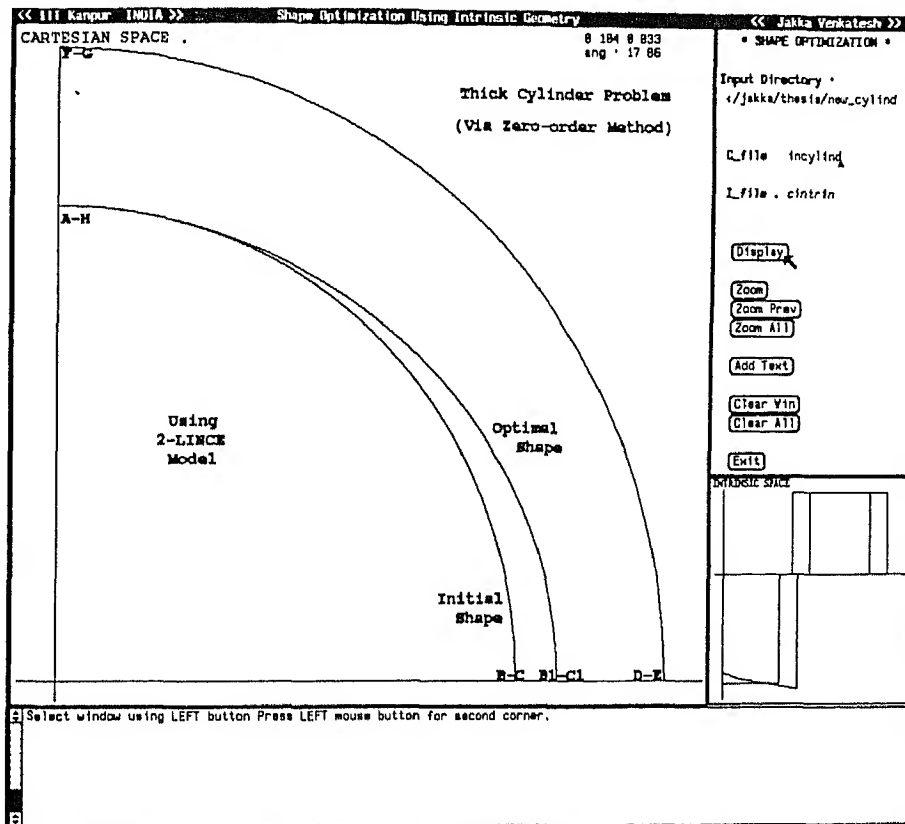


Figure 5.6 Cartesian and Intrinsic Profiles of Initial and Optimal Shapes of a Thick Cylinder on a Multi-Window SUN-view Graphics Environment.

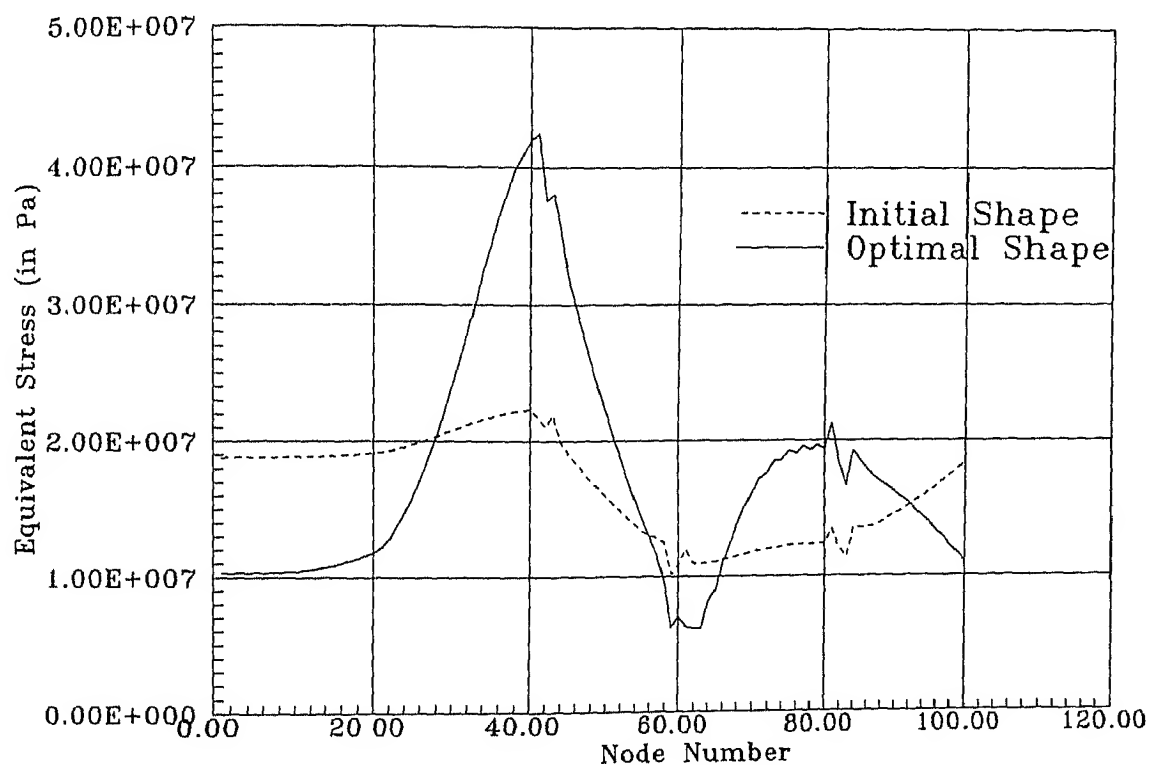
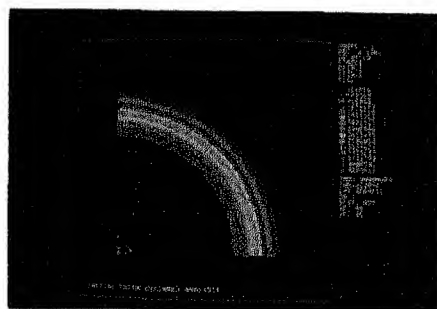


Figure 5.7 Equivalent Stress Vs Node Number along the Boundary of a Thick Cylinder.

(a)



(b)

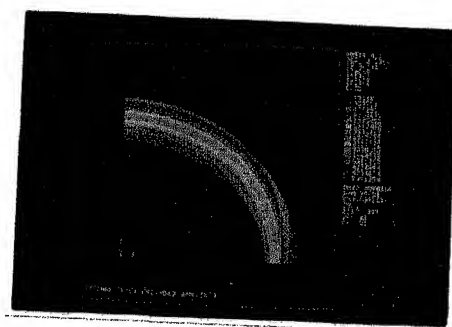


Figure 5.8 (a) Colour Stress Plot for an Initial Shape of a Thick Cylinder.  
(b) Colour Stress Plot for an Optimal Shape of a Thick Cylinder.

$\Phi_1$  - Area bounded by the outer curve E-F (for a quadrant section) =  $\frac{\pi}{4}(\text{radius of the outer boundary})^2$ .

$\tau_{max}$  - Peak value of Von-Mises stress at the surface boundary.

$\tau_{all}$  - Allowable stress or yield stress of the component.

Optimal shape has been obtained using shape optimization algorithm explained in Section 4.2. From Figure 5.10(b) the shape design variables related to initial shape including:  $\kappa_0 = -26.315789$ ;  $s_0 = 0.0$ ;  $\kappa_1 = -26.315789$ ;  $s_1 = 0.0298451$ ;  $\kappa_2 = -26.315789$ ; and  $s_2 = 0.0596902$ . And the Figure 5.11(b) shows SDVs related to an optimal shape include :  $\kappa_0 = -20.315789$ ;  $s_0 = 0.0$ ;  $\kappa_1 = -16.797924$ ;  $s_1 = 0.0120$ ;  $\kappa_2 = -33.063226$ ; and  $s_2 = 0.078075$ . The frontal-area (i.e. objective function) has been reduced 17.9% from the uniform ring section, with the inner radius the same as the smallest in optimum.

Figure 5.10(a) and (b) shows cartesian and intrinsic profiles for an initial shape of an elastic ring. Cartesian and intrinsic profiles of an optimal shape are shown in Figure 5.11(a) and (b). The cartesian and intrinsic profiles of an initial and optimal shapes together are included in the Figure 5.12(a) and (b) respectively.

Figure 5.13, show design history of an elastic ring in SUN-view graphics environment. Cartesian and intrinsic geometries of an elastic ring corresponding to initial and optimal shapes in a multi-window SUN-view graphics environment has been shown in Figure 5.14.

Von-Mises Equivalent stress versus Node number graphic plots of initial and optimal shapes are shown in Figure 5.15. The colour stress plots belong to initial and optimal shapes of an elastic ring problem have been shown in Figure 5.16.

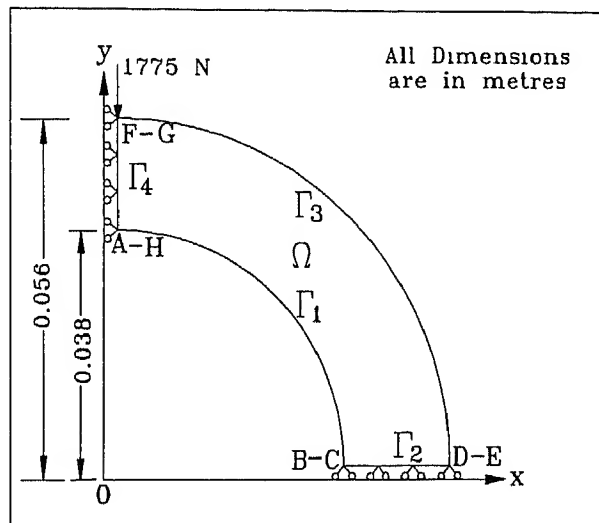
### 5.2.3 A Torque Arm Problem

The torque arm in Figure 5.17(a) has been optimized for minimum weight (i.e. minimization of frontal-area) according to the shape optimization procedure described in Section 4.2. The hole shown at the bigger end is where the device is fastened to the support taken with zero displacements, while the applied load is extended at the hole in the smaller end where force boundary conditions are given. The magnitude of the applied loads, allowable stresses and material properties are also given in Figure 5.17(a).

The objective is to minimize the weight of the arm by keeping the thickness of the material constant and finding the most suitable shape offering proper distribution of material, for the most efficient load carrying capacity.

Clearly, the problem is a plane-stress case and it is modelled with quadratic boundary elements. The whole boundary is divided into 80 elements and 160 nodes. Figure 5.17(b)

(a)



(b)

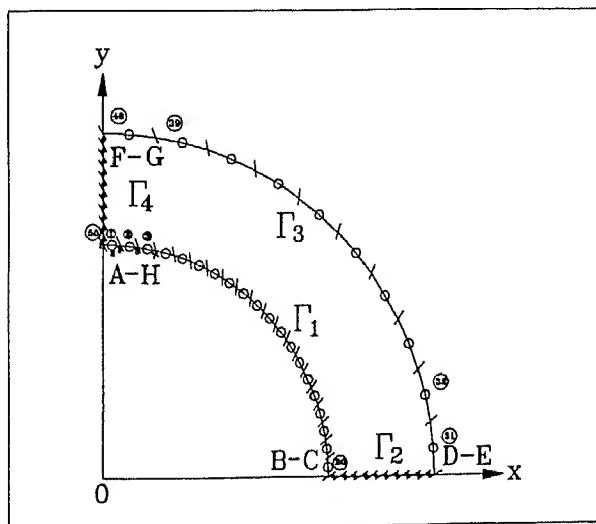
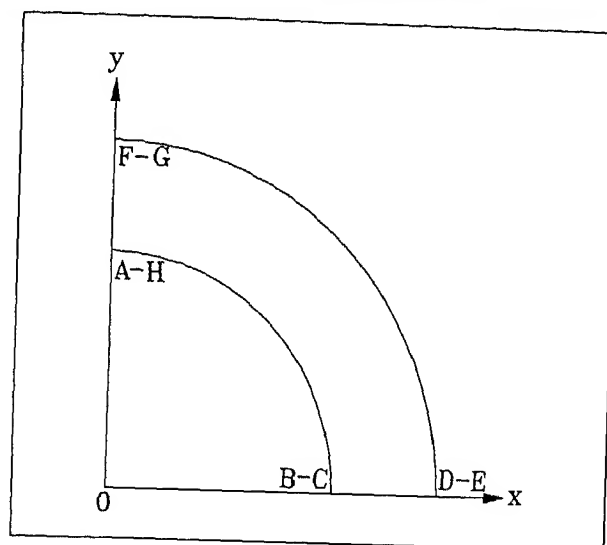


Figure 5.9 (a) Definition of An Elastic Ring Problem with Displacement and Stress Boundary Conditions.

(b) Boundary Element Mesh for An Elastic Ring.

(a)



(b)

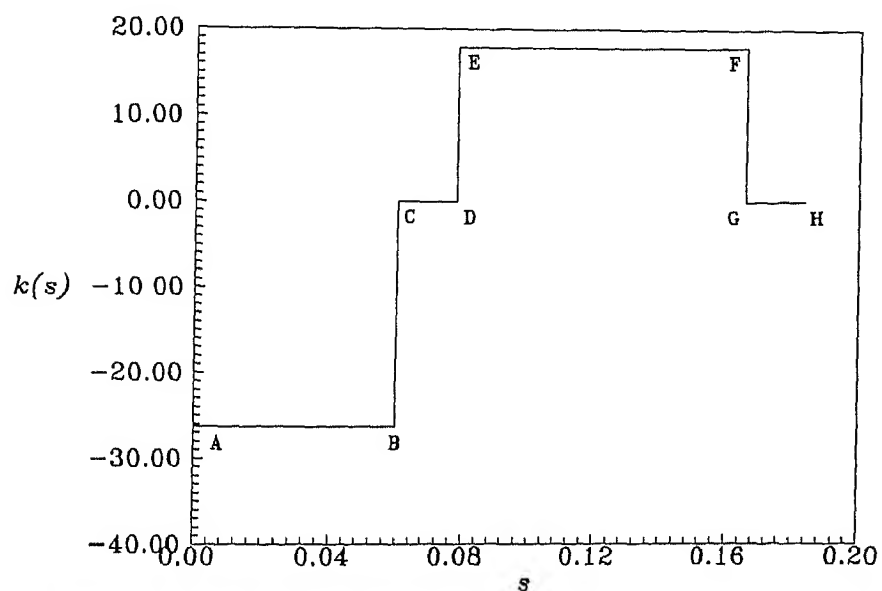
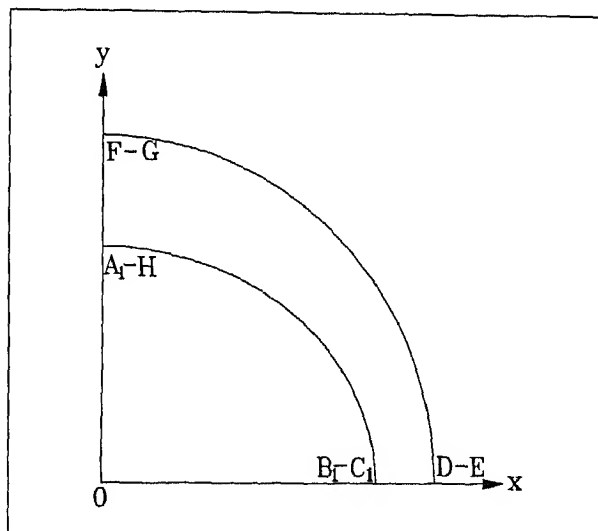


Figure 5.10 (a) Cartesian Profile for the Initial Shape of An Elastic Ring.  
 (b) Intrinsic Profile for the Initial Shape of An Elastic Ring.

(a)



(b)

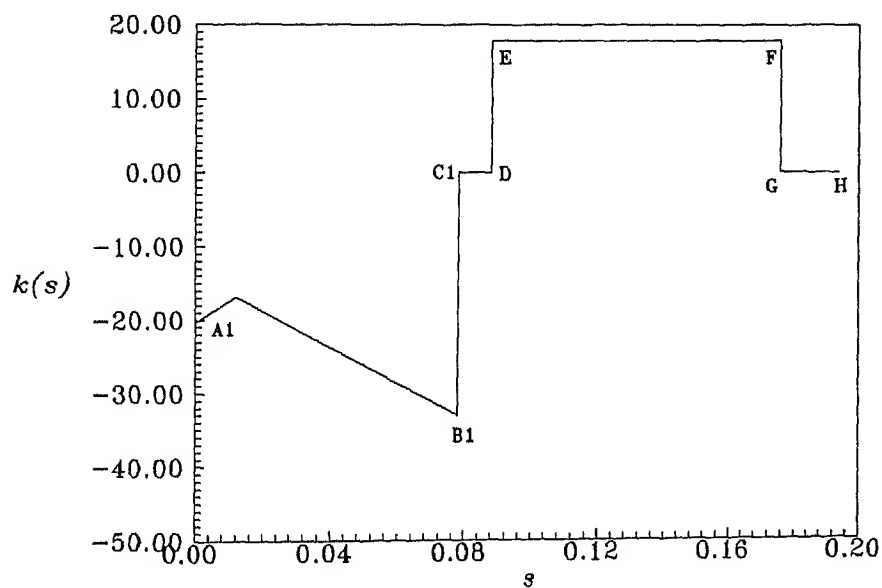


Figure 5.11 (a) Cartesian Profile for the Optimal Shape of An Elastic Ring.  
 (b) Intrinsic Profile for the Optimal Shape of An Elastic Ring.

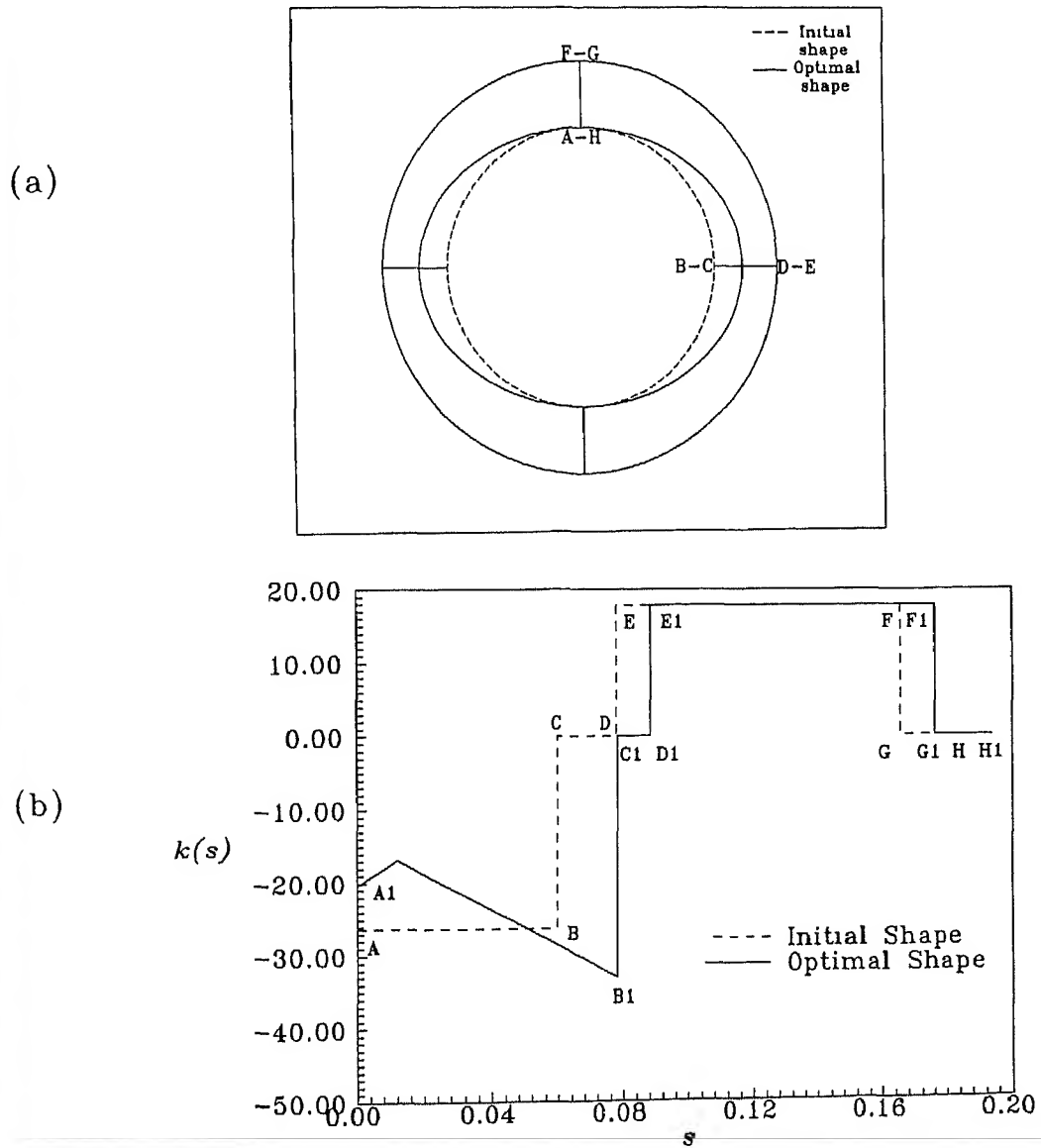
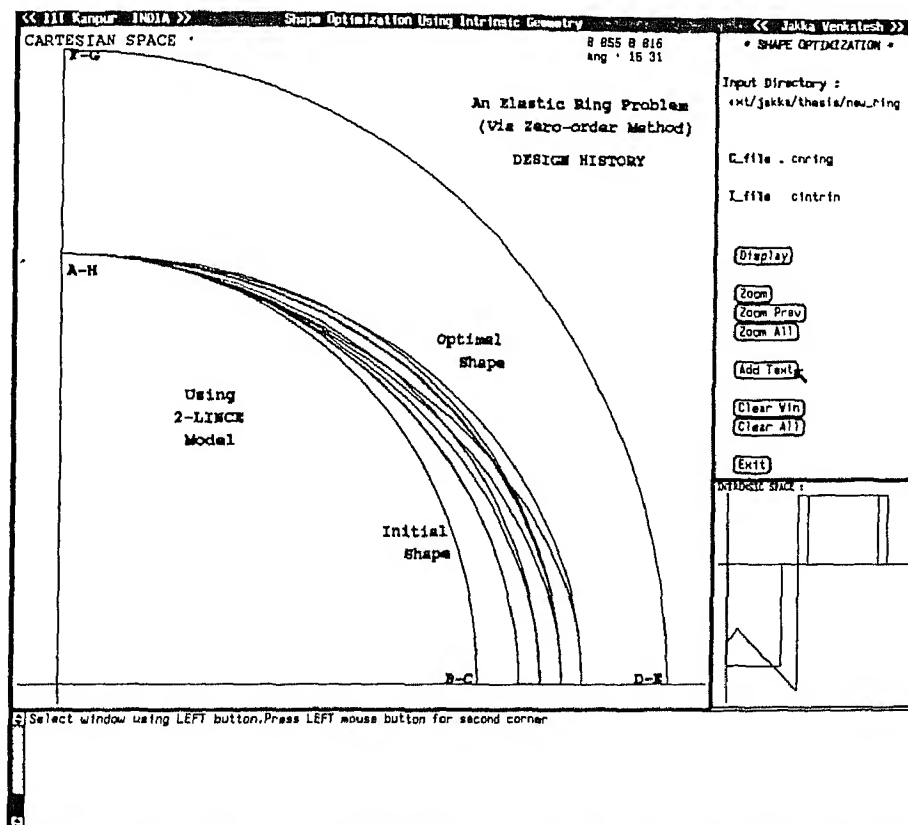


Figure 5.12 (a) Cartesian Profiles for the Initial and Optimal Shapes of An Elastic Ring.  
 (b) Intrinsic Profiles for the Initial and Optimal Shapes of An Elastic Ring.



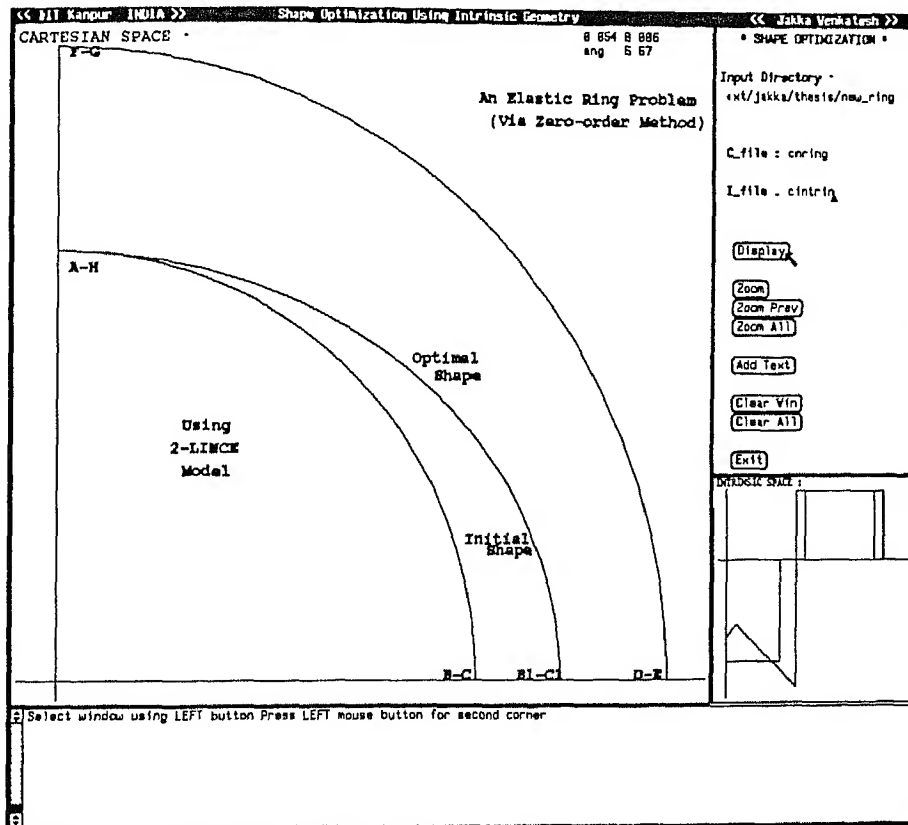


Figure 5.14 Cartesian and Intrinsic Profiles of An Elastic Ring on a Multi-Window SUN-view Graphics Environment.

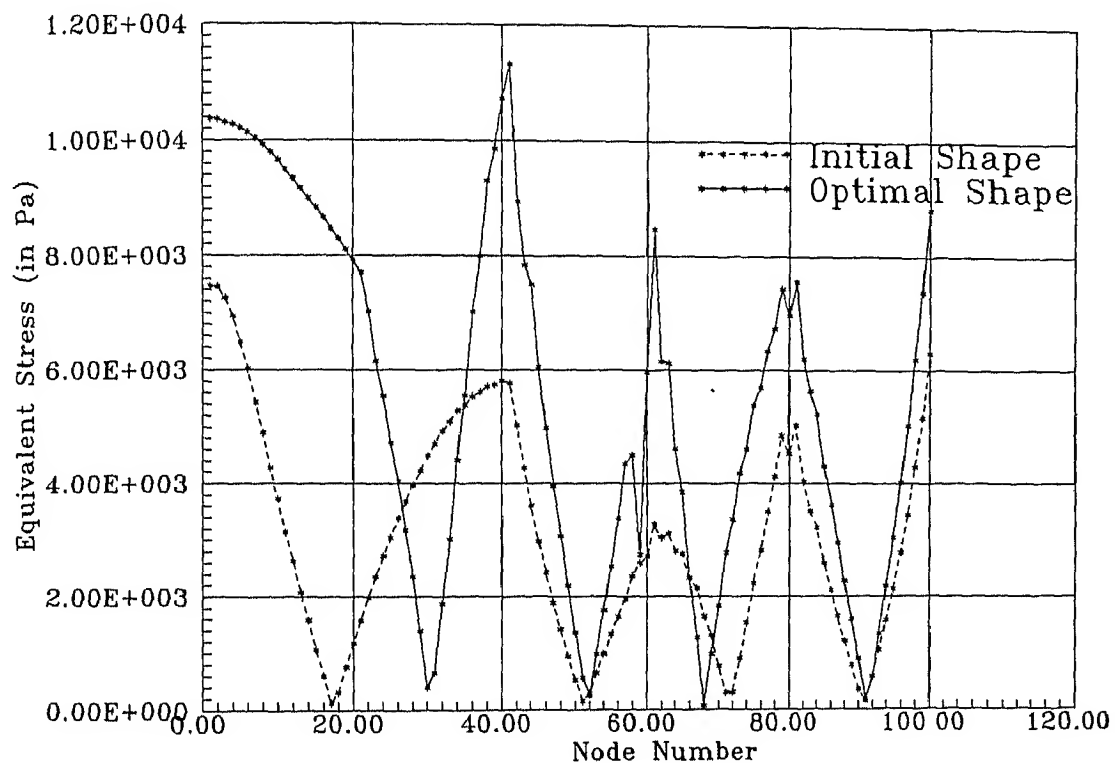
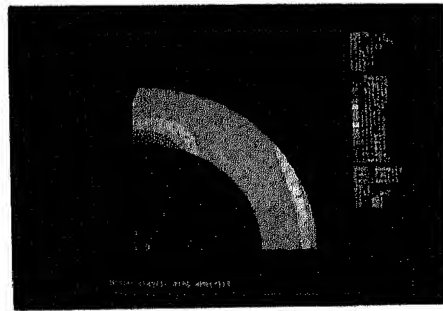


Figure 5.15 Graph Shows Equivalent Stress Vs Node Number along the Boundary of An Elastic Ring.

(a)



(b)

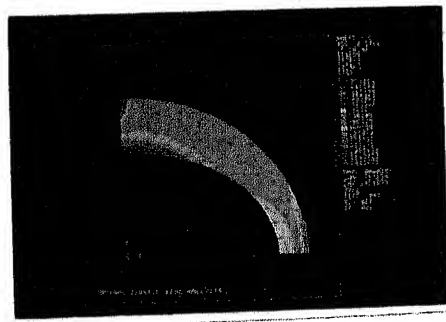


Figure 5.16 (a) Colour Stress Plot for an Initial Shape of An Elastic Ring.  
(b) Colour Stress Plot for an Optimal Shape of An Elastic Ring.

shows the boundary element mesh.

Allowing for the shape variations in the mid-section of the arm, located between the holes (i.e curve C-D and curve G-H). These two curves are modelled using 3-LINCEs model (R-R-R model) for each of the curves with suitable shape design variables. A limit on the maximum Von-Mises stress in an element is imposed. It is also to be noted that the modeling is to be done by keeping the holes and the semi-circular regions around the holes unchanged. The intrinsic SDVs related to an initial shape can be seen from the Figure 5.18(b) and the intrinsic SDVs related to an optimal shape are shown in Figure 5.19(b).

Starting from the shape given 5.18(a), and using the criterion for design as shown below.

Minimize

$$\Phi = \Phi(c_1, c_2, \dots, c_m(i_1, i_2, \dots, i_n)) \quad (5.5)$$

subject to

$$\tau_{max} - \tau_{all} \leq 0 \quad (5.6)$$

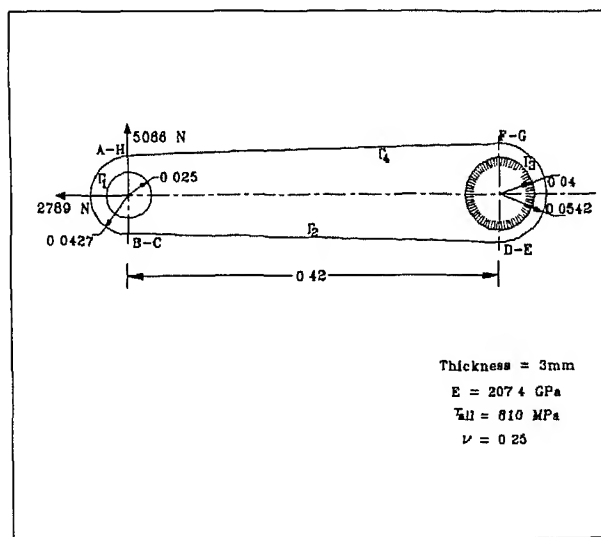
the design undergoes the process of changes according to the shape optimization methodology described in Section 4.2 and finally gives an optimal shape of the torque arm as shown in Figure 5.19(a). Figure 5.20(a) shows the cartesian profiles corresponding to initial and optimal shapes of the arm. The intrinsic profiles corresponding to initial and optimal shape of the arm are shown in Figure 5.20(b). The total of 45.6% reduction in frontal-area has been achieved.

In Figure 5.21 the cartesian and intrinsic profiles for initial and optimal shapes of the torque arm in a Multi-Window SUN-view graphics environment has been shown. The colour stress plots of initial and optimal shapes are shown in Figure 5.23.

#### 5.2.4 A Fillet Problem

It is required here to find the best shape of the fillet that makes a transition between two thicknesses of plate material connected in a butt joint. Figure 5.23(a) shows the problem with the tensile applied load and the material properties. A limit on the maximum Von-Mises stress in an element is imposed ( $\tau_{max}$ ). The objective function would be the area of material enclosed in the triangle ABC to be minimized. The BEM model is setup with 160 nodes, with 80 quadratic boundary elements, as shown in Figure

(a)



(b)

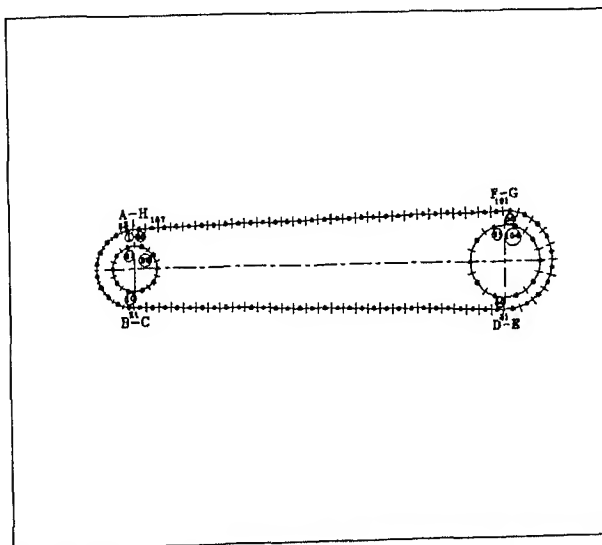
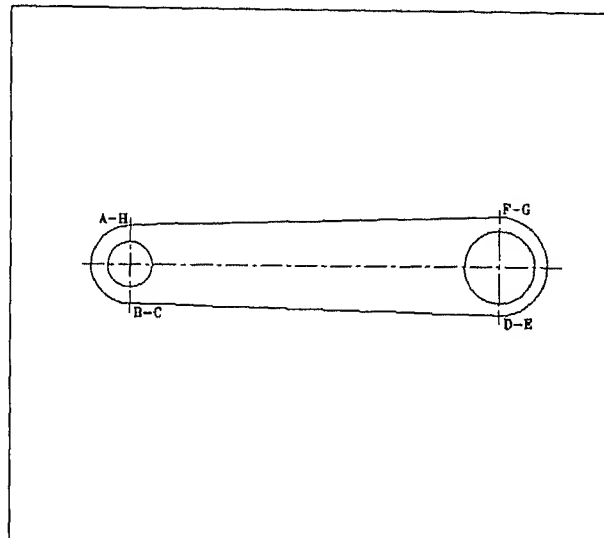


Figure 5.17 (a) Definition of a Torque Arm Design Problem with Displacement and Stress Boundary Conditions.  
 (b) Boundary Element Mesh for a Torque Arm.

(a)



(b)

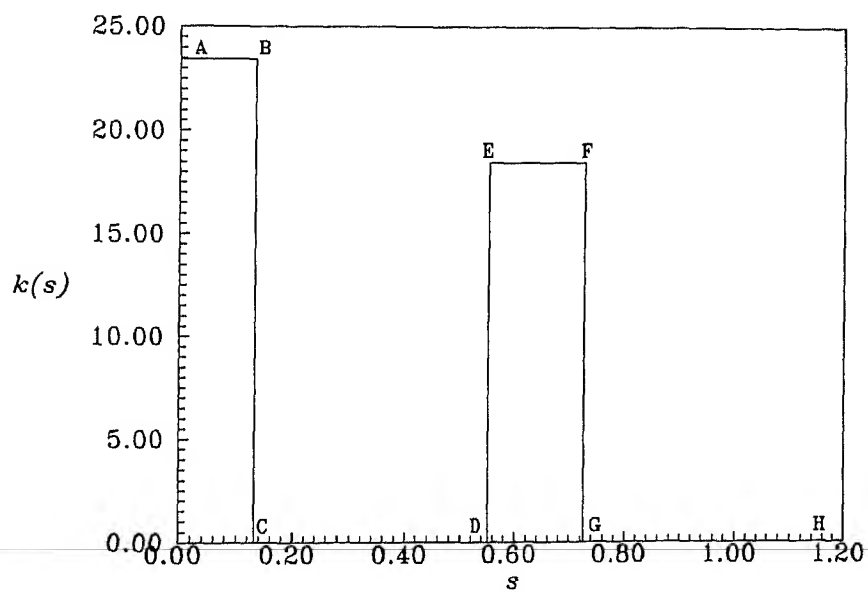
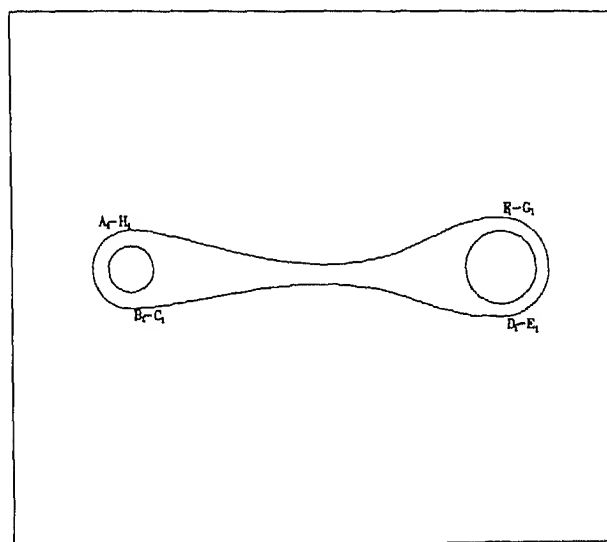


Figure 5.18 (a) Cartesian Profile for the Initial Shape of a Torque Arm.

(b) Intrinsic Profile for the Optimal Shape of a Torque Arm.

(a)



(b)

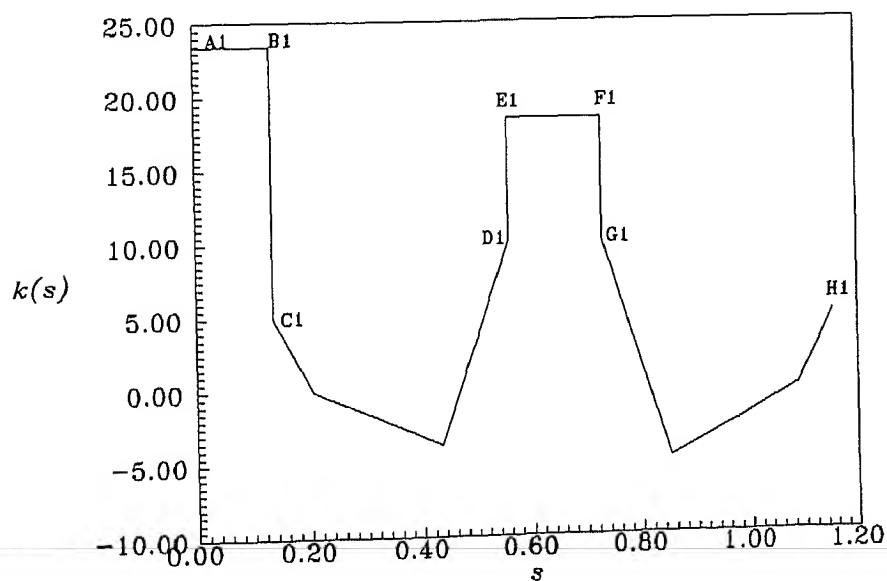
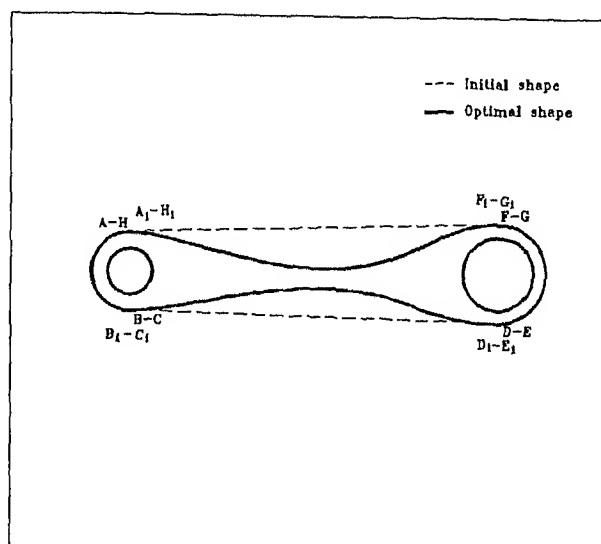


Figure 5.19 (a) Cartesian Profile for the Optimal Shape of a Torque Arm.  
 (b) Intrinsic Profile for the Optimal Shape of a Torque Arm.

(a)



(b)

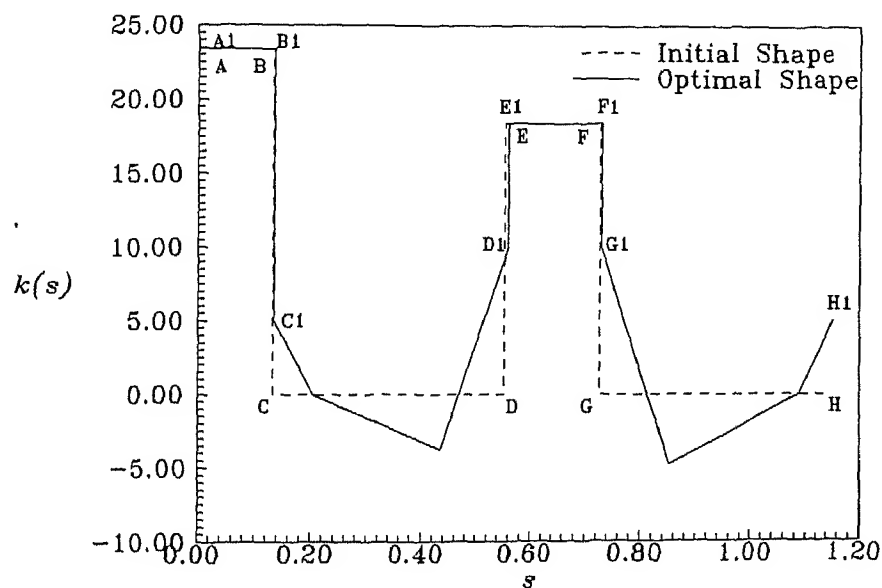


Figure 5.20 (a) Cartesian Profiles for the Initial and Optimal Shapes of a Torque Arm.

(b) Intrinsic Profiles for the Initial and Optimal Shapes of a Torque Arm.

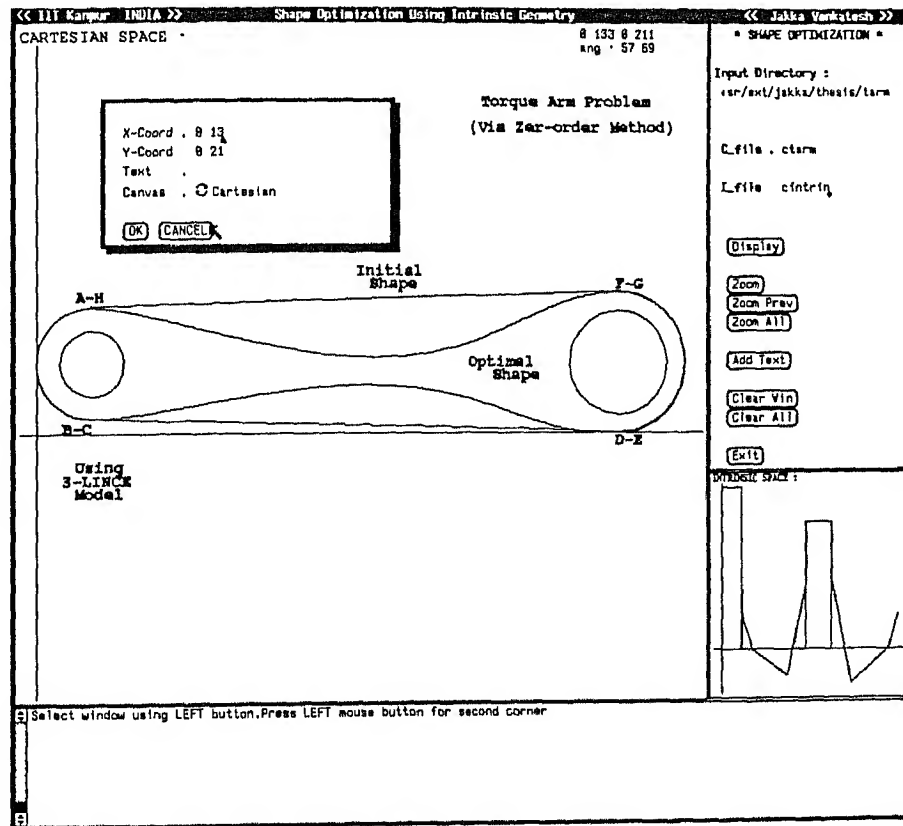
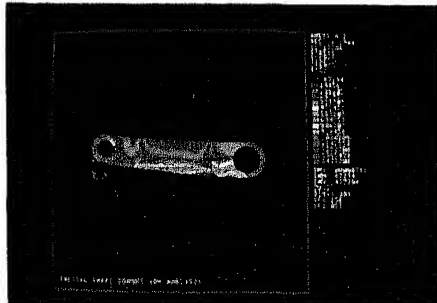


Figure 5.21 Cartesian and Intrinsic Profiles for the Initial and Optimal Shapes of a Torque Arm on a Multi-Window SUN-view Graphics Environment.

(a)



(b)

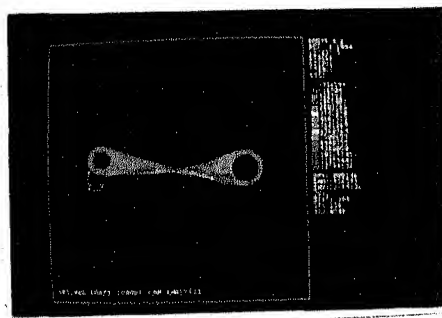


Figure 5.22 (a) Colour Stress Plot for an Initial Shape of a Torque Arm.  
(b) Colour Stress Plot for an Optimal Shape of a Torque Arm.

5.23(b). The applied load consists of 1777 N uniform on the cross-sectional net area. To define the shape of the transition section between fixed points A and B, a 3-LINCEs model (R-R-R model) is being used.

Formulation of the problem can be described as shown below.

Minimize

$$\Phi = \Phi(c_1, c_2, \dots, c_m(i_1, i_2, \dots, i_n)) \quad (5.7)$$

subject to

$$\frac{\tau_{max}}{\tau_{all}} - 1 \leq 0 \quad (5.8)$$

where

$\Phi$  - Frontal-area of the total cross-section of the plate-fillet joint assembly.

$\tau_{max}$  - Maximum Von-Mises stress at the surface boundary.

$\tau_{all}$  - Allowable stress of the fillet joint.

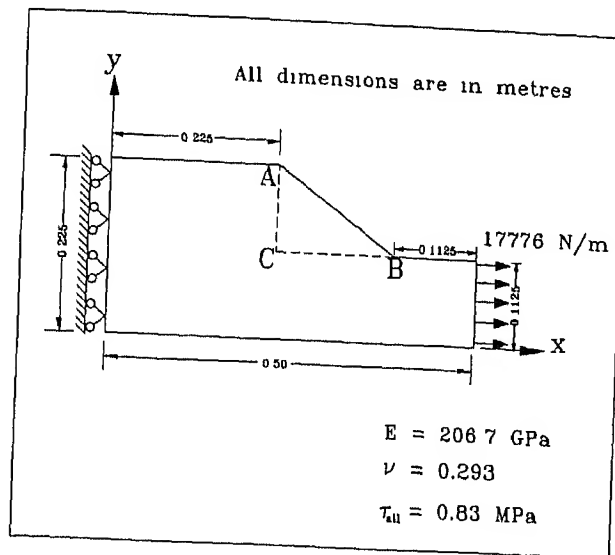
Figure 5.24(a) shows cartesian profile and Figure 5.24(b) shows intrinsic profile for an initial shape of a fillet. Cartesian and intrinsic profiles for an optimal shape are shown in Figure 5.25. Combined cartesian and intrinsic profiles for an initial and optimal shapes are shown in Figure 5.26. A multi-window SUN-view graphics environment with cartesian and intrinsic profiles of a fillet is shown in Figure 5.27. Colour stress plots corresponding to initial and optimal shapes are shown in Figure 5.28. A total 32.9% reduction in frontal-area of the fillet ABC has been achieved.

### 5.2.5 A Ladle Hook Problem

Application of the proposed shape optimization methodology for an elastic structural component is introduced as follows.

Consider the design of a hook for lifting hot metal ladles with minimum weight of 150 kN (hence the load on each hook is 75 kN). The dimensions of the critical elements of the hook (Figure 5.29 (a)) on the basis of stress, are presented by Dieter ([10]). These dimensions have been based on keeping the nominal stress at a level below 86.2 MPa. The remaining dimensions such as the bight section are set by engineering common sense.

(a)



(b)

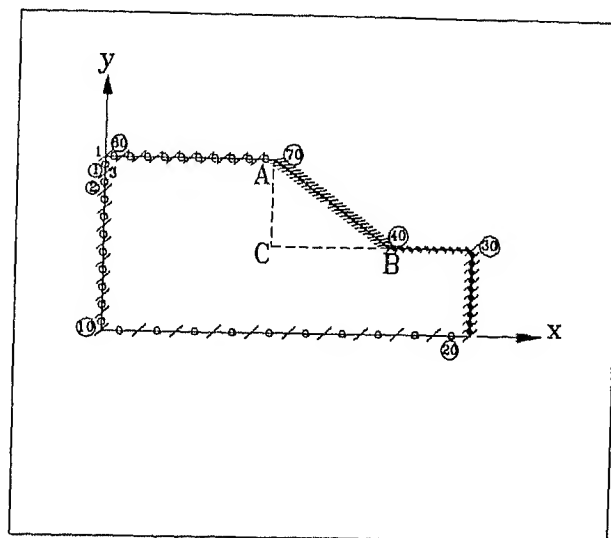
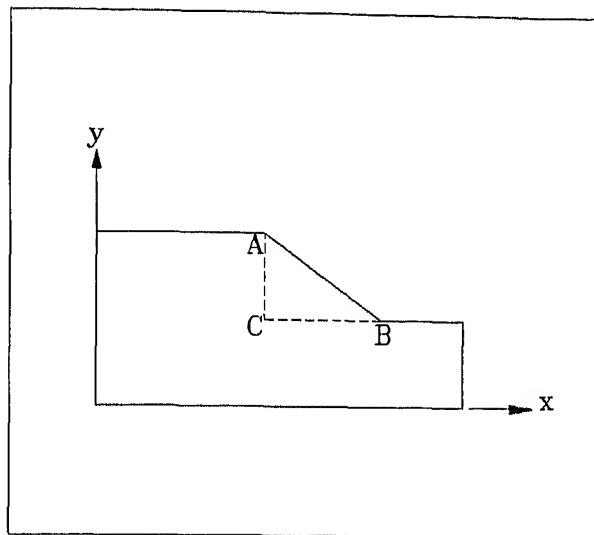


Figure 5.23 (a) Definition of a Fillet Problem with Displacement and Stress Boundary Conditions.

(b) Boundary Element Mesh for a Fillet Problem.

(a)



(b)

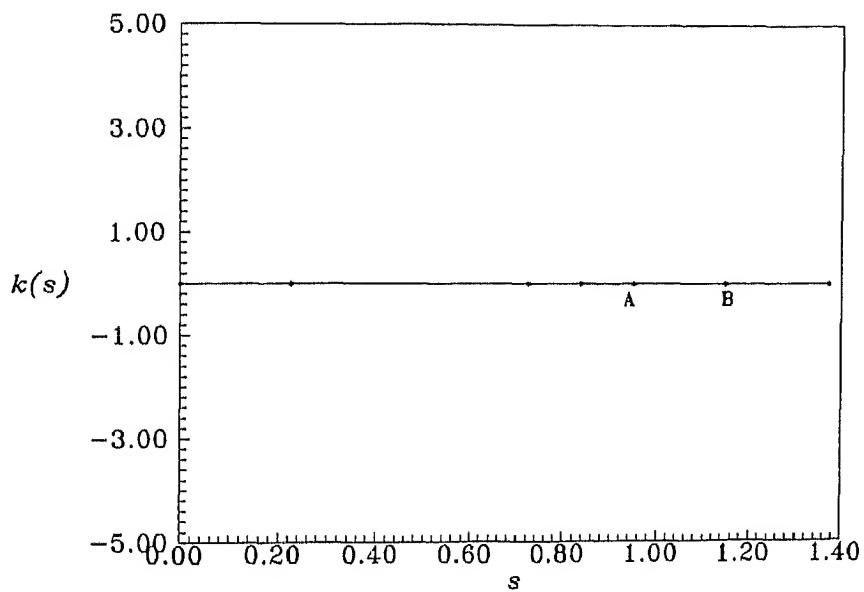
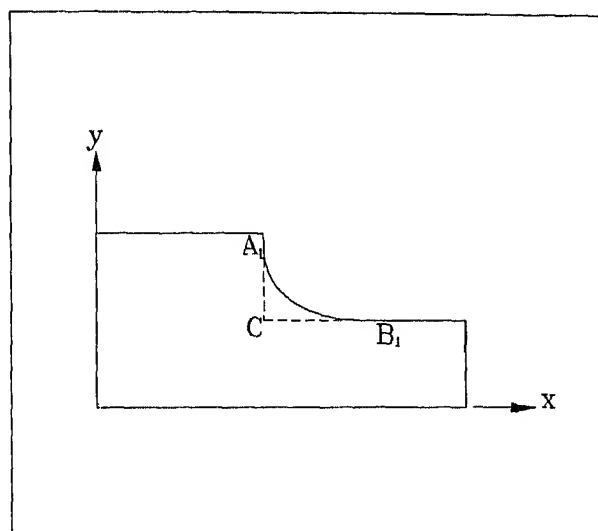


Figure 5.24 (a) Cartesian Profile for the Initial Shape of a Fillet.  
(b) Intrinsic Profile for the Initial Shape of a Fillet.

(a)



(b)

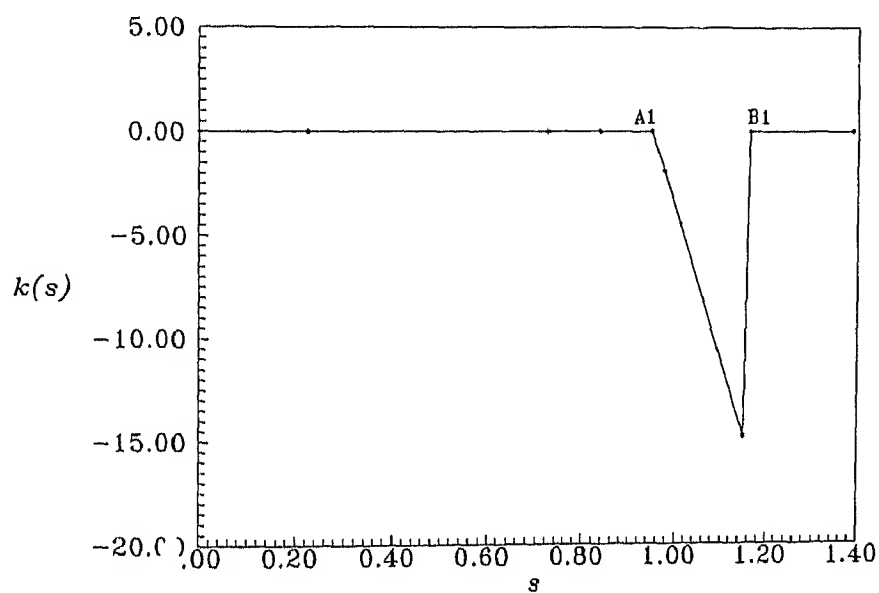
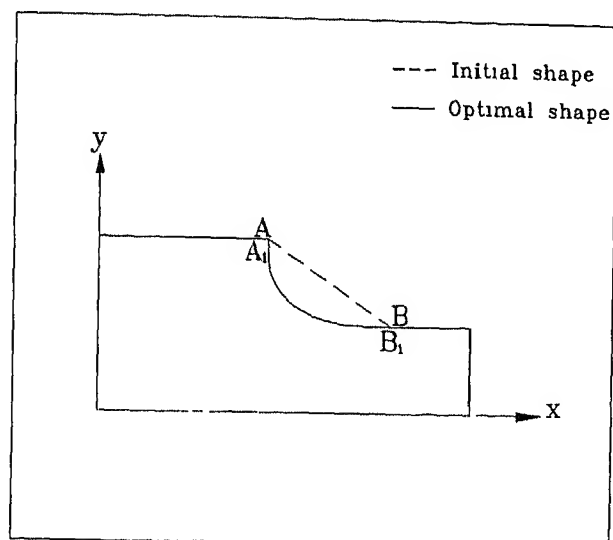


Figure 5.25 (a) Cartesian Profile for the Optimal Shape of a Fillet.

(b) Intrinsic Profile for the Optimal Shape of a Fillet.

(a)



(b)

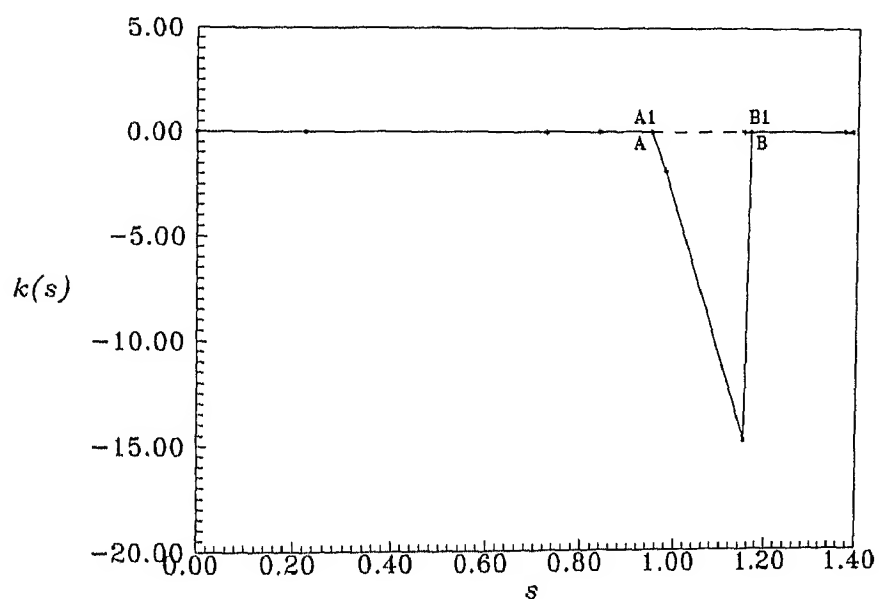


Figure 5.26 (a) Cartesian Profiles for the Initial and Optimal Shapes of a Fillet.  
 (b) Intrinsic Profiles for the Initial and Optimal Shapes of a Fillet.

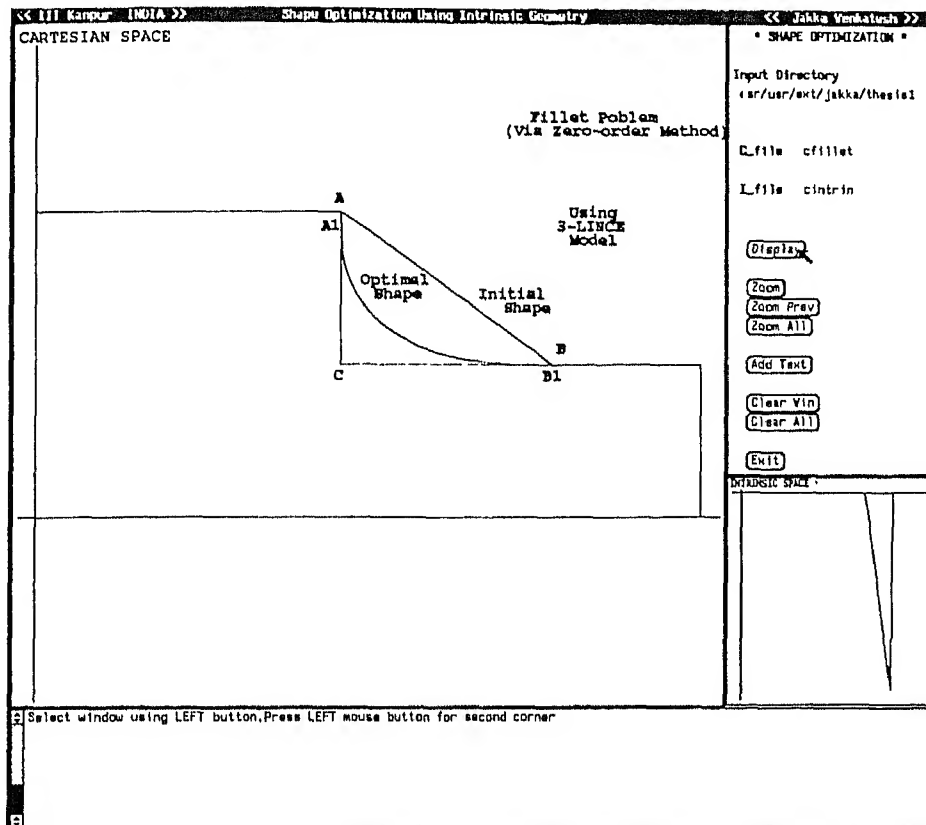
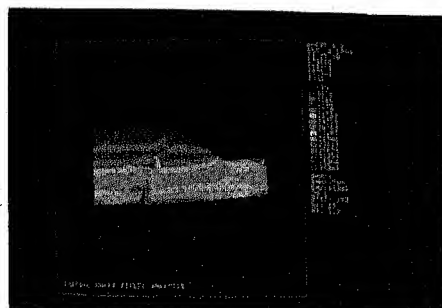


Figure 5.27 Cartesian and Intrinsic Profiles of a Fillet on a Multi-Window SUN-view Graphics Environment.

(a)



(b)

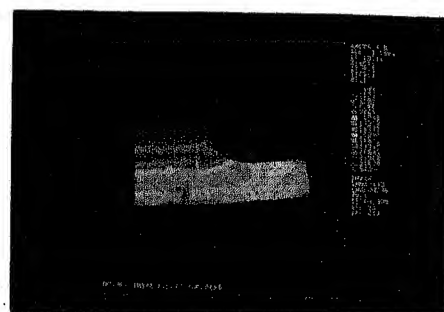
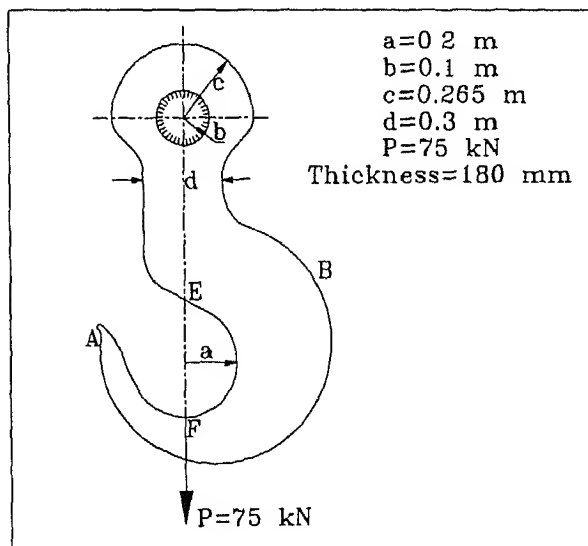


Figure 5.28 (a) Colour Stress Plot for an Initial Shape of a Fillet.  
(b) Colour Stress Plot for an Optimal Shape of a Fillet.

(a)



(b)

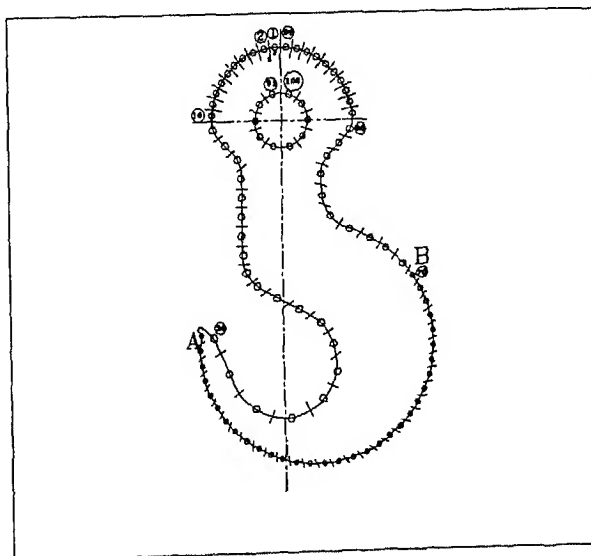


Figure 5.29 (a) Definition of the Ladle Hook Problem with Displacement and Stress Boundary Conditions.

(b) Boundary Element Mesh of a Ladle Hook Problem.

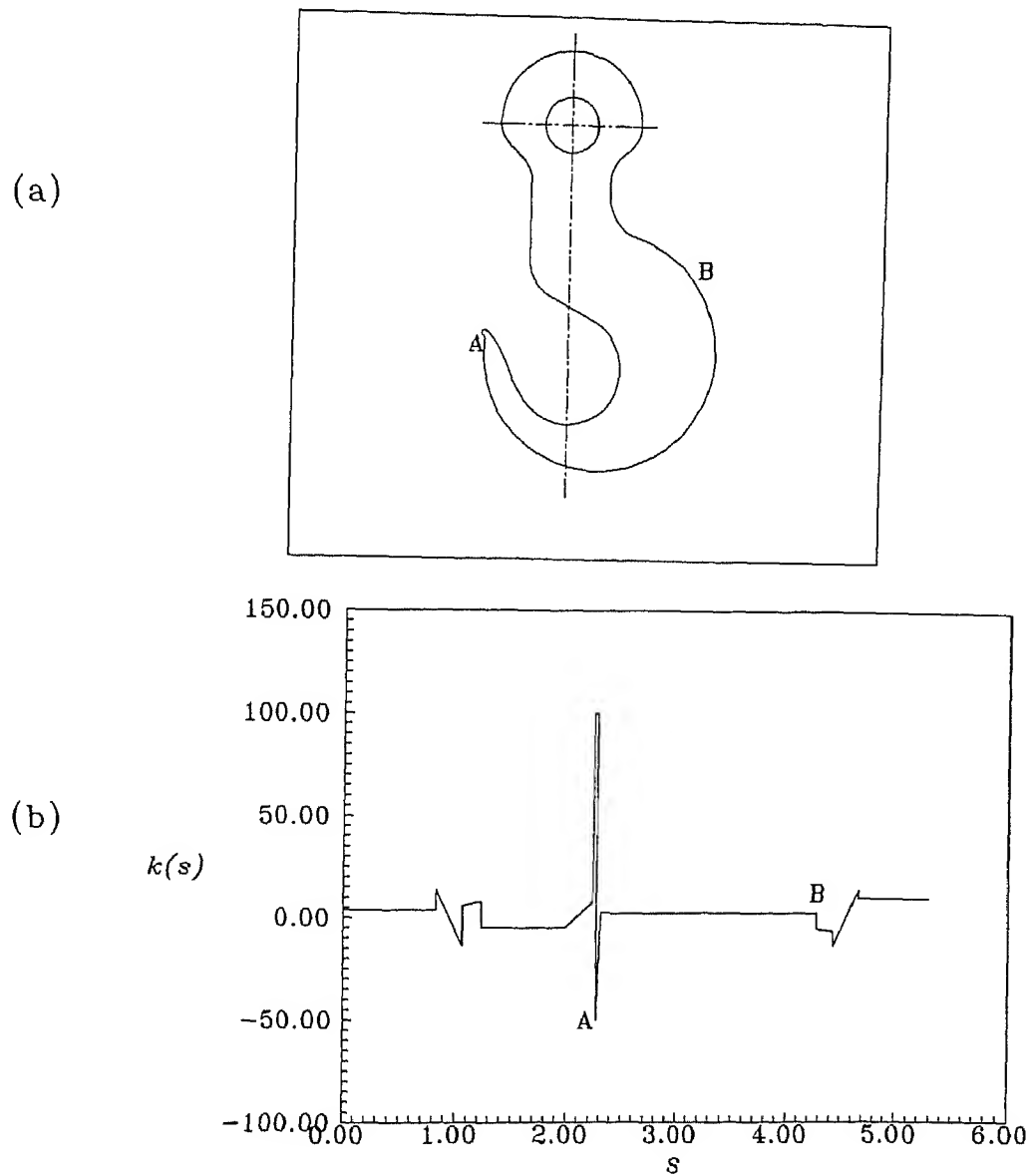
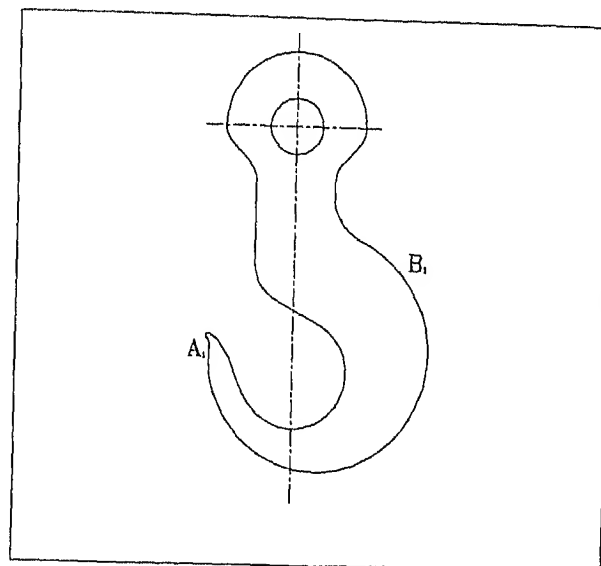


Figure 5.30 (a) Cartesian Profile for the Initial Shape of a Ladle Hook.

(b) Intrinsic Profile for the Initial Shape of the Ladle Hook.

(a)



(b)

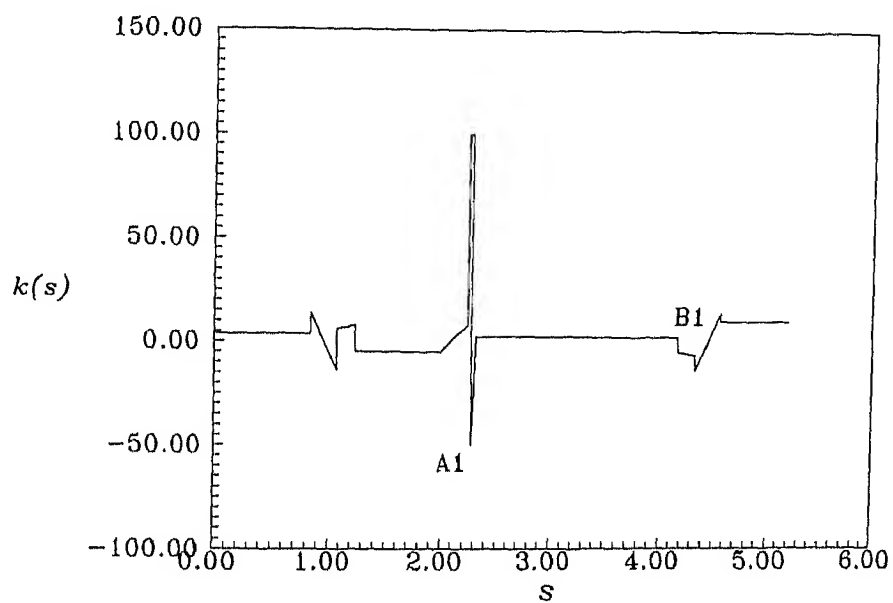
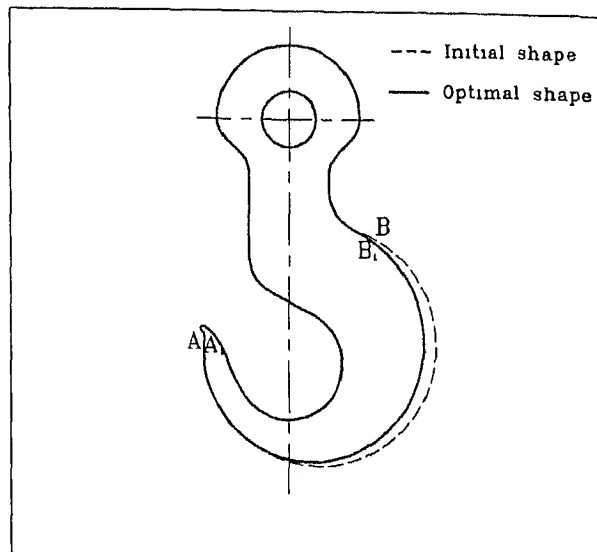


Figure 5.31 (a) Cartesian Profile for the Optimal Shape of a Ladle Hook.  
(b) Intrinsic Profile for the Optimal Shape Of a Ladle Hook.

(a)



(b)

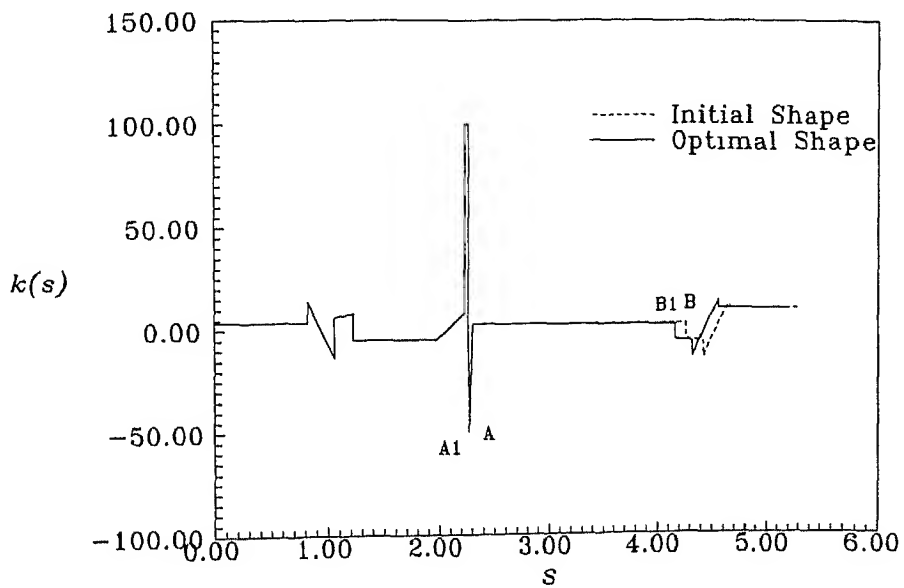


Figure 5.32 (a) Cartesian Profiles for the Initial and Optimal Shapes of a Ladle Hook.  
 (b) Intrinsic Profiles for the Initial and Optimal Shapes of a Ladle Hook.

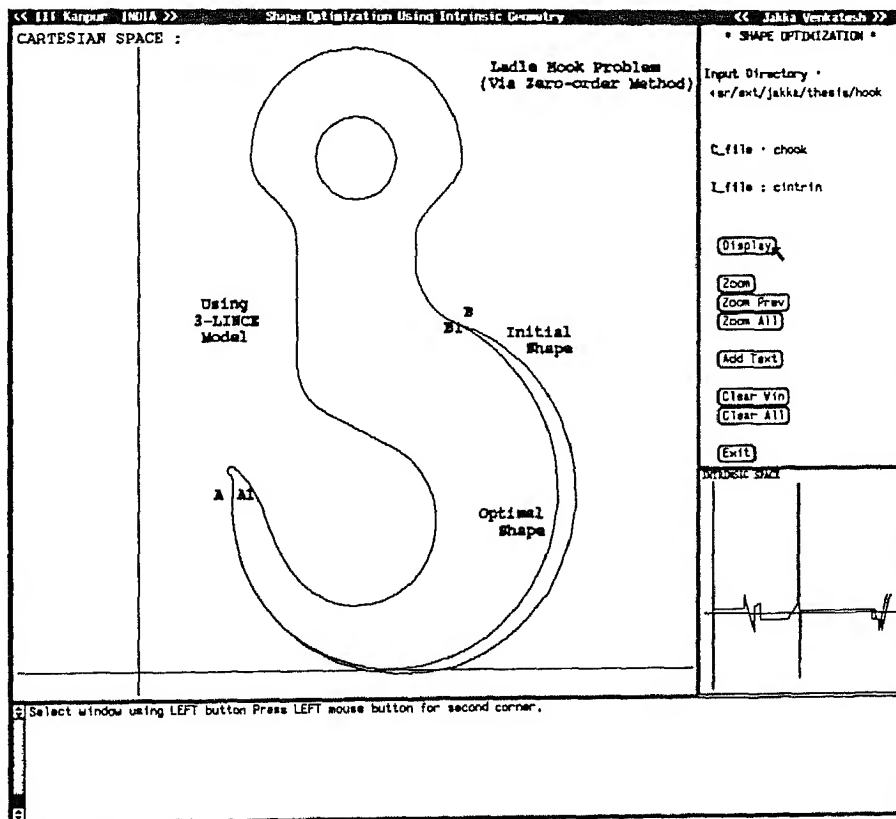


Figure 5.33 Cartesian and Intrinsic Profiles for the Initial and Optimal Shapes of a Ladle Hook on a Multi-Window SUN-view Graphics Environment.

### 5.2.6 Sensitivity Analysis of An Elastic Ring problem

The geometry belong to an optimal shape of an elastic ring has been considered here for sensitivity analysis. The effect of change in SDVs corresponding to an optimal shape has been studied via the sensitivity analysis procedure explained under Section 4.2.

The change in frontal-area (i.e. merit function) and the area sensitivity with respect to variation in optimal shape design variables including:  $\kappa_1$  and  $s_1$ . The variation in curvature  $\kappa_1$  is denoted by  $\Delta\kappa_1$  and arc length  $s_1$  denoted by  $\Delta s_1$ . The change in frontal-area and sensitivities have been estimated for 20 different perturbation sizes.

Figure 5.35 shows, the graph indicating frontal-area ( $\Phi$ ) versus changes in curvature ( $\Delta\kappa_1$ ). Figure 5.36 shows, the graph indicating area sensitivity versus change in curvature. Similarly Figures 5.37 and 5.38 shows, the variation in frontal-area ( $\Phi$ ) and area sensitivity with respect to the change in arc length ( $\Delta s_1$ ).

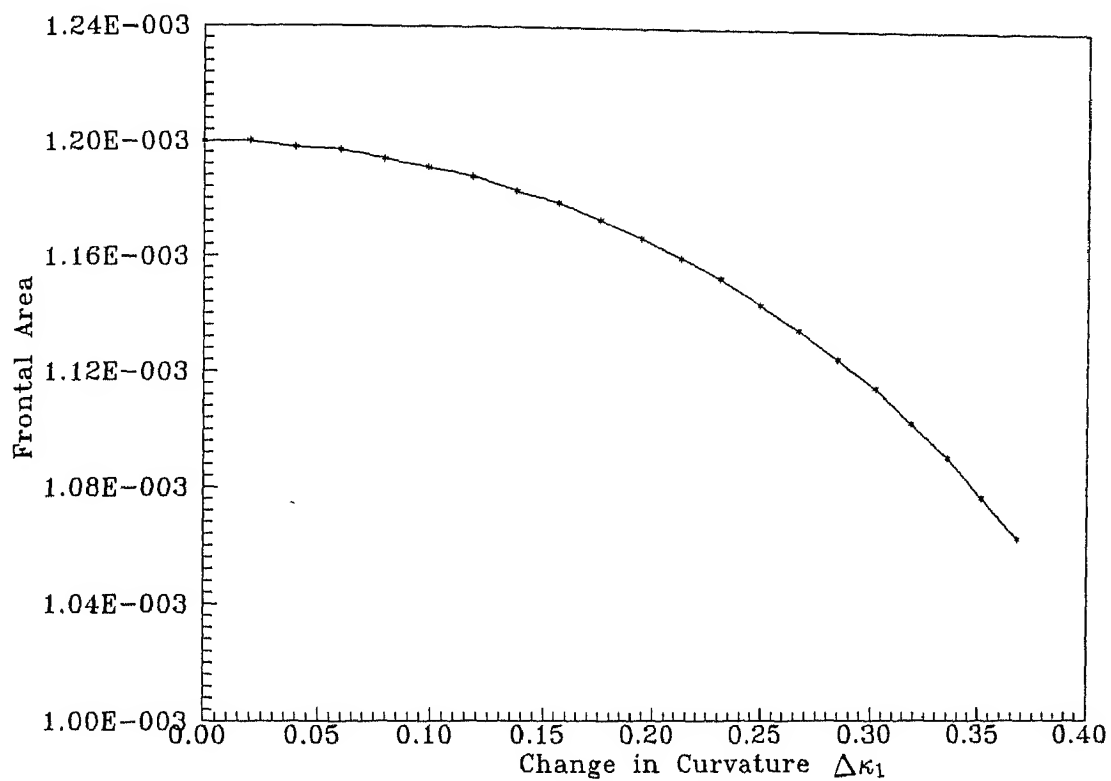


Figure 5.35 Graph shows Frontal-Area Vs Change in Curvature (  $\Delta\kappa_1$  ).

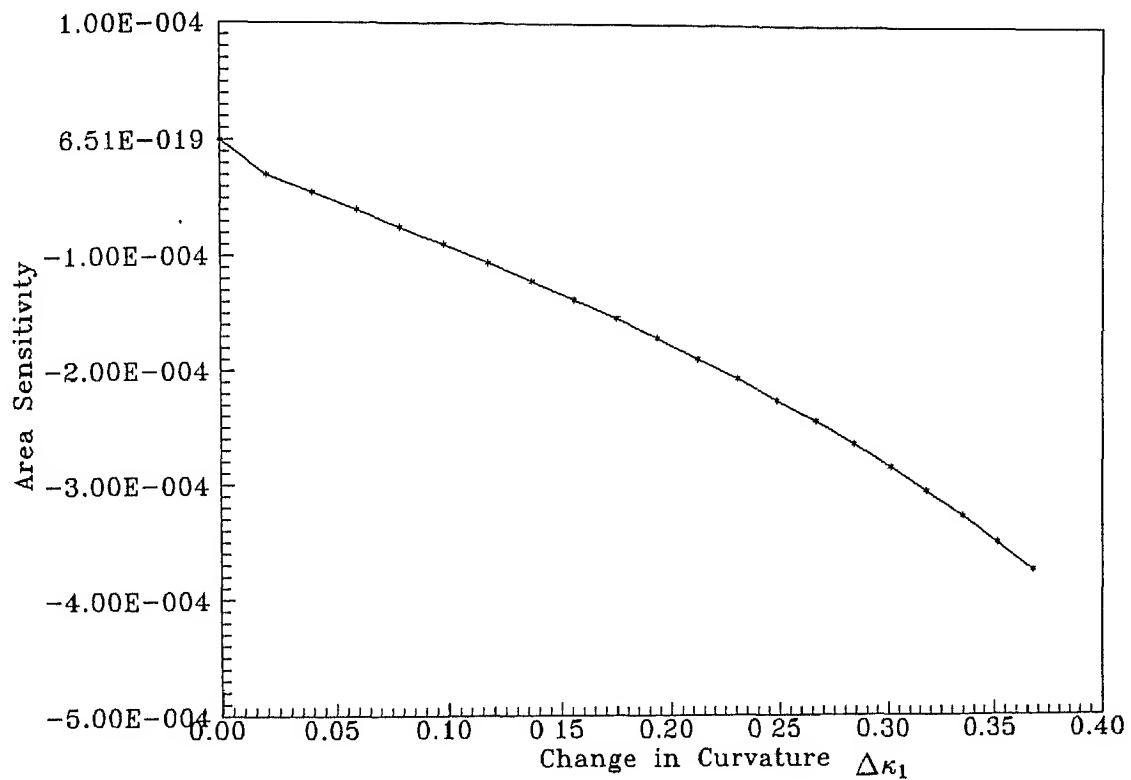


Figure 5.36 Graph shows Area-Sensitivity Vs Change in Curvature ( $\Delta\kappa_1$ ).

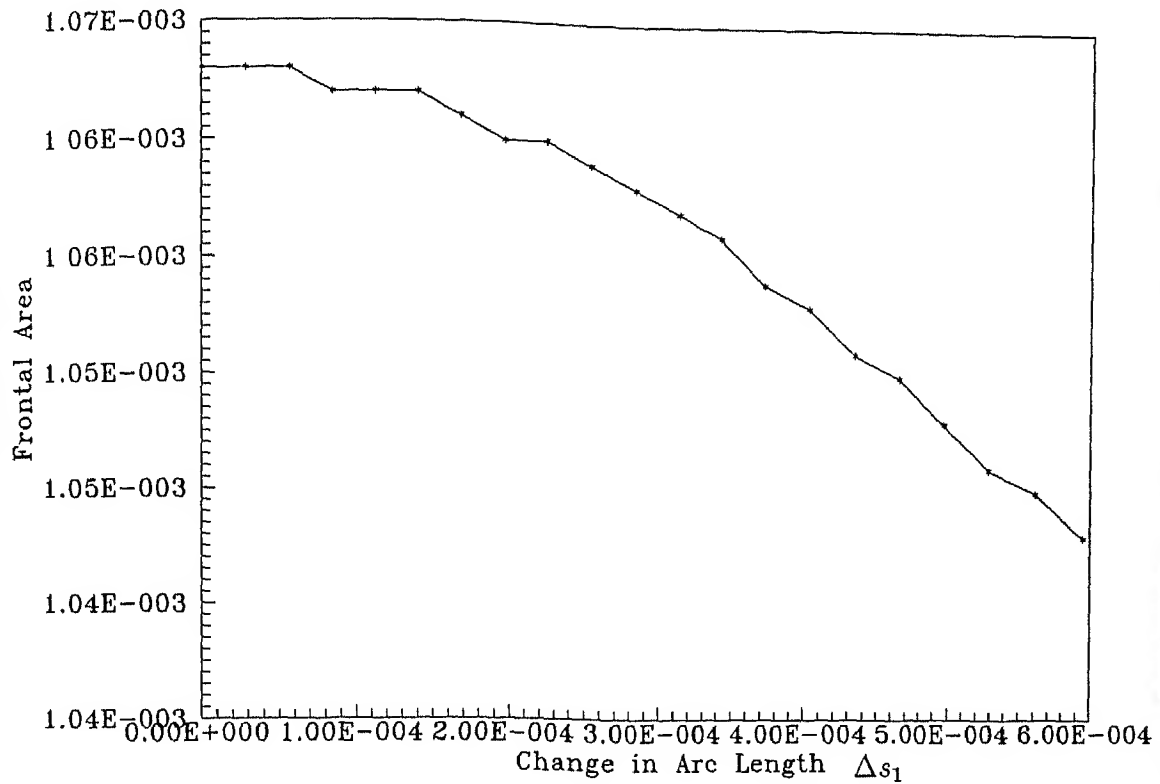


Figure 5.37 Graph shows Frontal-Area Vs Change in Arc Length ( $\Delta s_1$ ).

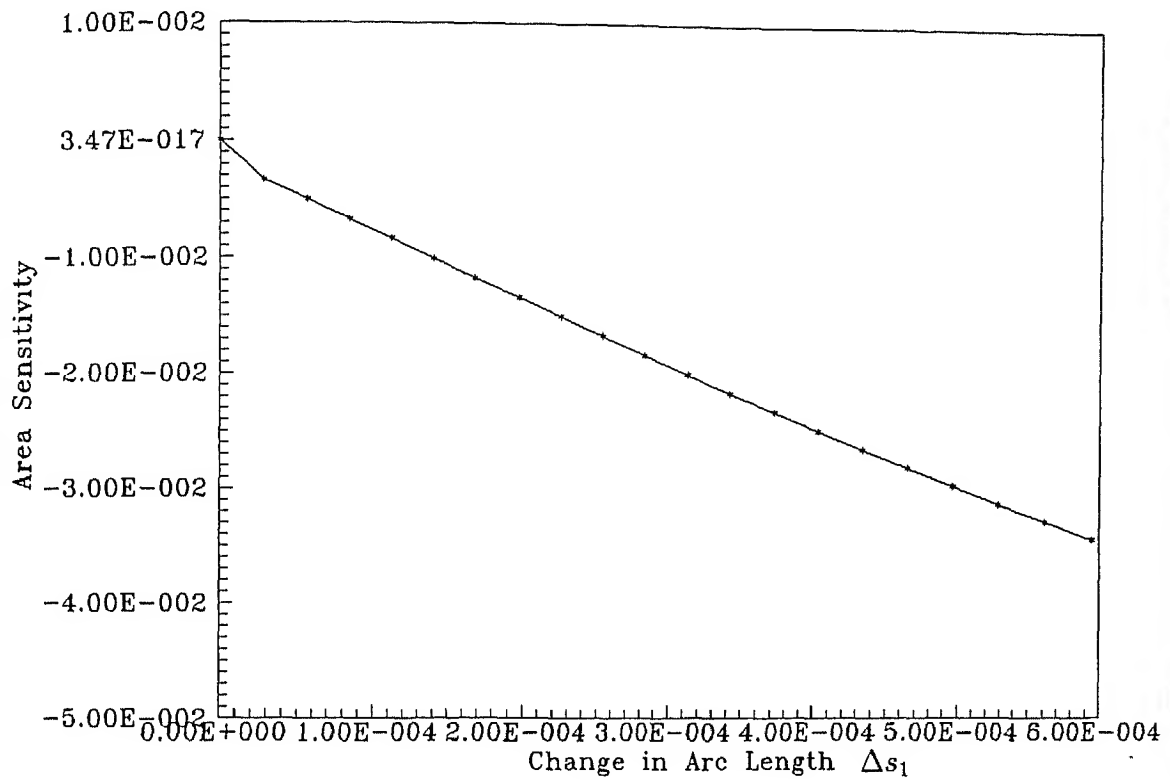


Figure 5.38 Graph shows Area-Sensitivity Vs Change in Arc Length ( $\Delta s_1$ ).

---

## CASE STUDIES VIA FIRST-ORDER METHOD

---

### 6.1 Software Development

The computer programs which have been developed for non-linear equation solver, numerical integration, shape synthesis, automatic boundary element mesh generation and refinement, and Boundary Element Analysis for Design (BEAD) in Section 4.2 are also used in this method. In addition, the optimization module based on first-order method has been developed in FORTRAN 77 using the optimization algorithm outlined in Section 4.3. The multi-window graphics environment created as described in Chapter 4 is also integrated with the proposed optimization cycle. In order to show the effectiveness of the proposed shape optimization methodology a numerical example of an elastic ring under diametral compression has successfully been implemented.

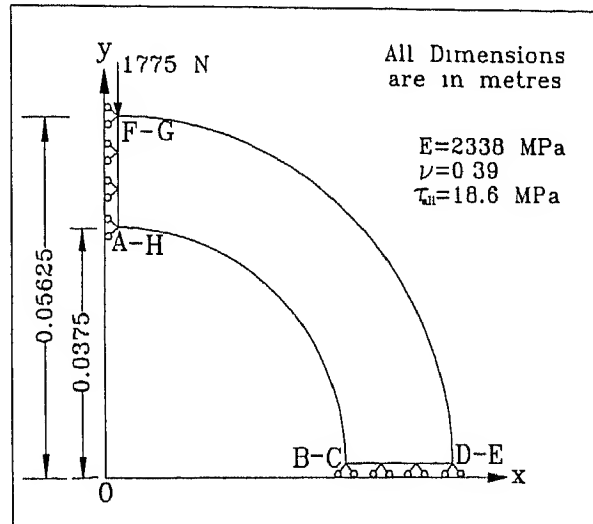
### 6.2 Numerical Example

The shape optimization methodology via First-order method described in Section 4.3 is now applied to a mechanical component. The problem is characterized as plane-stress case and the intrinsic 3-LINCEs model (R-R-R model) is used in order to have shape changes.

#### 6.2.1 An Elastic Ring Problem

This example shows an elastic ring under a single compressive load along its diameter, as shown in Figure 6.1(a). Taking the advantage of symmetry, one quarter of the ring is modelled, as shown in Figure 6.1. It is a case of plane-stress, and the objective is to minimize the weight (i.e. the minimization of frontal-area), while keeping the outer

(a)



(b)

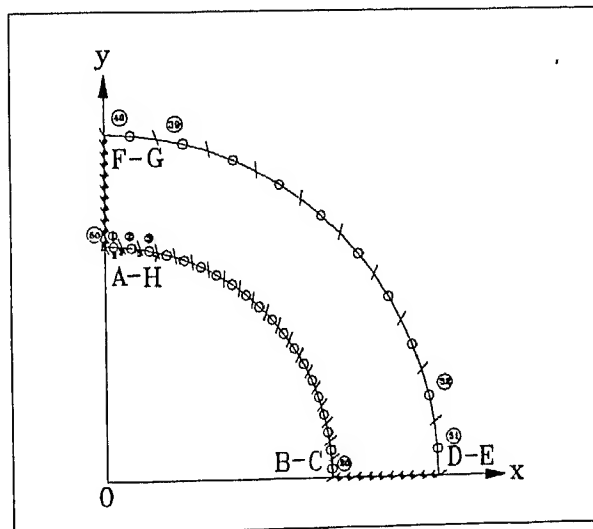


Figure 6.1 (a) Definition of An Elastic Ring under Diametral Compression with Displacement and Stress Boundary Conditions.

(b) Boundary Element Mesh for An Elastic Ring Problem.

boundaries defining the exterior shape of the ring unchanged. It is to be noted that the point B or C is allowed to move freely in the horizontal direction. A total of 100 nodes and 50 elements are used in the BEM analysis model.

The formulation of the problem can be stated as follows.

Minimize

$$\Phi = \Phi_1 - \frac{1}{2} \left[ \int_{s_0}^{s_1} \frac{1}{\left\{ \left( \frac{\kappa_1 - \kappa_0}{s_1 - s_0} \right) (s - s_0) + \kappa_0 \right\}} ds + \int_{s_1}^{s_2} \frac{1}{\left\{ \left( \frac{\kappa_2 - \kappa_1}{s_2 - s_1} \right) (s - s_1) + \kappa_1 \right\}} ds + \int_{s_2}^{s_3} \frac{1}{\left\{ \left( \frac{\kappa_3 - \kappa_2}{s_3 - s_2} \right) (s - s_2) + \kappa_2 \right\}} ds \right] \quad (6.1)$$

subject to

(i)

$$\begin{aligned} x_3 - x_0 &= \int_{s_0}^{s_1} \cos \left[ \left( \frac{\kappa_1 - \kappa_0}{s_1 - s_0} \right) \left( \frac{\sigma^2}{2} - s_0 \sigma \right) + \kappa_0 \sigma + C_1 \right] d\sigma \\ &- \int_{s_1}^{s_2} \cos \left[ \left( \frac{\kappa_2 - \kappa_1}{s_2 - s_1} \right) \left( \frac{\sigma^2}{2} - s_1 \sigma \right) + \kappa_1 \sigma + C_2 \right] d\sigma \\ &- \int_{s_2}^{s_3} \cos \left[ \left( \frac{\kappa_3 - \kappa_2}{s_3 - s_2} \right) \left( \frac{\sigma^2}{2} - s_2 \sigma \right) + \kappa_2 \sigma + C_3 \right] d\sigma = 0 \end{aligned} \quad (6.2)$$

$$\begin{aligned} y_3 - y_0 &= \int_{s_0}^{s_1} \sin \left[ \left( \frac{\kappa_1 - \kappa_0}{s_1 - s_0} \right) \left( \frac{\sigma^2}{2} - s_0 \sigma \right) + \kappa_0 \sigma + C_1 \right] d\sigma \\ &- \int_{s_1}^{s_2} \sin \left[ \left( \frac{\kappa_2 - \kappa_1}{s_2 - s_1} \right) \left( \frac{\sigma^2}{2} - s_1 \sigma \right) + \kappa_1 \sigma + C_2 \right] d\sigma \\ &- \int_{s_2}^{s_3} \sin \left[ \left( \frac{\kappa_3 - \kappa_2}{s_3 - s_2} \right) \left( \frac{\sigma^2}{2} - s_2 \sigma \right) + \kappa_2 \sigma + C_3 \right] d\sigma = 0 \end{aligned} \quad (6.3)$$

$$\psi_n - \psi_0 - \left( \frac{\kappa_0 + \kappa_1}{2} \right) (s_1 - s_0) - \left( \frac{\kappa_1 + \kappa_2}{2} \right) (s_2 - s_1) - \left( \frac{\kappa_2 + \kappa_3}{2} \right) (s_3 - s_2) = 0 \quad (6.4)$$

(ii)

$$\frac{\tau_{max}}{\tau_{all}} - 1 \leq 0 \quad (6.5)$$

$$-x_3 + 0.0375 \leq 0 \quad (6.6)$$

and

$$x_3 - 0.05625 \leq 0 \quad (6.7)$$

(iii)

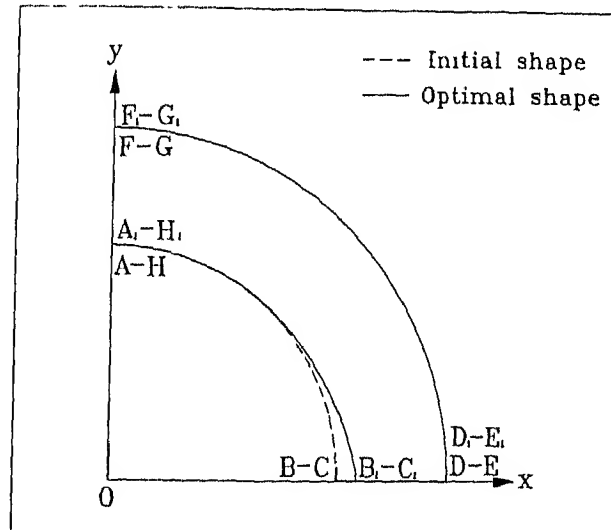
Constant values of

$$\begin{aligned} \Phi_1 &= \left(\frac{\pi}{4}\right)(0.05625)^2 \\ x_0 &= 0 \\ y_0 &= 0.0375 \\ y_3 &= 0 \\ s_0 &= 0 \\ \psi_0 &= 0 \text{ degrees} \\ \text{and } \psi_3 &= 270 \text{ degrees} \end{aligned} \quad (6.8)$$

Using the above formulation and shape optimization methodology via first-order method outlined in Section 4.3, an optimal shape of an elastic ring is achieved, as shown in Figure 6.2.

Figure 6.3 shows, the SUN-view graphics environment with cartesian and intrinsic geometries for the initial and the optimal shapes of the elastic ring.

(a)



(b)

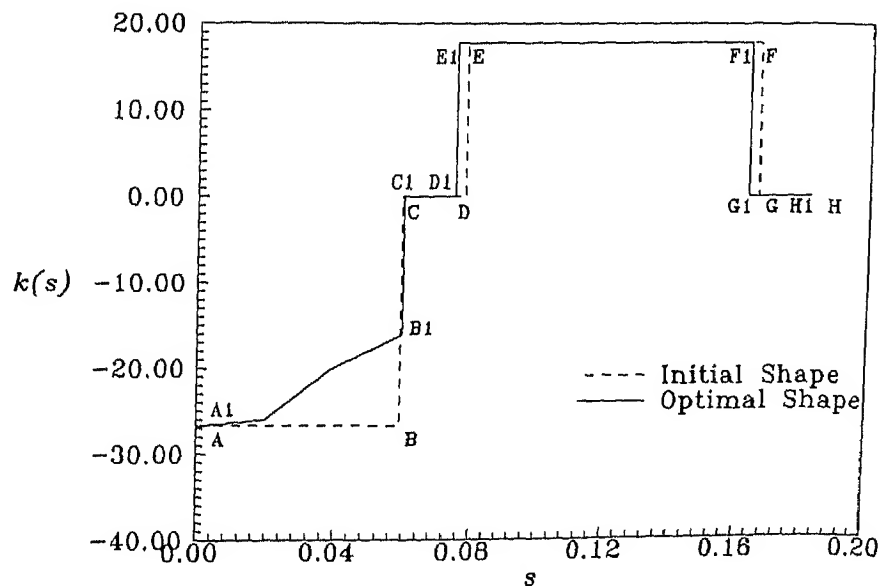


Figure 6.2 (a) Cartesian Profiles for the Initial and Optimal Shapes of An Elastic Ring (Via First-order Method).

(b) Intrinsic Profiles for the Initial and Optimal Shapes of An Elastic Ring (Via First-order Method).

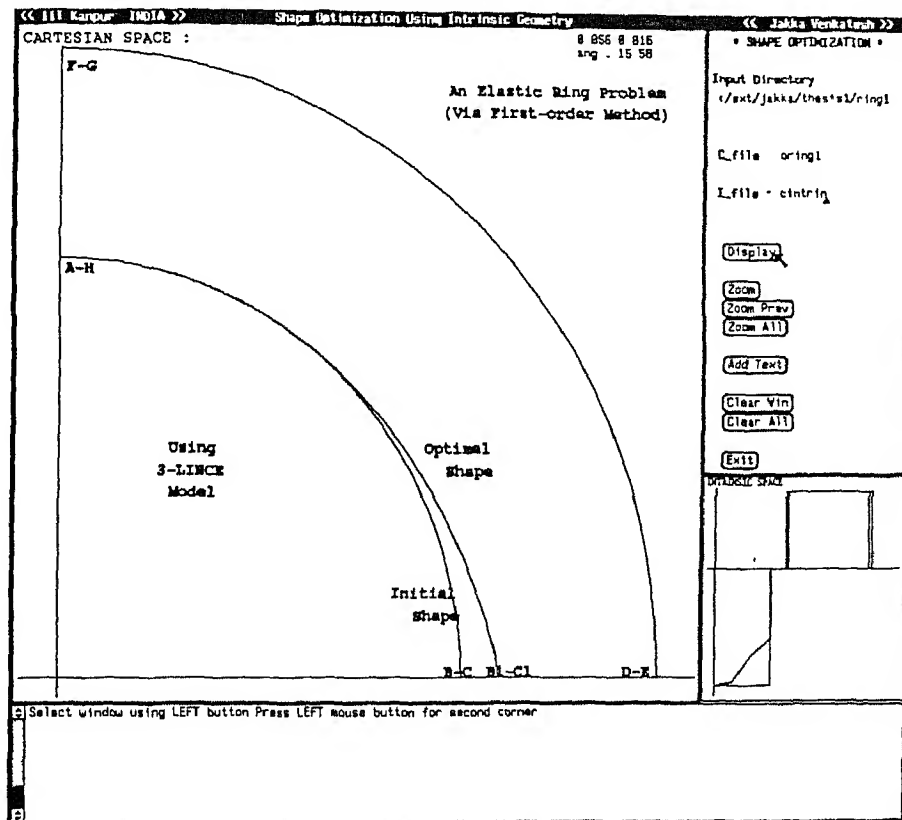


Figure 6.3 Cartesian Profiles for the Initial and Optimal Shapes of An Elastic Ring (Via First-order Method) on a Multi-Window SUN-view Graphics Environment.

---

## CONCLUSIONS

---

### 7.1 General Observations

The goal of CAD approach for shape optimization is to implement an interactive redesign system that integrates optimization methods within a flexible and efficient computational tool, easy to use by design engineers. *This interactive module is intended to create the missing link between BEM and CAD technologies and therefore it should constitute one of the key elements in the complex chain needed to computerize the design cycle.*

In particular, the shape optimization methodology proposed in this research requires a multi-window graphics environment. This is due to the fact that, the intrinsic definition of the curve and/or surface does not give the real feel of the geometry. In order to see the immediate effect of change in intrinsic shape design variables in cartesian space, the multi-window concept has been developed, thus the handicap of the intrinsic geometry would be eliminated. The multi-window concept developed on SUN-workstation using SUN-view graphics and UNIX-platform play an important role in the CAD based shape optimization cycle proposed in this research. The same optimization cycle on other systems, with the same multi-window concept has been developed on HP 9000/800-series workstation with UNIX-platform using STARBASE graphics in C language. It has been found that the optimization cycle is faster on HP-workstation than SUN-workstation. It is due to the supercomputing capability of HP-workstation. Figure 7.1 shows, such a graphics environment.

During the past two decades, the display technologies and computational tools have undergone a rapid change. Moreover, a unique integration of computational and display devices has occurred in the form of computer control display devices. As the means of *computations and display* have changed, it has become imperative to re-examine the

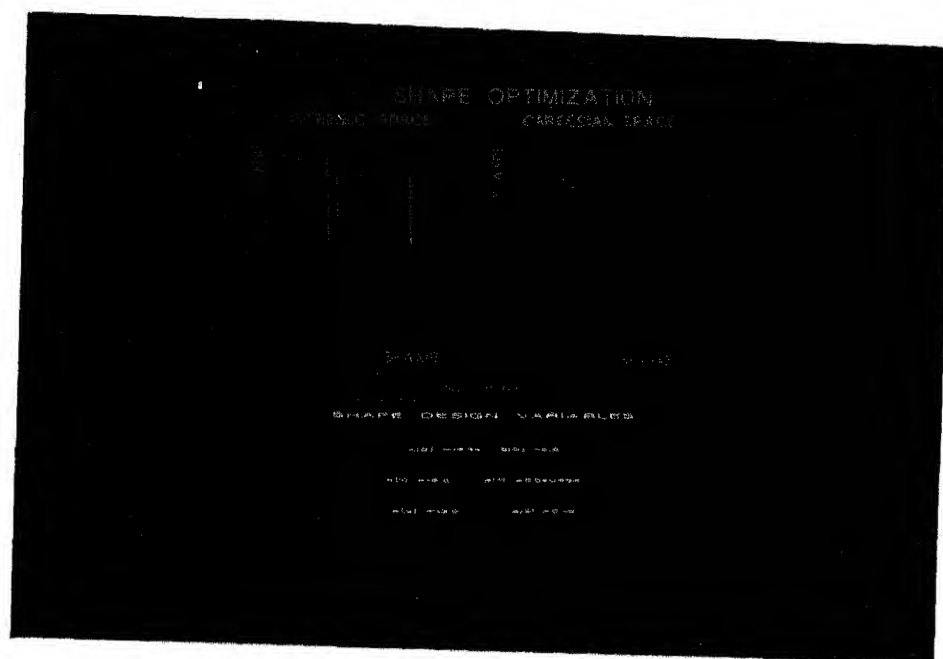


Figure 7.1 Multi-Window concept on HP-9000/800 series Workstation.

geometrical theories used for modeling design and manufacturing problems. It can be seen that research in the area of computational geometry during the past two decades has brought out many interesting techniques of geometric modeling such as, for example, solid modeling. The parametric form of modeling geometry has been found most attractive from two view points. In the first place, it is suitable for rendering the geometry in a parametric form or computer-controlled display devices. Secondly, by changing the position of some control points or auxiliary points, it is possible to manipulate the shape of the geometrical entities such as a curve or a surface. Extensive use of the parametric form has also brought into focus some drawbacks especially from engineering design view point. In particular, when a geometrical shape is to be manipulated for better or improved performance, then the relationship between the performance indices and the locations of the control points is not explicit. It is in this context that the proposed work has explored the role of one other form of representation of geometry, namely, the intrinsic form. It has been found that if the shape of a geometrical entity is presented in an intrinsic form, then it can be used for display purposes as well as for engineering analysis, optimization and manufacturing considerations. The proposed methodology of shape optimization utilizes intrinsic definition of surface boundary by selecting a shape model in the intrinsic space. For the selected shape model, it is possible to characterize a set of shape design variables by assigning suitable numerical values to the shape design variables. In this way, it is possible to define the geometry of a surface boundary completely. Any change in the values of design variables reflects in the corresponding change of the shape of the geometrical entity.

The proposed work consists of developing robust and stable numerical schemes in order to carry out shape synthesis as well as shape optimization using concepts of intrinsic geometry and BEM analysis. The shape synthesis of 2-dimensional surface boundaries can be accomplished by solving the Equations (2.31) through (2.33) provided that the curvature is given as a function of the arc length. The curvature can be represented using one of the proposed shape models. The shape models consists of a number of linear curvature elements ( $n$ -LINCEs). As the number of LINCEs increases, the number of shape design variables also increases, and hence the complexity of the optimization problem is augmented. The LINCE models seem to work for engineering design and optimization problems.

Any shape optimization problem requires a geometrical definition of shape. Traditionally, this has been accomplished by using parametric spline functions. The co-ordinates of the control vertices of the spline functions constitute the shape design variables. Such an approach invariably leads to a large number of design variables. In contrast the proposed investigation clearly indicates that the number of intrinsic shape design variables is definitely less than the number of shape design variables in the parametric approach.

In addition, it has been concluded that the intrinsic geometry approach seems to be

able to provide direct control for manipulation of the shape of a curve. The next important feature of intrinsic geometry shape definition is that, it provides an opportunity to include intrinsic properties like curvature and/or torsion in to the definition of the curve explicitly. These features of intrinsic geometry makes the shape synthesis module elegant and versatile, whereas the Bezier and B-spline representations do not provide the capability to control the intrinsic properties of a curve directly. The intrinsic geometry approach, however needs a scheme of mapping the intrinsic description on to a cartesian frame. This requires solving a set of non-linear equations and numerical integration schemes. In the present case Newton-Raphson modified method and Simpson's Numerical integration scheme were used for numerical analysis work. At this stage, it is important to note that while selecting  $(2n - 2)$  free shape design variables it is necessary rather must out of three dependent design variables, the arc length (i.e.  $s_i$ 's) variables can not be more than one. Otherwise, the numerical solution of non-linear equations (2.31) through (2.32) would not converge at all. This is due to the fact that the non-linear equations are too nonlinear in terms of arc length design variables ( $s_i$ 's) than curvature design variables ( $\kappa_i$ 's). The robust numerical schemes adopted in shape synthesis eliminates totally the user's intervention in the design cycle.

The versatility of this methodology is that the integration between shape synthesis module and BEM analysis module has been coupled through an automatic BEM mesh generation and refinement procedure. This eliminates the designer's intervention during the design process. Since BEM analysis is usually carried out in cartesian domain, the present investigation has shown that once the mapping of geometry from the intrinsic plane to the cartesian plane is completed, the stress analysis is relatively straightforward.

It is however, to be noted, that the proposed separation of the shape synthesis model from the analysis model, allows the designer to make a judicious choice in defining the shape via simple forms and low number of design variables, while at the same time using a highly refined BEM analysis model for sufficient accuracy of end results. Therefore, the matter of overall efficiency of the performance of methodology, remains to a great extent in the hands of the user.

The shape synthesis module and BEM analysis module has successfully integrated via zero-order (i.e. Exhaustive Search) and first-order (i.e. Interior penalty and hence DFP) Non-Linear programming (NLP) methods by taking proper precautions while formulating the objective function and other constraints of the problem. The proposed and very useful general CAD approach for shape optimal design of 2-D elastostatic problems consists of defining the boundary shape by Linear Curvature Elements (LINCES) model. It provides a flexible and compact geometric capability. The Boundary Element Method offers significant advantage over other engineering analysis tools like FEM, FDM etc. in shape optimization, especially for mesh data preparation. Using this method, the stress analysis could be rapidly performed, the regeneration and refinement of the

mesh elements representing the geometry was both straightforward and fast, and the optimization of the component shape could be carried out automatically.

The stress sensitivity and area sensitivity computational procedures explained in Sections 3.3 and 4.4 respectively, have successfully been implemented and the sensitivity plots are obtained.

The overall proposed shape optimization methodology has been implemented successfully for illustrative examples which include: a thick cylinder subjected to a constant internal pressure, an elastic ring under diametral compression, a torque arm subjected to an axial and transverse loads, a fillet under an axial load and a ladle hook subjected to tensile loading via zero-order method and an elastic ring problem via first-order method. The presented method of shape optimization approach can be applied to a broad range of applications in order to show its effectiveness over the parametric approach. The intrinsic geometry based shape optimization enables a designer to fulfil not only the functional requirements of an optimal design but also satisfy the manufacturing requirements. The proposed methodology will definitely become an effective tool in any CAD/CAM environment.

The following aspects must be considered while designing a computer software for the CAD approach to shape optimization.

The first one deals with the interactive computer graphics. It is present in most of the CAD systems as well as in analysis programs. It is concerned with the geometric transformations in 2-D and 3-D space and their graphical display. In the present case mapping the geometrical models from intrinsic to cartesian domain and then viewing them in an interactive SUN-view graphical display.

The second aspect is related to the geometric modeling. This poses a problem of conversion of models. The geometric models from CAD systems have to be converted in order to use in the analysis and optimization programs. For example, in the present research the shape has been defined in the intrinsic domain and the analysis and optimization are carried out in the cartesian domain.

The third aspect is the problem identification and the use of the design variables from the early step of shape design to the final step of optimization. The design variables are expected to be the parameters in the shape design, analysis, and optimization programs.

## 7.2 Future Work

Although it has been tried to include the intrinsic shape design variables directly into the shape functions of 2-D elastostatic BEM analysis, owing to the time limitations of

the research it has become necessary to leave this attempt incomplete. As a future work it has got a clear scope to implement. The description of the future work in this direction include defining the shape functions in terms of intrinsic shape design variables explicitly rather than presenting them in terms of cartesian  $x$ - $y$  co-ordinates. In addition the BEM analysis requires derivatives of the shape functions w.r.t the local co-ordinates of the boundary elements (i.e. w.r.t  $\xi$ ) and the evaluation of Jacobian of transformation,  $J(\xi)$ . Thus, the introduction of intrinsic geometric design variables directly into the shape function might pose numerical complexities and instabilities together with the programming difficulty. Robust numerical schemes must be selected in tackling this proposed approach of BEM analysis for shape optimization. The problem of imposing displacement and stress boundary conditions can be handled as usual case of BEM analysis. But at the same time the sensitivity computations become simpler.

Eventhough the present work utilized curvature function  $[\kappa(s)]$  is assumed to be a set of Linear Curvature Elements (LINCEs), the work can be extended using a set of cubic spirals. A cubic spiral is a curve whose tangent direction is described by a cubic function of arc length ( $s$ ). It can also be suggested that the same work can be extended using higher order curvature functions too. These approaches are expected to give more smooth profiles as compared to the one with Linear Curvature functions, at the cost of increased computational complexity. This proposed approach has got wide range of applications which include robot path planning and optimal design of trajectories etc. The other applications include designing of optimal cam shapes for jerk free cam-follower mechanisms.

The work can also be extended in the direction of designing optimal surface patches using intrinsic curve definition and lofted or ruled surface concept. For example, optimal blended transition surface patch design between air-craft fuselage surface and wing surface, optimal surface patch design for joining square or rectangular cross-section with the circular cross-section of air-conditioning ducts etc. by imposing suitable geometric and strength constraints.

Using the intrinsic definition of surface and the three-dimensional elastostatic BEM analysis, intrinsic geometry based shape optimization methodology can be developed in order to tackle 3-D problems. This widens the effective use of intrinsic geometry in the shape optimization process.

---

## REFERENCES

---

- [1] **Adams, J. A.**, 1975, "The Intrinsic Method for Curve Definition", *Computer Aided Design*, Vol. 7, No. 4, pp. 243-249.
- [2] **Akin, J. E.**, 1990, "*Computer-Assisted Mechanical Design*", Prentice Hall, Englewood Cliffs, New Jersey.
- [3] **Arora, J. S.**, 1989, "*Introduction to Optimum Design*", McGraw-Hill, New York.
- [4] **Becker, A. A.**, 1992, "*The Boundary Element Methods in Engineering*", McGraw-Hill, New York.
- [5] **Bennet, J. A., Botkin, M. E.**, 1986, "*The Optimum Shape Automated Structural Design*", Plenum Press, New York.
- [6] **Belegundu, A. D.**, 1993, "Optimizing the Shapes of Mechanical Components", *ASME Journal of Mechanical Engineering*, Vol. 115, No. 1, PP.46-48.
- [7] **Chan, W. P., Yung, M. Y., Kil, H. K.**, 1989, "Shape Design Sensitivity Analysis of An Axisymmetric Turbine Disk Using the Boundary Element Method", *Computers & Structures*, Vol. 33, No. 1, pp. 7-16.
- [8] **Chandrupatla, T. A., Belegundu, A. D.**, 1991, "*Introduction to Finite Elements in Engineering*", Prentice Hall of India Pvt. Ltd., New Delhi, India.

- [9] Choi, J. H., Kwak, B. M., 1988, "Boundary Integral Equation Method for Shape Optimization of Elastic Structures", *International Journal for Numerical Methods in Engineering*, Vol. 26, pp. 1579-1595.
- [10] Dieter, G. E., 1986, "*Engineering Design*", McGraw-Hill, New York.
- [11] Dimarogonas, A. D., 1989, "*Computer Aided Machine Design*", Prentice Hall International (UK) Ltd, London.
- [12] Ding, Y., 1987, "Shape Optimization of Two-Dimensional Structures with Optimal Thicknesses for Fixed Parts", *Computers & Structures*, Vol. 27, No. 6, pp. 729-743.
- [13] Do Carmo, M. P., 1976, "*Differential Geometry of Curves and Surfaces*", Prentice Hall, Englewood Cliffs, New Jersey.
- [14] Eschenauer, H. A., 1988, "On Shape Optimization of Satellite Tanks", *Structural Optimization*, Kluwer Academic Publishers, Dordrecht, The Netherlands, pp. 395-395.
- [15] Esping, B., Holm, D., 1988, "Structural Shape Optimization Using OASIS", *Structural Optimization*, Kluwer Academic Publishers, Dordrecht, The Netherlands, pp. 93-100.
- [16] Farshi, B., Moradi, S., 1992, "BESHOP : A Program Package for Shape Optimization in 2-D Elasticity Problems", *Advances in Design Automation*, Vol.1, pp. 37-41.
- [17] Faux, I. D., Pratt, M. J., 1983, "*Computational Geometry for Design and Manufacture*", Ellis Horwood Publishers, Chichester.
- [18] Fernand, E., 1988, "Shape Optimization of Intersecting Pressure Vessels", *Structural Optimization*, Kluwer Academic Publishers, Dordrecht, The Netherlands, pp. 77-84.
- [19] Fukushima, J., Suzuki, K., Kikuchi, N., 1992, "Topology Optimization of a Car Body with Multiple Loading Conditions", *American Institute of Aeronautics and Astronautics Journal*, AIAA-92-2250-CP, pp. 2499-2507.

- [20] Georgiades, P. N., Greenberg, D. P., 1992, "Locally Manipulating the Geometry of Curved Surfaces", *IEEE Computer Graphics & Applications*, January 1992, pp. 54-64.
- [21] Haftka, R. T., Grandhi, R. V., 1986, "Structural Shape Optimization A Survey", *The Optimum Shape: Automated Structural Design*, Plenum Press, New York.
- [22] Hajela, P., Jih, J., 1988, "Boundary Element Methods in Optimal Shape Design-An Integrated Approach", *Structural Optimization*, Kluwer Academic Publishers, Dordrecht, The Netherlands, pp. 109-116.
- [23] Haug, E. J., Choi, K. K., Komkov, V., 1986, "*Design Sensitivity Analysis of Structural Systems*", Academic Press, Inc., San Diego, CA.
- [24] Hou, J. W., 1985, "Techniques and Applications of Shape Optimum Design", *Computers & Structures*, Vol. 20, No. 1-3, pp. 467-473.
- [25] Kibsgaard, S., 1992, "Sensitivity Analysis-The Basis for Optimization", *International Journal for Numerical Methods in Engineering*, Vol. 34, pp. 901-932.
- [26] Kreyszig, E., 1964, "*Differential Geometry*", University of Toronto Press, Toronto.
- [27] Krishnamurthy, E. V., Sen, S. K., 1991 "*Numerical Algorithms*", East West Press Pvt. Ltd., New Delhi, India.
- [28] Lee, B. Y., Kwak, B. M., 1991, "Shape Optimization of Two Dimensional Thermo Elastic Structures Using Boundary Integral Equation Formulation", *Computers & Structures*, Vol. 41, No. 4, pp. 709-722.
- [29] Lord, E. A., Wilson, C. B., 1984, "*The Mathematical Description of Shape and Form*", Ellis Horwood Publishers, Chichester.
- [30] Luchi, M. L., Poggialini, C. V., Persiani, F., 1980, "An Interactive Optimization Procedure Applied to the design of Gas Turbine Disks", *Computers & Structures*, Vol. II, pp. 629-637.

- [31] Mortenson, M. E., 1985, "*Geometric Modeling*", Wiley, New York.
- [32] Mota Soares, C. A., Choi, K. K., 1986, "Boundary Elements in Shape Optimal Design of Structures", *The Optimum Shape: Automated Structural Design*, Plenum Press, New York.
- [33] Mota Soares, C. A., Leal, R. P., Choi, K. K., 1987, "Boundary Elements in Shape Optimal Design of Structural Components", *Computer Aided Optimal Design: Structural & Mechanical Systems*, Springer-Verlag, Berlin, Vol. 27, pp. 605-631.
- [34] Nutbourne, A. W., Martin, R. R., 1988, "*Differential Geometry Applied to Curve and Surface Design*", Vol. 1, Ellis Horwood Publishers, Chichester.
- [35] Olmsted, M. H. J., 1961, "*Advanced Calculus*", Appleton-Century-Crofts, Inc., USA.
- [36] Pal, T. K., 1978a, "Intrinsic Spline Curve with Local Control", *Computer Aided Design*, Vol. 10, No. 1, pp. 19-29.
- [37] Pal, T. K., Nutbourne, A. W., 1977, "Two Dimensional Curve Synthesis Using Linear Curvature Elements", *Computer Aided Design*, Vol. 9, No. 2, pp. 121-134.
- [38] Papalambros, P. Y., 1988, "*Principles of Optimal Design*", Cambridge University Press, Cambridge.
- [39] Pironneau, O., 1984, "*Optimal Shape Design for Elliptic Systems*", Springer-Verlag, New York.
- [40] Queau, J. P., Trompette, P., 1983, "Optimum Shape Design of Turbine Blades", *Journal of Vibrations, Acoustics, Stress, and Reliability in Design*, Vol. 105, pp. 444-448.
- [41] Rao S. S., 1991, "*Optimization Theory and Applications*", Wiley Eastern Limited, New Delhi.

- [42] Remash Chandran, N., 1982, "Synthesis of Curves Using Intrinsic Forms", M.Tech. Thesis Submitted to the Department of Mechanical Engineering, Indian Institute of Technology, Kanpur, India.
- [43] Rogers, D. F., Adams, J. A., 1990, "Mathematical Elements for Computer Graphics", McGraw-Hill, New York.
- [44] Sandgren, E., Sayed, M. El., 1988, "Shape Optimization : Creating a Useful Design Tool", *Structural Optimization*, Kluwer Academic Publishers, Dordrecht, The Netherlands, pp. 273-278.
- [45] Sandgren, E., Wu, S., 1988, "Shape Optimization Using Boundary Element Method with Substructuring", *International Journal for Numerical Methods in Engineering*, Vol. 26, No. 19, pp. 1913-1924.
- [46] Sastry, S. S., 1990, "Introductory Methods of Numerical Analysis", Prentice Hall of India, New Delhi, India.
- [47] Shigley, J. E., 1983, "Mechanical Engineering Design", McGraw-Hill, Tokyo, Japan.
- [48] Srinath, L. S., 1988, "Advanced Mechanics of Solids", Tata McGraw-Hill, New Delhi.
- [49] Struik, D. J., 1950, "Lectures on Classical Differential Geometry", Addison Wesley Press, Inc., Cambridge 42, Mass.
- [50] Tafreshi, A., Fenner, R. T., 1993, "Design Sensitivity Analysis Using The Boundary Element Method", *Journal of Strain Analysis*, Vol.28, No. 4, pp. 283-291.
- [51] Tavakkoli S., 1991, "Shape Design Using Intrinsic Geometry", Ph.D. Dissertation submitted to The Department of Mechanical Engineering, Virginia Polytechnic Institute and State University, Blacksburg, Virginia, USA.
- [52] Tavakkoli S., Dhande, S. G., 1991, "Shape Synthesis and Optimization Using Intrinsic Geometry", *ASME Journal of Mechanical Design*, Vol. 113, No. 4, pp. 379-386.

- [53] Timoshenko, S. P., Goodier, J. N., 1985, "*Theory of Elasticity*", McGraw-Hill, Singapore.
- [54] Vanderplaats, G. N., 1984, "Numerical Optimization Techniques for Engineering Design", McGraw-Hill, New York.
- [55] Venkatesh, J., Dhande, S. G., 1993, "A CAD Approach to Shape Optimization Using Intrinsic Geometry and Boundary Element Method", *INCARF-93, CAD, CAM, ROBOTICS AND AUTONOMOUS FACTORIES, Vol. II*, Tata McGrawHill, New Delhi, India, 44-66.
- [56] West, R. L., Sandgren, E., 1989, "A Direct and Indirect Approach to Shape Optimization Using The Boundary Element Method", *Proceedings of The International Symposium on Boundary Element Methods*, Springer-Verlag, New York, pp. 427-434.
- [57] Yamaguchi, F., 1988, "*Curves and Surfaces in Computer-Aided Geometric Design*", Springer-Verlag, Berlin, New York.
- [58] Yang, R. J., Choi, K. K., Haug, E. J., 1985, "Numerical Considerations in Structural Component Shape Optimization", *Journal of Mechanisms, Transmissions, and Automation in Design*, Vol. 107, pp.334-339.